Speciality and microstructured polymer optical FBG sensors

Woyessa, Getinet

Publication date:
2017

Document Version
Publisher's PDF, also known as Version of record

Speciality and Microstructured Polymer Optical FBG Sensors

PhD Dissertation

Getinet Taffesse Woyessa

DTU Fotonik
Department of Photonics Engineering

Technical University of Denmark

April 2017

Copyright

ISBN xxxxxxxxxxxxx

Preface

This dissertation is prepared in fulfillment of the requirements for acquiring a PhD in Photonics Engineering.

The presented works have been carried out in the period March, 2014 to April, 2017. The research activity took place mainly at the Department of Photonics Engineering, Technical University of Denmark, Lyngby, Denmark. Further scientific research was carried out during my secondments at Nano-photonics Research Laboratory, Cyprus University of Technology, Limassol, Cyprus and Aston Institute of Photonics Technologies, Aston University, Birmingham, UK. The research leading to the results presented in this thesis has received funding from the People Programme (Marie Curie Actions) of the European Union's Seventh Framework Programme FP7/2007-2013/ under REA grant agreement n° 608382. The research has been supervised by Professor Ole Bang and co-supervised by Dr. Christos Markos at the Department of Photonics Engineering, Technical University of Denmark, Lyngby, Denmark.

April , 2017

Getinet Taffesse Woyessa

Acknowledgements

I would like to acknowledge all people who have been supporting and contributing to the success of my PhD. First and foremost, I would like to express my deepest gratitude to my supervisor Ole Bang for his supervision, advice, encouragement and guidance throughout my research. I would like to thank my co-supervisor Christos Markos for the invaluable help during my research particularly down in the lab.

A special thanks goes to my project colleague Andrea Fasano for those numerous discussions and helpfulness. Big thanks to Alessio Stefani and Kristian Nielsen for the willingness to help me in the laboratory and for those countless scientific discussions.

Many thanks to Kyriakos Kali (Cyprus University of Technology) and David J. Webb and Kate Sugden (Aston University) for hosting me at their institute for my secondments. Amédée Lacraz and Antreas Theodosiou (Cyprus University of Technology) and Michael Zubel (Aston University) I thank you very much guys for the priceless time and support in the laboratory during my secondments.

Frank Persson, Martin Nielsen, Jan N. Mortensen and John Lauridsen from the mechanical workshop a million thanks for your excellent work, patience and helpfulness.

I would like to thank all my colleagues at DTU Fotonik as workplace is empty without good colleagues. I thank you very much all people in the TRIPOD project for bringing this project come true.

Finally, I would like to thank my friends and family, especially my father and mother, who have always provided wonderful support all the way through my life.

Abstract

In light of commercialisations of polymer optical fibre Bragg grating (POFBG) sensors, high performance and stable operation of the gratings are key requirements. Traditionally towards the development of such sensors, the polymer optical fibres (POFs) were annealed in conventional ovens before or after the grating inscriptions. In conventional ovens humidity is not controlled thus humidity significantly decreases as the temperature rises to the annealing temperature. This technique of thermal annealing did not allow obtaining high performance POFBGs sensors, particularly those based on polymethylmethacrylate (PMMA). During the PhD project it has been discovered that humidity plays a significant role in the annealing of PMMA POFBGs and the later sensor responsivity to environmental measurands. The investigation revealed that, PMMA POFBGs annealed at high level of humidity (I) provided a superior performance in humidity responsivity over a wide temperature range over the one annealed at low humidity (II) enabled tuning the Bragg wavelength by more than 200 nm which provide a way to produce gratings at short wavelengths and multiplexing several grating in a single fibre using only a single phase mask. The described humidity assisted annealing was performed in a climate chamber which was not cost effective despite it provided superior result. However, to combat this, new method of annealing at room temperature was proposed and investigated which only requires methanol-water solution but delivered a comparable result.

The most commonly used polymer material for POFs fabrication is PMMA. Although this polymer is ideal for humidity sensors development due to its high water absorption capability, the maximum operating temperature of PMMA POFBGs is limited to only 75 °C when they are operated at high humidity, for instance 90 % relative humidity (RH). In addition when PMMA POFBGs are applied for strain and temperature measurements, the high RH sensitivity pose a problem. Thus it was important to develop POFs that can mitigate the aforementioned problems. One of the objectives of the project

involved exploring and bringing speciality polymers which have different features than PMMA for fibre Bragg gratings (FBGs) based sensing applications.

The new polymers that were explored and exploited for the fabrication of solid core microstructured polymer optical fibres (mPOFs) were Polycarbonate (PC) and Zeonex 480R. In addition, a combination of Topas 5013S-04 and Zeonex 480R exploited for step index fibre realisation. PC has also moisture absorbing capability but not as strong as PMMA and it has excellent mechanical property. While Topas 5013S-04 and Zeonex 480R have a very low moisture absorbing capability. All of them have a glass transition temperature (T_g) greater than PMMA has and transmittance as good as PMMA but lower. Therefore, gratings fabricated in POFs produced from these polymers utilised to sense temperature beyond the operation limit of PMMA POFBGs. Not only this but also the strong effect of humidity cross sensitivity that were seen when temperature and strain were measured with PMMA mPOFBGs was avoided using these new polymers. PC POFBGs allowed sensing temperature up to 125 °C and this is a record temperature measured with currently existing POFBGs. In addition, with PC POFBGs it was possible to measure RH up to 90% at a temperature up to 100 °C which was limited to only up to 75 °C by PMMA based gratings. Wide range, hysteresis free and stable strain sensors were also realised with gratings fabricated in these new POFs.

Prior to the PhD Topas grade 8007F-04 and 5013S-04 mPOFs have been fabricated for humidity insensitive temperature and strain measurements. However, each of them has their own limitation. Topas 8007F-04 has a T_g 26 °C smaller than that of PMMA so the temperature sensing range is very narrow. Whereas Topas 5013S-04 has high flowability thus difficult to draw good quality microstructured fibres from it despite it has a T_g 28 °C larger than that of PMMA and suitable for high temperature sensing. Therefore, to fought back these challenges two solutions were proposed: to fabricate a step index Topas 5013S-04 fibre but yet single mode as the microstructured one or to explore another polymer which has low affinity to water as Topas but friendly to draw. Both of these solutions have been addressed and realised during the research period.

Zeonex 480R was the ideal candidate to replace Topas 5013S-04 as they share most properties in common but the former is easily drawable. Using these two polymers and by combining casting, drilling and injection moulding techniques a step index (SI) fibre was made. Heat and draw method was used to fabricate the fibre. The fabricated fibre was the first humidity insensitive and high operating temperature single mode SIPOF. The employed fibre production method was very efficient, flexible and cost effective as no doping was required. The fibre also presented grating inscription time shorter than PMMA mPOFs and much shorter that Topas mPOFs. Further, the 4.8 µm core size of the fibre was compatible and good for optimum coupling with standard silica fibre which is single mode in the 850 nm region. However, small core size caused high scattering loss which increases the overall loss of the fibre, and this was the main limitation.

The second proposed solution was to develop a Zeonex 480R mPOF as its flowability is suitable for mPOF drawing. This grade of Zeonex showed a superior drawablity over Topas 5013S-04 with wide range of drawing temperature. The realised Zeonex 480R mPOF was not only drawing friendly but also has low loss and presented a very good compatibility with PMMA for co-drawing applications compared to Topas 5013S-04. Further, grating realised in it provided high sensitivity to temperature.

The co-drawability feature of Zeonex 480R with PMMA enabled to draw a hybrid Zeonex 480R-PMMA mPOF for the development of the first fully polymeric thermo-hygrometer. The fibre had Zeonex 480R as core and cladding and PMMA as an over cladding. The thermo-hygrometer was developed based on dual in line gratings and operated in the range 20 °C-80 °C and 10-90 % RH, with a root means square error of 0.6 °C and 0.8 RH %. The device key advantages are being easy to fabricate, cost effective, fully polymeric and mechanically stable.

Resumé

For at sikre at polymer optisk fiber Bragg gitter (POFBG) sensorer får en kommerciel fremtid er det højest nødvendigt at garantere en stabil arbejdsgang og ydelse. Tidligere er disse faktorer forsøgt løst ved at afstresse polymer optiske fibrene (POF) i en konventionel ovn. I en konventionel ovn er der ingen fugt kontrol og dermed, pga. af de høje temperatur, er fugt niveau meget lavt når fiberen bliver forsøgt afstresset. Denne afstresnings teknik opnåede ikke særligt gode resultater, specielt når det kommer til POF lavet af polymethyl metha acrylat (PMMA). Med det resultat at POFBG kun kunne bruges ved temperaturer lavere end 50 °C og at sensorens respons udviste ulineær opførsel. I dette PhD projekt er det blevet påvist at fugt spiller en afgørende rolle når det kommer til afstresning af PMMA POFBG og dermed til POFBG respons. Undersøgelser har vist at PMMA POFBG der er afstresset ved høj fugt niveau har (I) en overlegen ydelse som fugt sensor over en større temperatur spænd end tidligere afspændings teknik og (II) muliggør at Bragg bølgelængden kan forskydes mere end 200 nm; hvilket gør det muligt at fremstille gitter ved meget lave bølgelængder og muliggør fremstilling af flere gitter i samme fiber ved brug af én phase maske. Den beskrevne høj fugt niveau afstresning blev gennemført i et klima kammer, hvilket medfører uønskede omkostninger. For at mindske disse omkostninger er en ny afstresnings teknik også blevet undersøgt, denne teknik er baseret på et opløsnings middel bestående af en blanding af methanol og vand. Denne simple teknik resulterede i lignende gode ydelser.

PMMA er det polymer materiale som er typisk brugt til fremstilling af POF. Denne polymer er velegnet som fugt sensor i og med at den absorberer meget vand. Dens brug er dog begrænset pga. dens lave maks. Temperatur grænse. Hvis PMMA POFGB udsættes for 90% relativ fugtighed (RH) så må den højest udsættes for 75 °C. Ligeledes når PMMA POFBG bruges som tøjning og temepratur sensor, udgør dens store fugt respons et problem. Det var derfor nødvendigt at udvikle en POF der kunne omgå disse problemer. En af målene

i dette projekt var at udforske nye polymerer og udnytte disse til at fremstille sensorer der har anderledes og komplimentære egenskaber mht. PMMA.

De nye polymer typer der er blevet undersøgt og brugt i fremstillingen af mikro-strukturerede polymer optiske fiber (mPOF) er polycarbonat (PC) og Zeonex 480R. Yderligere er en kombination af Topas 5013S-04 og Zeonex 480R også blevet brugt til at fremstille et step index fiber. PC optager også vand, dog ikke lige så meget som PMMA, og har fremragende mekaniske egenskaber. Mens Topas 5013s-04 og Zeonex 480R derimod har meget lavt vand optag. De nye polymerer har alle en glas transistions temperatur (T_g) der er højere end PMMAs og har optiske transmission der er like så god som PMMAs eller bedre. Disse nye polymerer kan derfor udnyttes til at lave sensorer der kan virke ved temepraturer højere end hvad PMMA kan. De nye polymerer har derud over ikke samme problem med krydsfølsomhed pga. fugt som er forstyrrende når PMMA mPOFBG bliver brugt til tøjning eller temperatur måling. PC POFBG tillader temperature målinger op til 125 °C, hvilket er en record hvad angår POFBGer. Derudover var det muligt at måle fugt op til 90 %RH ved 100 °C ved brug af en PC POFBG, hvor PMMA POFBG kun kan klare 75 °C. De nye polymerer blev også brugt til at fremstille tøjnings sensorer med vidt måle område, der var stabile og uden hysteresis.

Før dette PhD projekt var der blevet fremstillet mPOF ud af Topas, både 5013S-04 og 8007F-04, og demonstreret som fugt ufølsom temperatur og tøjning sensorer. Begge materiale typerne havde dog begrænsninger. Topas 8007F-04 har en T_g der er 26 °C lavere end PMMA, derfor var dens maks. Temperatur endnu lavere end PMMAs. Mens selv om Topas 5013S-04 har en T_g der er 28 °C højere end PMMAs, hvilket giver den en høj maks. Temperatur, så har den også en høj flowability under fremstilling, hvilket gør det svært at fremstille mPOF af dette polymer materiale. To løsninger blev forslået til at bekæmpe disse begrænsinger: At fremstille en step index Topas 5013S-04 fiber, som dog stadig er single mode, eller at finde en ny polymer som har samme vand afvisning som Topas, men som er fremstillings venlig. Begge af disse løsninger er blevet overvejet og realiseret i dette projekt.

Zeonex 480R var den idele kandidat til at erstatte 5013S-04 i og med at de deler mange af samme egenskaber, men Zeonex er nem at trække til mPOF. Ved at kombinerer støbning, boring og indsprøjtnings forming, var det muligt at samle disse to polymer typer i en step index fiber. Fiberen blev fremstillet ved varm og træk methoden. Den fremstillede fiber var den første fugt ufølsomme og højt temperaturs single mode SIPOF. Fremstillings methoden var meget effektiv, fleksibel og omkostnings lav, i og med at der ikke var brug for at dope. Fiberen var også bedre egnet til FBG indskrivning, med skrive tider kortere end PMMA og meget kortere end Topas mPOF. Derudover gjorde kernens størrelse på 4.8 µm at fiberen var velegnet til kobling med standard glas fiber I 850 nm bølgelængde området. Derimod gjorde den lille kerne at sprednings tabet var større og dette er fiberens største svaghed.

The næste forslag var at fremstille en mPOF ud af Zeonex 480R i og med at den flowability er bedre egnet til mPOf fremstilling. Denne type Zeonex udviste en overlegen drawability i forhold til Topas 5013S-04 med en bred vifte af egnede fremstillings temperaturer. Den fremstillede Zeonex 480R mPOF var ikke kun fremstillings venlig men den havde også lavt transmissions tab og fremviste også en god kompatibilitet med PMMA fremstilling, hvilket muliggjorde bedre fremstillings muligheder end hvad var muligt med Topas 5013S-04. Endvidere viste det sig at FBG skrevet i denne nye fiber var meget følsom overfor temperatur.

Den store kompatebilitet imellem Zeonex 480R og PMMA gjorde det muligt at fremstille en Zeonex 480R-PMMA hybrid mPOF hvilket medførte den første rent polymer termo-hygrometer. Fiberen havde Zeonex 480R som kerne og PMMA som kappe. Termo-hygrometeret blev fremstillet ved at skrive to FBG efter hinanden og kunne bruges i området 20-80 °C og 10-90 %RH med en root mean square fejl på 0,6 °C og 0,8 %RH. Denne sensors store styrker er at den er nem at fremsille, lav omkostning, ren polymer og mekaniskt stabil.

Summary of Original Work

This thesis is based on the following journal publications produced during the PhD project:

Paper 1 **G.Woyessa**, K.Nielsen, A.Stefani, C.Markos and O.Bang, "Temperature insensitive hysteresis free highly sensitive polymer optical fibre Bragg grating humidity sensor," Optics Express 24(2), 1206-1213 (2016).

Paper 2 A.Fasano, **G.Woyessa**, J. Janting, Henrik K. Rasmussen, and O.Bang, "Solution-mediated annealing of polymer optical fiber Bragg gratings at room temperature," IEEE Photonics Technology Letters 29(8), 687-690 (2017).

Paper 3 A.Fasano, **G.Woyessa**, P.Stajanca, C. Markos, A.Stefani, K.Nielsen, H. K. Rasmussen, K. Krebber, and O. Bang, "Fabrication and characterization of polycarbonate microstructured polymer optical fibers for high-temperature-resistant fiber Bragg grating strain sensors," Optical Materials Express 6(2), 649-659 (2016).

Paper 4 **G. Woyessa**, A. Fasano, C. Markos, H.K. Rasmussen, and O. Bang, "Low loss polycarbonate polymer optical fiber for high temperature FBG humidity sensing," IEEE Photonics Technology Letters 29(7), 575-578 (2017).

Paper 5 **G.Woyessa**, A.Fasano, A. Stefani, C.Markos, K.Nielsen, H.K. Rasmussen and O.Bang, "Single mode step-index polymer optical fiber for humidity insensitive high temperature fiber Bragg grating sensors," Optics Express 24(2), 1253-1260 (2016).

Paper 6 **G.Woyessa**, A.Fasano, C. Markos, A. Stefani, H. K. Rasmussen, and O. Bang, "Zeonex microstructured polymer optical fiber: fabrication friendly fibers for high temperature and humidity insensitive Bragg grating sensing," Optical. Material Express 7(1), 286-295 (2017).

Paper 7 **G. Woyessa**, J.M.Pedersen, A. Fasano, K. Nielsen, C. Markos, H.K. Rasmussen, and O. Bang, "Zeonex-PMMA microstructured

polymer optical FBGs for simultaneous humidity and temperature sensing," Optics Letter 42(6), 1161-1164 (2017).

Other Journal papers produced during the PhD project:

1. I.-L. Bundalo, K. Nielsen, **G.Woyessa** and O.Bang, "Long-term strain response of polymer optical fiber FBG sensors," Optical Materials Express 7(3), 967-976(2017).
2. D. Ganziy, O. Jespersen. **G. Woyessa**, B. Rose, O. Bang, "Dynamic gate algorithm for multimode fiber Bragg grating sensor systems," Applied Optics 54(18), 5657-5661 (2015).
3. X. Hu, **G. Woyessa**, D. Kinet, J. Janting, K. Nielsen, O. Bang, and C. Caucheteur, "BDK-doped core microstructured PMMA optical fiber for effective Bragg grating photo-inscription," Optics Letter 42(11), 2206-2212 (2017).
4. J.M.Pedersen, **G. Woyessa**, K. Nielsen, and O. Bang, "Improved pressure sensitivity of pre-strained polymer optical fiber Bragg-gratings," Optics Letter(In review).

Conference papers produced during the PhD project:

1. **G.Woyessa**, A.Fasano, A. Stefani, C.Markos, K.Nielsen, H.K. Rasmussen, O.Bang, "Humidity insensitive step-index polymer optical fibre Bragg grating sensors," *Proc. SPIE* 9634, 24th International Conference on Optical Fibre Sensors, 96342L (September 28, 2015); doi:10.1117/12.2194963.
2. I.-L Bundalo, K. Nielsen, **G. Woyessa**, O. Bang, "Long term strain behavior of PMMA based polymer optical fibers," *Proc. SPIE* 9634, 24th International Conference on Optical Fibre Sensors, 96347Y (September 28, 2015); doi:10.1117/12.2195267.
3. **G.Woyessa**, K.Nielsen, and O.Bang, "The effect of humidity on annealing of polymer optical fibre Bragg grating and their response," Proceedings of the 24th International Conference on Plastic Optical Fibers 2015 (POF2015), Nuremberg, Germany, September 22-24, 2015.

4. A. Fasano, **G. Woyessa**, P. Stajanca, C. Markos, A. Stefani, K. Nielsen, H.K. Rasmussen, K. Krebber, O. Bang, "Production and characterization of polycarbonate microstructured polymer optical fiber Bragg grating sensor," Proceedings of the 24th International Conference on Plastic Optical Fibers 2015 (POF2015), Nuremberg, Germany, September 22-24, 2015.
5. C.Broadway, D.Gallego, **G.Woyessa**, A.Pospori, O.Bang, D.J. Webb, G.Carpintero, H.Lamela, "Polymer Optical Fibre Sensors for Endoscopic Opto-Acoustic Imaging," *Proc. SPIE* 9539, Opto-Acoustic Methods and Applications in Biophotonics II, 953907 (July 16, 2015); doi:10.1117/12.2183452.
6. C.Broadway, D.Gallego, **G.Woyessa**, A.Pospori, G.Carpintero, O.Bang, K.Sugden, H.Lamela, "Fabry-Perot micro-structured polymer optical fibre sensors for opto-acoustic endoscopy," *Proc. SPIE* 9531, Biophotonics South America, 953116 (June 19, 2015); doi:10.1117/12.2181095.
7. A.Fasano, **G.Woyessa**, P.Stajanca, C. Markos, A.Stefani, K.Nielsen, H. K. Rasmussen, K. Krebber, and O. Bang , "Creation of a microstructured polymer optical fiber with UV Bragg grating inscription for the detection of extensions at temperatures up to 125 °C," *Proc. SPIE* 9886, Micro-Structured and Specialty Optical Fibres IV, 988619 (April 27, 2016); doi:10.1117/12.2227843.
8. **G.Woyessa**, A.Fasano, C. Markos, H. K. Rasmussen, and O. Bang , "Zeonex Microstructured Polymer Optical Fibre Bragg Grating Sensor," article in conference proceedings, Photonics and Fiber Technology Conference (ACOFT, BGPP, NP), Sydney, Australia, September 5-8, OSA 2016, ISBN: 978-1-943580-17-02016, doi:10.1364/ACOFT.2016.AW3C.4.
9. **G.Woyessa**, A.Fasano, C. Markos, H. K. Rasmussen, and O. Bang, "Polymer Optical Fibre Bragg Grating Humidity Sensor at 100 °C", 25th International Conference on Plastic Optical Fibers 2016 (POF2016), Birmingham, UK, September 13-15, 2016, ISBN 978 1 85449 408 5.

10. J.M.Pedersen **G.Woyessa**, A.Fasano, K. Nielsen, H.K. Rasmussen, and O. Bang, "Intrinsic Pressure Response of a Single-Mode Cyclo Olefin Polymer Microstructured Optical Fibre Bragg Grating," 25th International Conference on Plastic Optical Fibers 2016 (POF2016), Birmingham, UK, September 13-15, 2016, ISBN 978 1 85449 408 5.
11. A.Fasano, **G.Woyessa**, J. Janting, Henrik K. Rasmussen, and O.Bang, "Investigation of the in-solution relaxation of polymer optical fibre Bragg gratings," Proceedings of the 25th International Conference on Plastic Optical Fibers 2016 (POF2016), Birmingham, UK, September 13-15, 2016, ISBN 978 1 85449 408 5.
12. X.Hu, **G.Woyessa**, D.Kinet, J.Janting, K.Nielsen, O.Bang, P.Megret and C.Caucheteur, "Bragg grating photo-inscription in doped microstructured polymer optical fiber by 400nm femtosecond laser pulses," Proceedings of the 25th International Conference on Plastic Optical Fibers 2016 (POF2016), Birmingham, UK, September 13-15, 2016, ISBN 978 1 85449 408 5.
13. H. U. Hassan, A. Fasano, J. Janting, G. Demirci, O. Çetinkaya, **G.Woyessa**, H. K. Rasmussen, O. Bang, "Study of doping non-PMMA polymer fibre canes with UV photosensitive compounds," Proceedings of the 25th International Conference on Plastic Optical Fibers 2016 (POF2016), Birmingham, UK, September 13-15, 2016, ISBN 978 1 85449 408 5.
14. M. G. Zubel, A. Fasano, **G. Woyessa**, K. Sudgen, H. K. Rasmussen, O. Bang, "3D printed PMMA preform for hollow-core POF drawing," Proceedings of the 25th International Conference on Plastic Optical Fibers 2016 (POF2016), Birmingham, UK, September 13-15, 2016, ISBN 978 1 85449 408 5.
15. **G.Woyessa**, J.M.Pedersen, A.Fasano, K. Nielsen, C. Markos, H.K. Rasmussen, and O. Bang, "Simultaneous measurement of temperature and humidity with microstructured polymer optical fiber Bragg gratings," *Proc. SPIE* 10323, 25th International Conference on Optical Fibre Sensors, 103234T (April 25, 2017); doi:10.1117/12.2265884.
16. J.M.Pedersen, **G.Woyessa**, K. Nielsen and O. Bang, "Effects of pre-strain on the intrinsic pressure sensitivity of polymer optical fiber

Bragg-gratings," *Proc. SPIE* 10323, 25th International Conference on Optical Fibre Sensors, 103234U (April 25, 2017); doi:10.1117/12.2265885.

Book chapters produced during the PhD project:

1. C.-A. Bunge, K. Bremer, B. Lustermann, **G. Woyessa**: "Special fibres and components" in Polymer Optical Fibres, Fibre Types, Materials, Fabrication, Characterisation and Applications, P119-151. Published by Elsevier 01/01/2017; ISBN 9780081000397. DOI: 10.1016/B978-0-08-100039-7.00004-X.
2. **G.Woyessa**, A. Fasano and C. Markos, "Microstructured polymer optical fibre gratings and sensors'', book chapter of "Handbook of Optical Fibres'' to be edited by Gang-Ding Peng and published by Springer (In production).

Patent:

1. **G. Woyessa** , C.Markos and O. Bang, "Multimode polymer optical fibre Bragg grating sensors", in filing process, to be submitted to EPO.

Contents

Chapter 1 - Introduction

This chapter provides the main motivation behind the PhD project and the main achievements that obtained during the research period. It also details how the thesis is organised and highlights the contents of each chapters.

1.1 Motivation

The field of measuring environmental physical quantities such as strain, temperature, humidity, pressure and so on has been growing very rapidly. To this end, sensors with high sensitivity to the measurands, high resolution and accuracy, low failure rate, low installation and operation cost, immunity to external environmental influences that affects the operation of the sensors are highly required. To measure environmental quantities electro-mechanical sensors were developed, get matured and widely implemented. However, these sensors have several limitations in some application areas such as being not immune to electromagnetic interferences and they require continuous electrical power supply for their operation which increases both the installation and operation costs. In addition, they easily fail in hazardous areas for instance at high temperature and fast chemical reaction environments. Further, they are large in size and heavy in weight which upturns the difficulty to integrate them in a composite structures and sophisticated areas.

The emerging of optical technologies has opened a door in finding of a solution that overcomes the limitations of the conventional electro-mechanical sensors. The rapid improvement and mass production of optoelectronic components in the field of optical technology born new sensors called fibre optic sensors. Over the years, the replacement of the conventional electro-mechanical sensor by fibre optic sensors have been proceeding due to the production of high quality and cost-effective components in optoelectronic and fibre optic communication industries [1], [2]. In comparison to the conventional electro-mechanical sensors, fibre optic sensors have numerous and inherent advantages such as immunity

to electromagnetic interference, high sensitivity, light weight, environmental ruggedness, multiplexing and distributed capabilities to form sensor networks. These advantages of fibre optic sensors enabled to reach in several application areas that were not reliable, effective and efficient with the conventional electro-mechanical sensors, for instance in hostile, high electric and magnetic field areas and also biomedical and chemical industries. In addition, fibre optic sensors employed to measure large variety of environmental parameters that were difficult with electronic sensors like current, voltage, magnetic field, and so on [3], [4]. Moreover, various researches and developments have been made to detect damages in composite and aircraft wing and to detect acoustic emission using fibre optic interferometric method [5]–[7] among some of them. Nevertheless, interferometric based fibre optic sensors have some limitations for example they lack of multiplexing capabilities and cause ambiguity in strain direction detection. However, in the realm of fibre optic sensors, the discovery of optical fibre photosensitivity emerged a dominant technology called fibre Bragg grating (FBG) which overcomes these problems. As a result, the development of optical FBG sensors has attracted great attentions and has become the leading type of sensors in the field.

Fibre optic Bragg grating sensors have distinguished advantages over other types of fibre optic sensors mainly they are compact, lightweight and have high sensitivity. In addition, they are insensitive to fluctuations in the power of light in the sensor components. Moreover, low cost of manufacturing of FBGs in large volume decreases the total cost of the sensor system development and more importantly they have multiplexing and distributed capabilities to form sensor networks. Furthermore, FBGs are excellent to monitor varies parameters using multiplexing technology [8], [9].

FBG was first developed in silica optical fibres [10]. Due to a rapid development in the production of silica FBGs and a considerable study in the area, gratings in silica fibres is matured, and widely and extensively used in different applications. Due to low attenuation of silica optical fibres, grating sensors made of silica fibres are suitable for distributed and remote monitoring of extensive areas. Although they have these important advantages, they do have

also some limitations in some application areas due to their intrinsic material properties. Some of them are narrow strain sensing range due their low elastic limit and not suitable for biomedical application as they are not biocompatible.

The promising solution to address these problems is to use a fibre made of different material which have unique material properties which could overcome the aforesaid problems of silica based fibres. The good candidates are polymer optical fibres (POFs) as they have non-brittle nature, high flexibility in bending, low Young's modulus, high elastic strain limits, giving them great potential for FBG based sensing applications [11]–[14]. POFs have also excellent compatibility with organic materials, making them ideal candidates for biomedical applications [15]–[19]. In addition, POFs have very low processing temperature and are easy to handle, hence low processing cost and safe disposability. Moreover, it was possible to realise the integration of metals, insulators and semiconductors structures into an extended length of polymer fibre for various applications [20], [21]. Furthermore, production of microstructured polymer optical fibres (mPOFs) is easy and cost effective compared to that of silica photonic crystal fibres.

There are different types of polymers available and most of them have their own unique properties. The unique intrinsic features of various polymers make them suitable to develop POFBGs for a specific measurand sensing application. Therefore, by exploring new polymer materials for the development of high performance FBGs sensors for different applications are the primarily motivations of this PhD project. Towards these, this thesis present the design, development, realisation and characterisation of stable, hysteresis free and highly sensitive polymer optical fibre Bragg gratings (POFBGs) strain, temperature and humidity sensors. Fabrications of both step index and microstructured types POFs were carried out with various polymer materials. Solution to sensors high performance and stability has been proposed and experimentally demonstrated. Grating inscription optimisations in order to obtain high quality gratings have been carried out for POFs fabricated from various polymer materials. A multi-parameters POFBGs sensor was also realised with a new fibre design and fibre grating technology.

1.2 Thesis Organisation

Chapter 2 contains a review and basic principles pertinent to this thesis. It begins with a detailed description of history, fabrication techniques and the fundamentals of POFs in general. Then, it follows with a brief review of FBGs in POFs and their development till to date. Later, a review on fibre optic sensors and particularly FBG sensors are detailed. Finally, the key features of POFBGs sensors over their counterpart silica FBGs sensors are compared with respect to the material properties. This chapter is closed by giving a short summary on the basic principle behind the strain, temperature and humidity sensing characteristics of POFBGs.

Chapter 3 describes the main contribution and achievements during the PhD by directly referring to the journal papers published during the research period. It also involved some relevant but unpublished results. It describes the fibres fabrication method used, characterisation of the fabricated fibres, grating fabrication and optimisations for fibres fabricated from various polymer materials, followed by the key step in the development of stable and high performance POFBGs sensors. Then, the humidity, temperature and strain characterisations of the produced gratings are summarised and described. Finally, a thermo-hygrometer developed from purely polymeric fibres is reported.

Chapter 4 comprises conclusions drawn from the research performed during the project period. The key achievements of the PhD study are also provided in this chapter. Finally the chapter closes by providing recommendations on what can be done in the future in the realm of POF and POFBGs which are quite important from the commercialisation point of views.

Chapter 2 - Thesis Background

This chapter comprises mainly a literature review and basic principles pertinent to this thesis. It begins with descriptions on history, fabrication techniques and the fundamental theories POFs in general followed by brief review of FBGs in POFs and their development till to date. Later, a review on fibre optic sensors is given focused on FBG sensors. Finally, the key features of polymer FBG sensors over their counterpart silica FBGs sensors are discussed. This chapter close by giving the basic principle behind strain, temperature and humidity sensing with POFBGs.

2.1 Polymer Optical Fibres (POFs)

In the realm of fibre optics, the very first optical fibres were developed from polymeric materials. The first POF was invented by Du Pont in 1968 at almost the same time when silica was proposed as a transmission medium for communication. Dupont's fibre was having a step index refractive index profile with polymethylmethacrylate (PMMA) core and fluoropolymer cladding [22]. Although POFs showed their appearance before silica optical fibres, their higher intrinsic losses pushed back their development. However, the extensive research made on silica fibres improved their purity considerably. Currently, silica fibres used for long haul telecommunication has a transmission loss of 0.15 dB/km at 1550 nm [23] which is way smaller than the lowest loss POF available commercially now-a-days. Although POFs are not competent for long haul communications, they serve as a complement for silica fibres for short short-haul communications links as they are flexible, easy to handle, and economical.

Transmission losses in POFs are due to both intrinsic and extrinsic loss factors which are caused by absorption, scattering, bending and so on. Intrinsic absorptions are mainly caused by electronic transitions between energy levels in the material molecular bonds particularly in the ultraviolet and blue wave-

length region; and the molecular vibrations of the groups C-H, N-H and O-H, predominantly in the red and infrared wavelength region. Rayleigh scattering is also another main cause of intrinsic loss which resulted principally due to fluctuation in composition, density and orientation in the fibre. Dopants introduced to increase the refractive index of the core of an optical fibre are an example that causes fluctuation in composition of a fibre. Intrinsic losses exhibit the ultimate transmission loss limit.

Transmission loss in POF at short wavelengths (ultraviolet and visible) region is mainly dominated by Rayleigh scattering and it is proportional to λ^{-4} while at longer wavelengths (near infrared) it is dominated by absorption due to carbon-hydrogen (C-H) bond vibration, where Rayleigh scattering is almost vanish [23]. However, C-H bonds are the fundamental of polymers thus overcoming absorption due to their presence in polymer material is difficult. Despite the challenge, some solutions have been proposed and implemented to overcome this problem. One solution proposed was to substitute the hydrogen atoms with heavier elements. By this way it was possible to push the bond vibration to longer wavelengths (7.7 μm – 10 μm [24]), and reduced the loss in the visible and near infrared region (see Figure 2.1). Two elements used to realise this were fluorine [25] and deuterium [26]. The theoretical minimum loss of a pure fluorinated optical fibre is 0.3 dB/km at 1300 nm [27], which is almost close to the one achieved for silica optical fibre. The theoretical transmission loss of optical fibres is basically given by the sum of intrinsic losses only but the actual transmission loss is always larger. This is due to the fact that there are also extrinsic losses factors which increase the total attenuation of the optical fibre.

Extrinsic losses mechanism in optical fibres are light absorption provoked by dust or organic pollutants, scattering of light from micro-fracture and bubbles, and radiation losses due to light out-coupling of the fibre due to micro and macro bending [28], [29]. Thus including extrinsic loss, the actual experimentally achieved transmission loss of currently commercially available fluorinated optical fibre (Cytop, commercial name) is around 15 dB/km at 1300 nm [30], which is two orders of magnitude higher than the theoretical one.

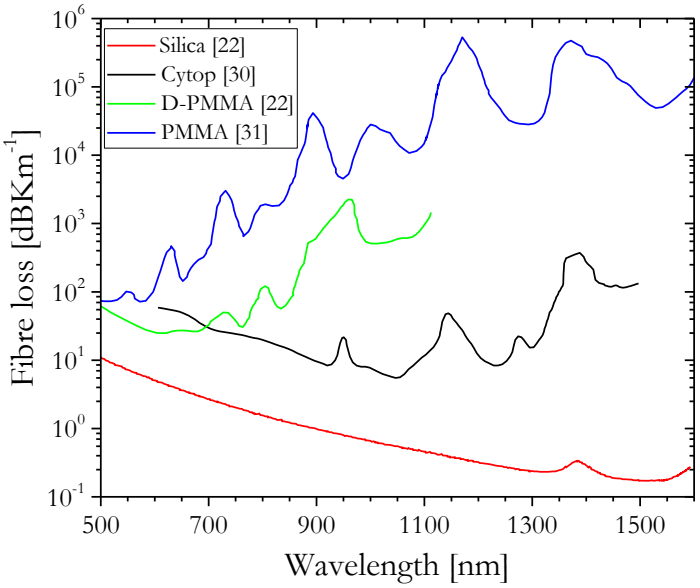

Figure 2.1 Transmission loss of standard silica optical fibre and various POFs.

The lowest loss measured for Cytop is around 5 dB/km at 1050 nm. This loss figure is promising and allowed increasing the usable wavelength range up to infrared. As a result it enabled to use low-cost components that are commercially available and were originally developed for silica fibre. In spite of this, the additional cost of deuteriation and fluorination is expensive and these materials were not able to be widely used for fabrication of POFs. Nowadays, the most commonly used material for the fabrication of POFs is PMMA. This is due to the fact that PMMA is widely available, low cost, and easy of processing and safe disposability although it has higher transmission loss [31] than the deuterated PMMA and Cytop POFs as shown in the Figure 2.1.

Optical fibre is fundamentally a length of cylindrical dielectric waveguide which consists of a central core region surrounded by an outer ring of material called cladding. In the solid core optical fibres the refractive index of the core (n_{co}) is greater than that of the cladding (n_{cl}) and light is guided by the phenomenon of total internal reflection. The two refractive indices define the numerical aperture (NA) of an optical fibre which defines the range of angles at

which light can be accepted into or emitted out of the waveguide and is calculated by [32]:

$$NA = \sqrt{n_{co}^2 - n_{cl}^2} \tag{1}$$

Depending on the number modes they support optical fibres can be either single mode or multimode whereas depending on the structure of the fibre they can be grouped as step index or microstructured. The normalised frequency (V) of a step index optical fibre defines the number of modes supported in the core of the fibre and is given by:

$$V = \frac{2\pi\rho}{\lambda_c} NA \tag{2}$$

where ρ is the core diameter of the fibre and λ_c is the cut off wavelength. For $V = 2.405$, the optical fibre is single mode (SM) for $\lambda > \lambda_c$, otherwise it is multimode.

2.1.1 Microstructured Polymer Optical Fibres

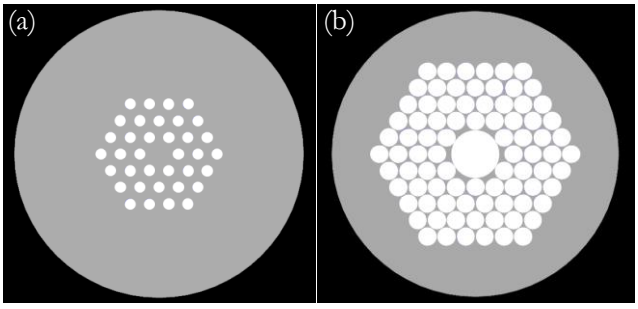

Figure 2.2 The illustration of (a) solid and (b) hollow core MOFs.

The first microstructured optical fibres (MOFs) have been first made of silica by Knight *et al.* in 1996 [33]. Based on the guiding principle, MOFs can be divided into two: solid and hollow core. The illustrations of both types of MOFs are shown in the Figure 2.2. In the case of solid core, the cladding section of the fibre is made of an array of holes running along the length of the fibre. The microstructured holes contain air which thus reduces the average

refractive index of the cladding compared to the solid core. Thus, like a step index fibre light is guided by total internal reflection. In the latter case, both the core and the cladding sections are made of microstructured holes and light is guided by a photonic bandgap effect [34].

One of the unique and potential advantage of MOFs is the capability of endlessly single mode (ESM) guidance, meaning being single mode for a wide range of wavelength, independent of the material they are fabricated from [35]. For MOF where the holes are arranged in a hexagonal lattice the necessary and sufficient condition for ESM guidance is [36]:

$$\frac{d}{\Lambda} < 0.42 \tag{3}$$

where d is holes diameter and Λ hole to hole distance or pitch. MOFs can be designed and fabricated either endlessly single mode or single mode for a certain wavelength region or multimode by engineering the holes and pitch size relative to wavelength of the light.

Figure 2.3 displays MOFs single mode multi-mode phase diagram depending on the hole to pitch ratio and the wavelength to pitch ratio [37].

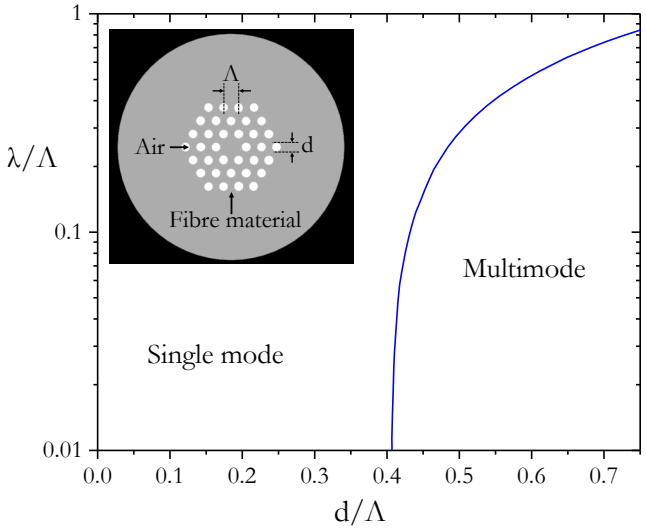

Figure 2.3 The single mode and multimode regime of a typical MOF where the holes are arranged in a hexagonal lattice.

Despite the first MOF is demonstrated with silica, they are also fabricated from polymers as well. The first mPOFs has been demonstrated in 2001 by van Eijkelenborg *et al.* [28]. The fibre was fabricated from PMMA and the holes were arranged in a uniform hexagonal structure, which are the most commonly used microstructure designs. However, there are also several different designs that have been realised for different purposes such as suspended core [38] , hollow core mPOF (HCmPOF) [39], rectangular core[40], graded index mPOF (GImPOF) [41], high birefringence fibres [42], dual cores [43] and multi core [44] as illustrated in the Figure 2.4.

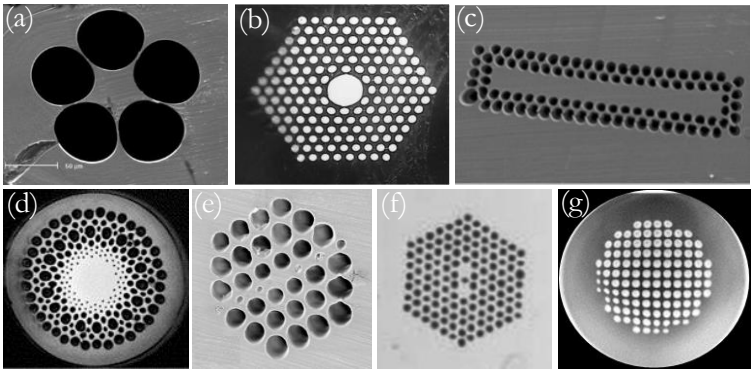

Figure 2.4 Various types of mPOFs.

One of the challenges in the production of step index polymer optical fibres (SIPOFs), particularly single mode POFs, is that it is very problematic to control the dopant diffusion and keep the refractive index uniform along the length of the fibre. In addition, when doped SIPOFs are exposed to high temperature and humidity the dopant properties are affected, this leads to changing the refractive index profile in the cross-section [45]. Thus when doped POFs are applied to grating based sensors the responses to measurands are not consistent [46]–[48]. Thus one of the significant advantages of mPOFs comes here where no dopant is required in the core to increase its refractive index as in the case of step index fibre to achieve light guidance. In addition, the fabrication of single mode mPOF is easy, flexible and cost effective compared to their step index counterpart.

Various types of polymer materials have been explored for the development of mPOFs in addition to PMMA material with the intention to exploit their unique intrinsic properties for grating based sensors, for instance cyclic olefin copolymers (COCs) (Topas, trade name). These groups of polymers have a very low moisture uptake, chemical inertness to acids and bases and many polar solvents [49]. The first Topas mPOF was fabricated from Topas grade 8007F-04 [50] which has a glass transition temperature (T_g) lower than PMMA but very low water absorption. Microstructured POFs has been also fabricated from another grade of Topas, grade 5013S-04 [51]. This grade of Topas had a glass transition of temperature (T_g) higher than PMMA and the same water absorption capability as the other grade of Topas. The main advantage of this Topas 5013S-04 is that it has very good thermal resistance which is suitable for FBG strain sensing at high temperature. However, this grade of Topas has a high flowability so that it is difficult to fabricate fibres compared to Topas 8007F-04. In addition to polymer Topas other types of polymers, namely polycarbonate (PC) and Zeonex, have been explored for the development of grating based sensors during the PhD study and are described in the next chapter.

2.2 Fabrication of POFs

As described in the previous section, in general, there are two types of POFs based on the structure owning: SIPOFs and mPOFs. The most common SIPOFs fabrication methods are continuous extrusion method and preform method. Continuous extrusion method was developed by Mitsubishi rayon [52], and it is one of the most efficient method for fabrication of SIPOFs. In this method, a purified monomer, a chain transfer agent and an initiator are fed into a polymerisation reactor, where polymerisation is takes place. When the chemical composition in the reactor reaches about 80% polymer and 20% monomer, it is fed into an extruder by a gear pump and this form the core material of the final SIPOF. A cladding material is then applied from a separate extruder and conveyed into a die or spinning block where core-cladding structure of the SIPOF is formed. The main characteristics of this manufacturing method are high production rate and excellent purity of the optical fibre.

However, the complexity to control polymerisation and extrusion process and the high investment costs are the limitations [53]. Unlike the continuous extrusion method, fabrication of SIPOFs by preform method involves two separate process stages. In the first stage, a cylindrical preform of 1-5 cm in diameter and up to one meter in length is made. The intended refractive index profile is achieved by introducing dopants in the core of the preform. In the second stage, the preform is drawn into a fibre by the heat and draw method using POF drawing tower [54]–[56]. The main advantages of this fabrication technique are its technical flexibility and low cost of production. However, is difficult to control dopant diffusion from core to cladding during the polymerisation of monomers in the preform making process. This challenge is particularly pose a problem in the production of single mode SIPOF as it is difficult to maintain the refractive index profile.

Unlike SIPOF, manufacturing of mPOFs do not require introducing dopant in the core to obtain a refractive index difference between the core and the cladding. These types of POFs are drawn from a single independent material. This is one of the most important fabrication advantages of mPOFs over SIPOFs particularly for single mode fibre production. The most common method to fabricate mPOFs is preform method where the microstructured preform is made first and the fibre is drawn from it [28]. There are different methods to fabricate microstructured preforms. Some of them are:

Capillary stacking: In this method several capillaries and a rod stacked together in the desired pattern to form the fibre preform [57]. The silica microstructured preforms are fabricated by this technique.

Extrusion: In this mechanism, the polymer is molten in an extruder and forced through a die. The pattern of the die determines the structure of the fibre preform [58].

Casting: In this approach, rods arranged in the desired holes pattern within a cylindrical casting form and liquid preform is filled into it directly produce microstructured preform [59]. This method can be either chemical (polymerisa-

tion) or mechanical (casting from polymeric pellets). Homogenous preforms can be also produced with this technique.

Drilling: In this method of microstructure preform production, first a solid homogenous fibre preform is made either by casting or extrusion method, which is the bigger version of the final fibre. Then the structure required in the final fibre is designed and the holes pattern is drilled into the preform using a computer numerically controlled (CNC) mill [60]. This method has been used extensively during the PhD study to produce microstrcutured preforms.

Currently the most common fabrication method of mPOFs comprises casting/extruding homogenous preform, drilling the hole patterns, and heat and draw techniques. The first mPOF was also fabricated using this combinations [28]. To easily control the fabrication process, in most case drawing of mPOFs consist of two steps. First the initial preform is drawn into a cane. Usually the sizes of the canes are 4-6 mm in diameter and 50 -70 cm in length. In the second stages, the cane is sleeved with a tube of the same material from where the preform is made to produce a secondary preform. The choice of the diameter of the secondary preform depends on the desired final fibre dimensions. The secondary preform is then drawn to a fibre by using POFs drawing tower (see Figure 2.5). It is also possible to draw the fibre directly from the preform. However, as the size of the preform is big compared to the final fibre, it is difficult to control the fibre parameters such as hole diameter and pitch size, which determine the final optical characteristic of the mPOF [23].

In the process of fabrication of POFs using a draw tower, the preform is first mounted on the preform feeder. Then it is feed into the furnace by lowering the feeder. Once the preform is in the furnace, it is heated above the glass transition temperature (T_g) of the polymer where it softens and the bottom part slowly drops out of the furnace by gravity when it has acquired the necessary viscosity. The drop out is then manually cut and the thin section of the preform is pulled by either a cane puller or fibre puller if the production is either a cane or a fibre, respectively.

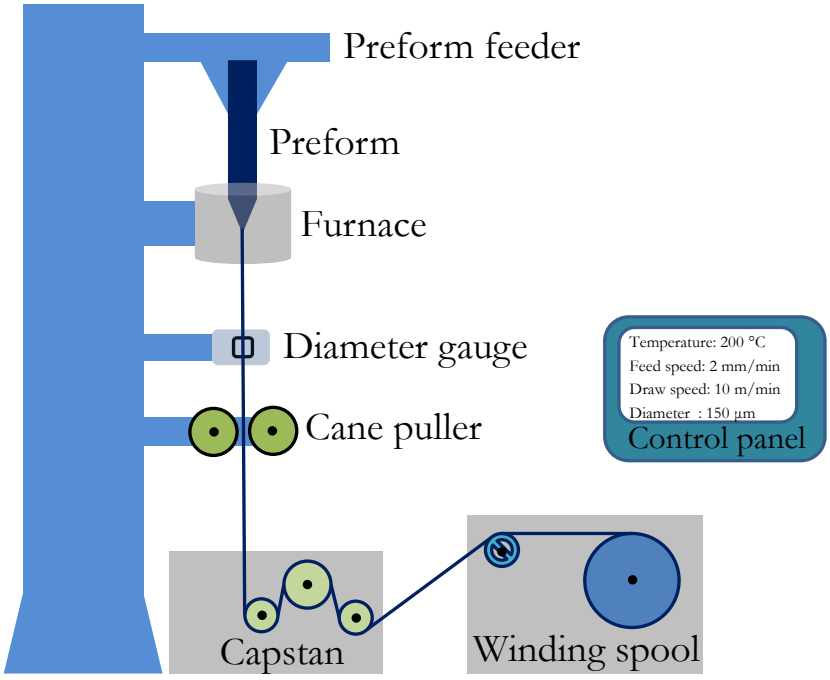

Figure 2.5 The schematic diagram of POFs draw tower.

The desired thickness of the cane or the fibre is achieved by controlling the temperature of the furnace, feeding speed and drawing speed. The draw rate along with the preform feed rate determines the diameter of the fibre. Under steady-state operating conditions, mass conservation gives the diameter of the fibre D_f :

$$D_f = D_p\sqrt{\frac{V_f}{V_d}} \tag{4}$$

where V_f is the feed speed of the preform, V_d is the drawing speed of the fibre and D_p is the diameter of the preform [23].

A typical polymer optical fibre draw tower has the following main parts: preform feeder, furnace, diameter gauge, cane puller, capstan, and winding spool which are controlled by electronic controller unit.

Preform feeder: The preform feeder is a translation stage which is driven by a motor which can be controlled manually or by electronic controller unit. A preform holder is attached to the preform feeder so as to hold the preform which has to be drawn to canes or optical fibres. The preform is lowered into the furnace by the preform feeder.

Furnace: The fibre preform is heated inside a furnace to draw canes or fibre. An ideal furnace should have very good temperature stability and temperature profile suitable for fibre drawing. The furnace can be either inductive or radiative. In inductive furnaces, usually a heating coil is wound over a ceramic tube which is heated by current passing through the coil. Radiative furnaces use lamps arranged symmetrically.

Diameter gauge: The diameter gauge, usually it is a laser micrometer, and used to continuously monitor the diameter of the cane or fibre during fabrication.

Cane puller: The cane puller is another important unit of the fibre draw tower. It has two rollers which are close to each other and use to pull a cane during cane drawing.

Capstan: The capstan is a three wheel system which pulls the fibre and also measures the tension in the fibre while fibre drawing.

Winding spool: After the fibre is collected by the pickup pulley it is spooled on the winding spool.

2.3 Fibre Bragg Gratings (FBGs)

FBG was first discovered by Hill *et al.* [10] in 1978 at the Canadian Communications Research Centre. Since then, the development of FBGs have been grown dramatically, due to their extensive application in the telecommunication industry and fibre optic sensors systems.

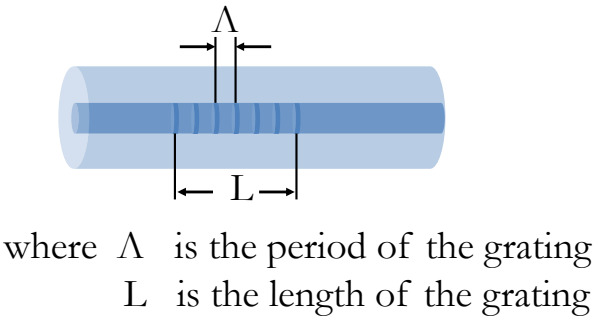

Figure 2.6 The schematics diagram of typical FBG.

FBG is fundamentally a longitudinal periodic variation of the refractive index of the core of a short segment of an optical fibre which is created by exposing an intensity pattern of ultraviolet (UV) light to a photosensitive optical fibre core. As depicted in the Figure 2.6 a typical FBG consists of periodic grating planes that are perpendicular to the fibre longitudinal axis.

The principle of operation of a FBG is essentially based on Bragg reflection [29]. When light is traveling from one medium to another medium that have different refractive indices, at the interface, both reflection and refraction of the light may occur. Similarly, when a broadband optical light source is directed into one end of an optical fibre with FBG in it, at each successive periodic grating planes a reflection of the propagating light will occurs. Depending on the period of the grating relative to the wavelength of the light, the relative phase of the reflected light waves from each grating planes are in phase at particular wavelengths and out of phase at other wavelengths. Those reflected light waves that are in phase are at wavelengths that satisfy the Bragg resonance condition. The centre of wavelength that satisfies the Bragg resonance condition is called the Bragg wavelength. Thus, reflected light from each periodic grating plane with wavelength matching the Bragg wavelength, added constructively and one large reflection signal at Bragg wavelength observed. The input light at wavelength different from the Bragg wavelength transmitted through the grating.

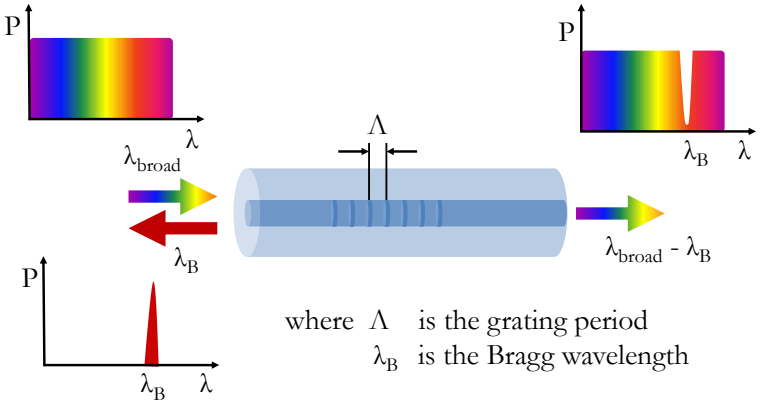

Figure 2.7 The fundamental principle operation of FBG.

From Figure 2.7 it can be seen that an FBG has only one strong resonance which occurs at the Bragg wavelength and this resonance is observed both in the reflection and transmission spectrum as peak and dip, respectively. The Bragg wavelength λ_B is determined from the period of the grating Λ and the effective refractive index of the fibre core n_{eff} by the relationship:

$$\lambda_B = 2\Lambda n_{eff} \tag{5}$$

2.4 Polymer Optical Fibre Bragg Gratings (POFBGs)

The first grating inscribed in POF was reported in 1999 by Xiong *et al.* [61]. The fibre was single mode step index fabricated from PMMA. Nevertheless, the photosensitivity of PMMA polymer was first reported by Tomlinson *et al.* in 1970 [62] where they claimed an index changes of up to 3×10^{-3} and a density increase of 0.8% at 325 nm UV radiation. They speculated that, the main factor for the refractive index change was that of density increase which was assumed due to photo-crosslinking. Since after, different photosensitivity mechanisms of polymer, such as photo-polymerisation, chain scission, and the induction of cross-links between polymer chains, have been suggested [63]. However, the widely accepted photosensitivity mechanism is photo-polymerisation which is polymerisation of the unreacted monomers. It is also

contemplated that, the photosensitivity of POFs to UV exposure could be depending on both the fabrication process of the fibre and the grating inscription process [12].

FBGs have been inscribed in POFs with different techniques namely interferometric method, phase mask method and point by point methods. Various types of lasers have been used for inscription such as He-Cd laser, excimer laser and femtosecond (fs) lasers and gratings have been also inscribed at various wavelengths. Although the first grating fabricated in POFs was inscribed by a modified interferometric method, this technique is not widely used [61]. This is because it requires highly coherent UV laser beam source and this coherence must be maintained throughout the exposure otherwise a shift in the interference fringes may occur and leading to erosion of the grating. In addition, the alignment is time consuming and the mechanical stability is poor. However, it gives flexibility to control the period of the gratings over the other methods.

Phase mask method is the most widely used technique to inscribe grating in POFs as it allows the use of low cost UV light source by lowering the requirement of coherent UV light unlike interferometric technique. It also permits an easier arrangement of the fibre to be grated and also the stability requirements on the grating apparatus are reduced. This configuration set up is mechanically stable and reliable, and the FBGs are relatively easy to inscribe. Therefore, this method produces the most consistent and reproducible inscriptions, and hence the most commonly used techniques of FBG writing in POFs. Grating in POF with phase mask technique was first demonstrated by Yu *et al* in 2004 [64]. Figure 2.8 illustrated a complete schematic of POFBG inscription setup using the phase mask approach. The main drawback of the phase mask technique is that, to fabricate gratings with different grating pitches a separate phase masks are required. However, this problem can be solved to some extent by tuning the Bragg wavelength of the grating inscribed using a single phase mask. The Bragg wavelength can be tuned either by applying axial pre straining before inscription or post inscription annealing [65], [66].

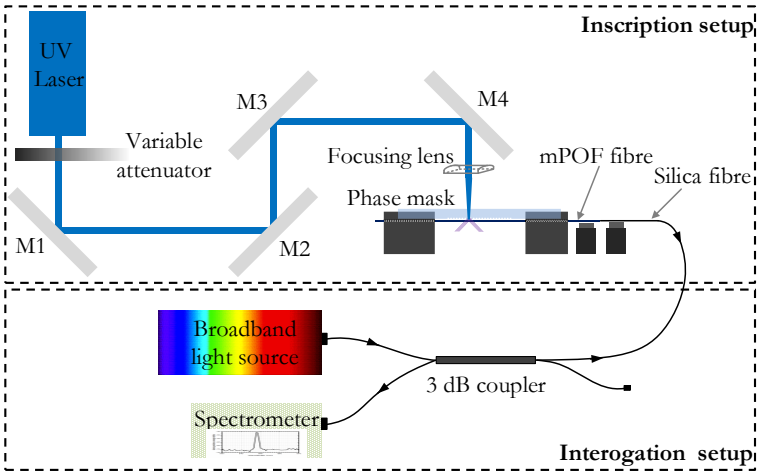

Figure 2.8 The most commonly used POFs grating inscription setup using the phase mask technique and the corresponding interrogation setup.

A typical interrogation system to monitor the grating in the reflection while inscription, is also shown as a part of Figure 2.8 which mainly consists of a broad band light source, a 3 dB optical coupler and a spectrometer. A broadband light source or a supercontinuum white light source is used to interrogate the light into the core of the POF via 3dB coupler. A silica fibre is used to butt couple the light into the POF. Index matching oil is usually used in the gap between the silica fibre and the interrogated POF to reduce the reflection noise. The light reflected from the POFBG is coupled back through the coupler and finally to spectrometer. Majority of FBGs inscribed in POFs used the phase mask writing techniques depicted in Figure 2.8.

In contrast to interferometric and phase mask methods, which write the whole grating at once, using point-by-point (direct writing) approach each grating plane in the POF core is photo-inscribed point by point [67], [68]. In such technique, the POF is first placed on a mechanical stage which enables the fibre to be translated along its length during the inscription process. Then a pulse or excimer laser is focused in the core of the fibre to photoimprint one grate at a time. The stage is then translated, hence the fibre, by a length which is the intended period of the grating to write the next grating plane. By

repeating the irradiation of the laser beam and the translation of the stage, a periodic grating is fabricated in the POF core. The significant advantage of point-by-point grating technique is that, it provides the choice of the length and pitch of the grating to be determined independently, which enables the grating spectral response to be controlled precisely and also avoids the high expense of phase masks. Direct writing also allows grating inscription in POFs made of non-photosensitive materials [69]–[71]. The potential limitations of this method is that, the alignment of the fibre core with the pulsed laser beam, and also the discontinuous irradiation and translation process, make the production time much longer than that of the previously described techniques which required only a single exposure. The point by point method of inscription was first demonstrated in POFs using 800 nm fs laser by Stecher *et al.* in 2009 [72].

Unlike in SIPOFs, grating inscription in mPOFs is not straight forward. The microstructured air holes along the length of the fibre significantly affect the writing process. Hence, the fibre should be aligned in such a way that the laser reaches the core easily, so that the inscription time is short and the grating strength is comparable with that of SIPOFs. One of the most common challenges occurring when gratings are inscribed in mPOFs is the scattering of the laser beam from the microstructured air holes and hence hindering the laser beam from reaching the core the fibre efficiently. This resulted in longer inscription time and poor quality gratings. Thus, in order to achieve rapid and high quality grating in the mPOFs, the orientation of the fibre should be in such a way that the coupling of the laser beam to the core of the fibre is the strongest. And this occur only for certain angles close to X but not exactly X (see Figure 2.9), the angular direction that offers direct access for the laser beam to the core of the mPOF from the side [73], [74]. Gratings could be obtained at almost any angle but their quality would be lower if the orientation is not in the desire range, for instance if it is at X' or/and in the vicinity of X' [75].

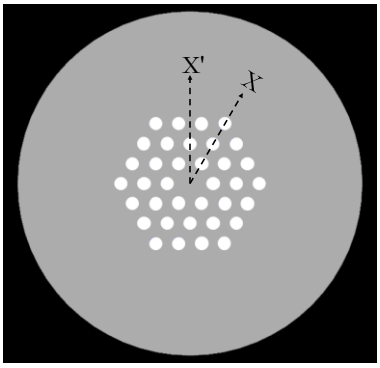

Figure 2.9 The schematic diagram of a 3-ring hexagonally arranged holes mPOF with marked symmetry directions for FBG inscription.

The first FBG in mPOFs was inscribed by Dobb *et al.* in 2007 in the 1550 nm wavelength region [13]. The fibres used were endlessly single mode and few modes PMMA mPOFs. The technique used for inscription was the phase mask method and the gratings were inscribed by using a 325 nm He-Cd continuous wave UV laser with a power of 30 mW. The FBGs were saturated almost an hour after the exposure was started. Long grating inscription time, usually ranging from several tens of minutes to hours [47], [76]–[78], has been remained one of the most common challenge of grating inscription in POFs for several years. However, in 2014 Bundalo *et al.* reported FBG inscription in PMMA mPOFs with writing time less than 7 minutes, which was 5-10 times shorter than were previously reported[79]. The setup used by Bundalo *et al.* was also a standard phase mask writing technique. It was demonstrated that there was a strong correlation between laser power and the grating inscription time, claiming that high intensity of laser power in the core is required in order to achieve a fast writing time. A year later Oliveira *et al.* reported inscription of FBG in a PMMA mPOF in less than 30 seconds using the phase mask method [80] but the inscription laser used was KrF excimer laser (Bragg Star *TM* Industrial-LN). They claimed that the key factors leading to reducing the writing time were the use of low number of pulses, low repetition rate and low fluence, and energy density below the threshold for the PMMA ablation. This inscription time is the record of writing time in POFs till now with a UV

laser. However, the fastest writing time recorded in POFs to date was in 2.5 sec with direct writing technique with fs laser [69]. One of the advantages of having a fast inscription time is avoiding the constraints related with the stability of the mechanical setup during the inscription process.

Bragg gratings in PMMA mPOFs have been fabricated at different wavelengths, 632 nm [79], 827 nm [81], 850 nm [76], and 980 nm [82] using phase mask writing method and 325 nm He-Cd UV laser using different phase masks. Multiple gratings have also been inscribed in PMMA mPOFs using a single phase mask but with several diffraction orders [83].

PMMA microstructured polymer optical fibre Bragg gratings (mPOFBGs) discussed above were inscribed in an undoped fibres. In 2013, Sáez *et al.* doped a core of PMMA mPOF with BDK to increase the photosensitivity of the fibre and obtained a shorter writing time and a higher index change compared to undoped PMMA mPOFs [84]. A He-Cd UV laser and a standard phase mask inscription technique were used. They reported that a grating with 23 dB strength in transmission with a 10 dB bandwidth of 0.3 nm was obtained in 13 minutes. Hu *et al.* also inscribed FBGs in BDK doped PMMA mPOF [85]. Unlike the He-Cd laser used by Sáez, Hu used 400 nm fs laser pulses and it is claimed that a grating with 40% reflectivity in 20 seconds was achieved. Although the writing time can be reduced by doping, it increases the transmission loss of the fibre and doped fibre less suitable for in-vivo biosensing.

In addition to PMMA mPOFs, FBGs have been also inscribed in mPOFs made of different materials for instance in Topas. Johnson *et al.* reported the first Topas mPOFBG fabricated from Topas grade 8007F-04 [50]. The grating was inscribed with a standard phase mask method and 30 mW 325 nm He-Cd UV laser. The grating had a Bragg wavelength of 1567.9 nm and it took around 45 minutes for the grating to reach a saturation level. Yuan *et al.* demonstrated also the inscription of an FBG in the same grade of Topas but in 850 nm spectral region, using a phase mask of a uniform period of 572.4 nm [78]. The main advantage of inscribing FBGs in the 850 nm region is that, the

loss of the fibre in this wavelength region is very low compared to 1550 nm region which enables to use longer fibres. Markos *et al.* reported the fabrication of FBGs in another grade of Topas, grade 5013S-04 in 850 nm regions [51]. The grating was fabricated with the same method and phase mask as used by Yuan *et al.* [78]. During the PhD study, FBGs have been inscribed in mPOFs that have been fabricated from two different polymers, PC and Zeonex, for the first time and it is described in the next chapter.

2.5 Fibre Optics Sensors

One class of sensors technologies that brings a tremendous applications ranging from civil, aerospace and medical industries, to distributed sensors in gas and oil industry are the fibre optic sensors. Development of fibre optic sensors in many application areas attracted due to their superior advantages over the conventional electro-mechanical sensors. Fibre optic sensors are immune from electromagnetic interference and high voltages, have high sensitivity, light weight, small size, wide operating range, higher resolution and accuracy, low power consumption, robust and environmental ruggedness, multiplexing and distributed capabilities to form sensor networks and so on [86]–[88].

Fibre optic sensor system is fundamentally composed of an optical light source, a sensing element or transducer, an optical detector and optical fibre as depicted in the Figure 2.10. The general principle of operation of such sensor systems is that, the light sent from the optical source through the optical fibre experiences a change in either of its optical properties as it passes through the sensing element, and when the sensing element is perturbed by external environmental measurand. The optical signal which is modulated in the sensing medium in response to the external perturbations is then passes through an optical fibre to an optical detector to measure the sensing signal. Therefore, fibre optic sensor can measure any environment measurand which can change the characteristics of the light (intensity, wavelength, phase and polarisation) that propagates through it.

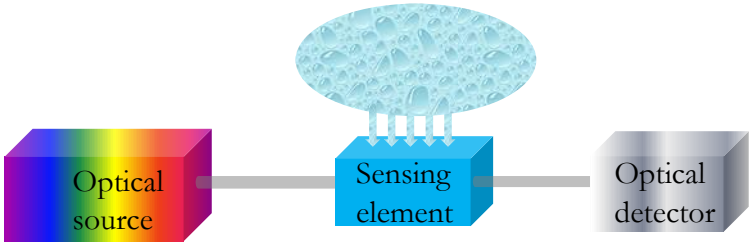

Figure 2.10 The schematic diagram of the basics of fibre optic sensor system.

Depending on the sensing medium implemented in the fibre optic sensing system, they are basically classified into two groups: extrinsic and intrinsic fibre optic sensors. In the former case, the actual sensing element or transducer is not an optical fibre, rather an external optical device, hence sensing does not take place in the region inside the optical fibre. However, optical fibre is used to carry a light signal to and from the transducer. One of the limitations of these types of sensors is a loss in optical power as the light is entering and out of the sensing element. Although these sensors are simple and suitable for applications that require low cost and low resolution, they are not in general keen to high quality measurements.

In contrast to extrinsic sensors, in the case of intrinsic sensors the actual sensing takes place in the optical fibre itself. Thus, it is the optical fibre that acts as a sensing element. The basic principle of operation of intrinsic fibre optic sensors lies in the response of the optical fibre either geometrically (e.g. size and shape) and /or optically (e.g. refractive index) to the external perturbation on the fibre. The geometrical and optical changes in the fibre cause a change in any one of the characteristics of the light as it passes through it [89]. As light propagate from the optical source to detector it is confined in the fibre so no power loss occurs as it entering and leaving the sensing element unlike extrinsic sensors. This feature of intrinsic sensors offers a key benefit in distributed and remote sensing applications.

An example of simple, most common and relatively mature type of intrinsic type of optical fibre sensor is FBG sensor. FBG is used as sensing element in

this project. Thus a review and a brief discussion on the fundamental motivation, principles and distinguished advantages of FBG based optical sensors over other types intrinsic fibre optic sensors will be given in the next section.

2.6 Fibre Bragg Grating Sensors

An FBG sensor is an intrinsic fibre optic sensor that uses FBG as a sensing element. When an FBG is perturbed by an environmental measurands the reflected optical signal from the grating will show an induced shit in the Bragg wavelength in response to the effect of measurands. It is this special characteristic of FBG that predominately inspire its use as sensor.

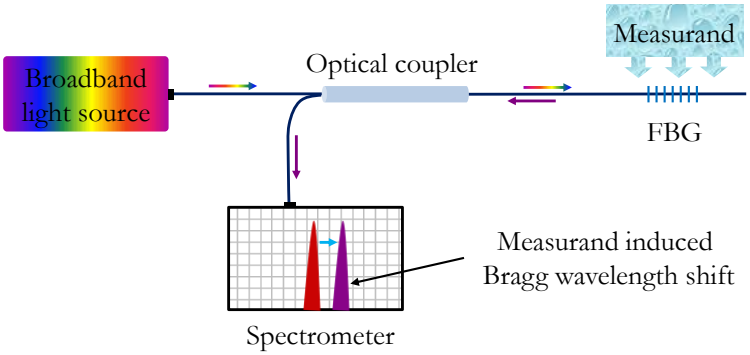

Figure 2.11 The schematic diagram of basic FBG optical sensing system.

As shown in the Figure 2.11, a typical FBG sensor system consists of a broadband light source, an optical coupler, FBG as a sensing element, and a wavelength monitoring device. In these kinds of sensor systems, the light directed from a spectrally broadband source propagates through the optical coupler to the grating. As the broadband light reaches the grating a narrow spectral band of the incident light is reflected from the FBG. When the grating is perturbed by the environmental measurand, it reacts by changing its physical and optical properties and the wavelength of the reflected optical signal will shift accordingly. The amount of shift depends on the magnitude of the measurand. Then, the reflected light from the FBG propagate back through the optical coupler to the wavelength monitoring device. Using the wavelength monitoring

device the shift in the wavelength induced by the measurand is measured and subsequently the value of the measurand is determined.

Although FBG optical sensors share all the advantages attributed to fibre optics sensors, they have several distinctive advantages. As the influence of external environmental parameters is encoded directly in the induced wavelength shift of the light propagating in the optical fibre, which is an absolute parameter, FBG sensors are immune to fluctuations in the power of the light. That is, the sensed information does not depend directly on the total light levels, losses in the source power, couplers, connectors and the fibres itself. In addition, multiple grating can be inscribed in a single optical fibre and number of parameters can be measured using wavelength multiplexing techniques. This feature of FBG sensors is suitable for quasi-distributed measurements. Moreover, as the grating is imprinted directly into the optical fibre, FBG sensors are relatively very small in dimension compared to other types of intrinsic fibre optic sensors. As a result, they are compatible and suitable to be embedded in wide range of devices which are very small in size with increased system portability and stability. Furthermore, because FBGs are simple to manufacture in large volume at reasonable cost, FGB sensors can be competitive with other types of fibre optic and electro-mechanical sensors. Last but not least, as the response of FBGs to most of measurands such as temperature and strain is linear and additive, FBG optical sensors do not require on-site calibration [90].

FBG sensors have been developed from both silica and polymer optical fibres. However, FBGs sensors made from POFs have distinct advantages over their silica counterpart due to their unique material properties. In the next section, a comparison between these two materials and FBG sensors developed from these materials is described. The superior advantages of POFs over that of silica optical fibres which is the motivation behind of this PhD project will be discussed in detail from the materials properties point of view.

2.7 Polymer Optical Fibre Bragg Grating Sensors

Despite POFs shares many of the merits of silica optical fibres have for sensing applications, they have unique features that silica fibres do not have for many sensing applications, albeit with higher transmission losses. POFs have the ability to survive higher strain levels i.e. high elastic strain limits. For instance, the elastic limit of PMMA can be up to 10% while that of silica is around 1-3 % [91], [92]. POFs have also a Young's modulus much smaller than silica. For example, the most commonly used polymer material for POFs production PMMA has a Young's modulus of 1.6-3.4 GPa while silica has 72-73 GPa [63], [92], [93]. POFs have also non-brittle nature and flexibility in bending [63], [94]. These unique features of POFs provide them immense potential in the development of FBGs based high strain and acceleration sensing applications [11], [12], [14]. The Bragg wavelength shift obtained by applying tensile strain to POFBGs is an order of magnitude larger than silica optical fibres gratings, and this is the result of the large yield strain and the increased stress sensitivity of POFs. The other important advantage of POFs is their excellent compatibility with organic materials, making them ideal candidates for biomedical sensors applications [15]–[19]. In addition, POFs have very low processing temperature and are easy to handle, hence low processing cost and safe disposability. Moreover, polymers have density lower than silica, for instance the density of silica is almost twice as much that of PMMA, which is quite important as it minimise the weight of the optical fibre hence the final sensor [23], [95].

In the development POFBGs sensors for a specific parameter measurement, for instance relative humidity, some polymers such as PMMA showed a distinct advantage over silica fibres. To develop a humidity sensor based on silica based fibre, the fibre needs to be coated first with hygroscopic material as the silica do not absorb water intrinsically [96]–[98]. This increases the sensor production cost. However, polymers like PMMA naturally have moisture absorbing capability and it does not require coating to developed PMMA POFBGs humidity sensors [99]–[101]. This is one of the key characteristics of PMMA based POFs for FBG based humidity sensor development. PMMA

based POFBGs showed a humidity sensitive 125 times larger than polyamide uncoated silica FBGs [102]. Other polymer materials such Topas has also been explored for POFBG sensors fabrication [50], [51], [78]. This polymer has very low water absorption and hence ideal for FBG based temperature and strain sensors development as it avoids humidity cross sensitivity.

2.7.1 Sensing Characteristics

2.7.1.1 Strain Sensing

Mechanical strain in a material is simply a change in the physical length when stressed. Mathematically, in the linear elastic region, one dimensional strain is defined as the ratio of a change in the physical length of the material when stressed to the original length of the material.

$$Strain \quad \varepsilon = \frac{\Delta L}{L} = \frac{L' - L}{L} \tag{6}$$

where L is the original length of the material and L' is the length after the material is stretched or compressed due to the external applied force.

When a section of a fibre containing a grating is subjected to axial strain, the load is directly transferred to the core of the fibre and the length of the grating experience a physical elongation. Subsequently, the period of the grating undergoes a fractional change. Due to photo-elastic effect in the optical fibre, the refractive index of the core also varies accordingly. According to equation 5, the Bragg wavelength is a function of the period and effective refractive index of the grating. Thus, the effect of the strain which changes the physical and optical properties of the grating can be monitored by measuring the shift in the Bragg wavelength.

For a FBG with a length L, a grating period Λ and effective refractive index n_{eff}, the fractional Bragg wavelength shift , $\Delta\lambda_B$, for strain variation $\frac{\Delta L}{L}$ is given by:

$$\Delta\lambda_B = 2(\Lambda\frac{\partial n_{eff}}{\partial \Delta L} + n_{eff}\frac{\partial \Lambda}{\partial \Delta L})\Delta L \tag{7}$$

Equation (7) can also be expressed as:

$$\Delta\lambda_B = \lambda_B(1 - P_e)\varepsilon \tag{8}$$

where ε is the axial strain and P_e is strain-optic (photo elastic) constant defined by:

$$P_e = \frac{n_{eff}^2}{2}(P_{12} - \nu(P_{11} + P_{12}))$$

P_{11} and P_{12} are strain optic coefficients and ν is the Poisson's ratio of the POF.

2.7.1.2 Temperature Sensing

When FBG is subjected to a temperature change, the grating will undergo thermal expansion or contraction and the grating period does so. The refractive index of the core also varies due to photo-thermal effect in the optical fibre. Therefore, the effect of the external temperature perturbation which changes the physical and optical properties of the grating can be monitored by measuring the corresponding Bragg wavelength shift $\Delta\lambda_B$. For a FBG with a grating period Λ and effective refractive index n_{eff}, the fractional Bragg wavelength shift $\Delta\lambda_B$ for a temperature change ΔT is given by:

$$\Delta\lambda_B = \lambda_B(\frac{1}{\Lambda}\frac{\partial \Lambda}{\partial T} + \frac{1}{n_{eff}}\frac{\partial n_{eff}}{\partial T})\Delta T \tag{9}$$

Equation (9) can also be expressed as:

$$\Delta\lambda_B = \lambda_B(\alpha + \xi)\Delta T \tag{10}$$

where λ_B is the initial Bragg wavelength, α is the thermal expansion and ξ thermo-optic coefficient of the POF.

2.7.1.3 Humidity Sensing

When moisture is absorbed by POFs, the fibre swell and consequently the grating pitch undergoes a fractional change. Due to photo-hygroscopic effect in the optical fibre, the refractive index of the core also varies accordingly. For a FBG with a grating period Λ and effective refractive index n_{eff}, the fractional Bragg wavelength shift $\Delta\lambda_B$ for a relative humidity (RH) change ΔH is given by:

$$\Delta\lambda_B = \lambda_B\left(\frac{1}{\Lambda}\frac{\partial\Lambda}{\partial H} + \frac{1}{n_{eff}}\frac{\partial n_{eff}}{\partial H}\right)\Delta H \tag{11}$$

Equation (11) can also be expressed as:

$$\Delta\lambda_B = \lambda_B(\beta + \eta)\Delta H \tag{12}$$

where λ_B is the initial Bragg wavelength, β is the swelling coefficient of the POF related to RH induced volumetric change, η is the normalised refractive index change with RH and ΔH is the RH change (%).

Chapter 3 - Thesis Contributions

This chapter reports the main achievements of the researches during the PhD project. It summarises the whole processes towards the development of high performance POFBGs sensors which involved annealing, fibres fabrication, characterisations and connectorisations, and grating inscriptions and characterisations. The report is based on the attached published journal papers and some unpublished but relevant results during the research period.

3.1 Fibres Fabrication

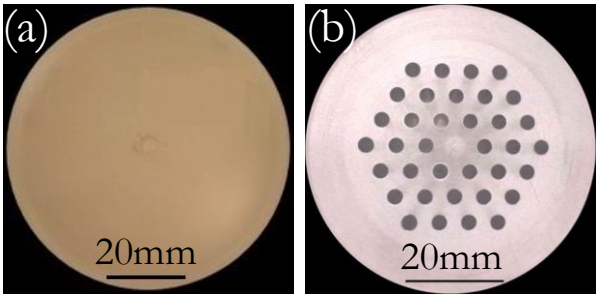

Figure 3.1 The facet of typical (a) step index (b) microstructured polymer optical preforms prepared for fibres fabrication.

During the project period several POFs have been fabricated from different polymer materials namely: PMMA, PC, Topas 5013S-04 and Zeonex 480R. Both step index and microstrctured fibre types have been considered. PMMA and Topas based fibres were used for the development of POFBGs sensors prior to this PhD project [50], [51], [61], [101], [103]. However, PC and Zeonex 480R are the two new polymers that have been introduced to the table during the PhD for the fabrication of POFs for FBGs based sensing applications considering their unique features. Hereinafter, Topas and Zeonex refer to Topas grade 5013S-04 and Zeonex grade 480R, respectively, unless stated otherwise.

The homogenous fibre preforms for all polymers except PMMA have been cast at DTU Mechanic whereas for PMMA a commercial rod from Nordisk Plast A/S [104] was used, which was extruded. The microstructured preforms were prepared at mechanical workshop by drilling method. First the polymer rods were machined to have a dimension of 60 mm in diameter and 100 mm in length. Then in a three rings hexagonal pattern holes were drilled with hole and pitch size of 3 mm and 5 mm, respectively. For the step index preform preparation only a single hole was drilled at the centre of the host preform and a guest polymer was injected in the drilled hole. The production of a step index preform is reported in detail in paper 5. Figure 3.1 displays a facet of a typical step index and microstructured fibre preforms prepared for SIPOFs and mPOFs fabrications, respectively.

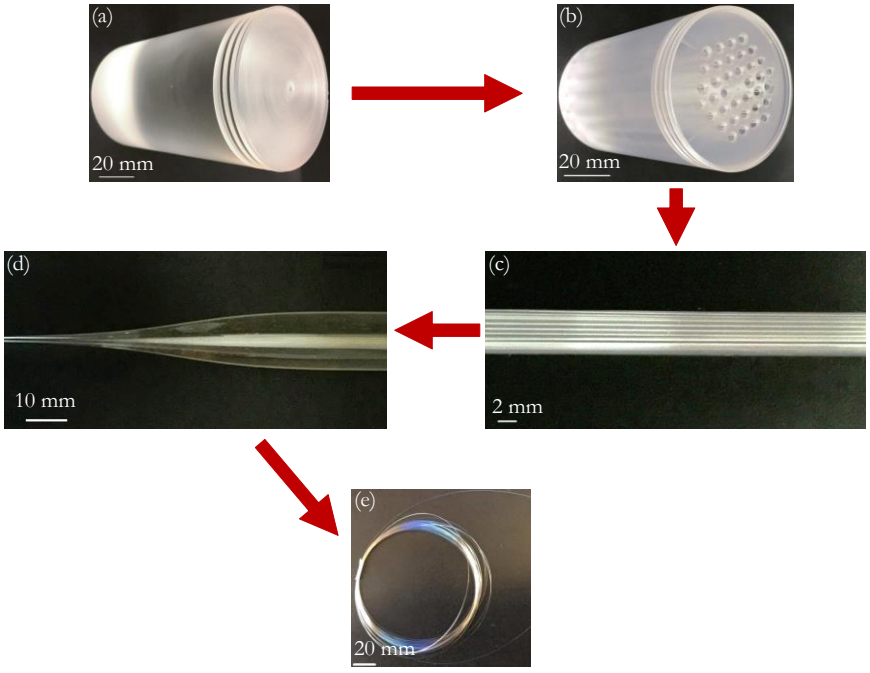

Figure 3.2 POFs drawing process (a) homogenous preform (b) microstructured preform (c) microstructured cane (d) secondary preform: a cane sleeved with a tube (e) the final fibre.

A two steps heat and draw technique were used to fabricate the fibres. For all cases, first a cane was drawn from the preform and then the cane was sleeved with a sleeving tube of the same material the preform was made. The secondary preform was then drawn to a fibre as it is described in section 2.2. Figure 3.2 illustrated the implemented process for the fibres fabrication.

Both the canes and the fibres produced during the project were fabricated at DTU Fotonik with POFs drawing tower (see Figure 3.3). The optimum fibre drawing temperature and the corresponding drawing stress implemented to fabricate PMMA, PC and Zeonex mPOFs and Topas-Zeonex SIPOF are summarised in Table 3.1. Topas-Zeonex SIPOF is a step index POF with Topas core and Zeonex cladding.

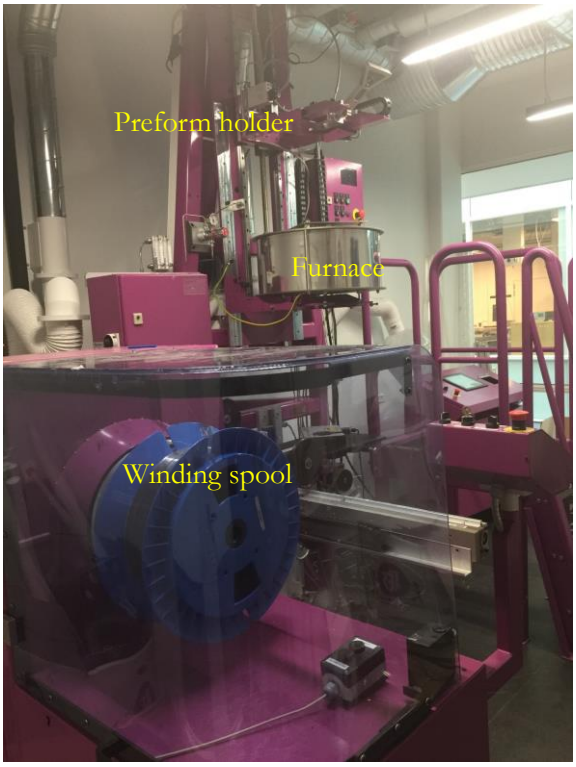

Figure 3.3 DTU Fotonik POFs drawing tower.

Table 3.1 Drawing temperature and stress applied for the fabricated fibres.

Fibres	Average drawing temperature (°C)	Average drawing stress (MPa)
PMMA mPOF	~178	~9.8
PC mPOF	~185	~11
Zeonex mPOF	~180	~10
Topas-Zeonex SIPOF	~180	~8

There was an important additional and integral step in POFs drawing processes, which was annealing. For each polymer types, both the primarily and the secondary preforms, before drawing the canes and the fibres, respectively, were annealed in a conventional oven. This step was particularly essential when the preform was made from moisture absorbing polymers such as PMMA and PC. In such a case, if the preform was not annealed and stored in an oven at their annealing temperature before drawing, bubbles appear during drawing as shown in the Figure 3.4 and thus increasing the final fibre losses significantly. Sometimes the preforms even were not drawable at all. But this problem has not been seen for the polymer Topas and Zeonex as they have a very small affinity to water. The water absorption a capability at room temperature and T_g of PMMA [105], PC [106], Topas [107] and Zeonex [108] polymers and the corresponding applied annealing temperature and time are listed in Table 3.2.

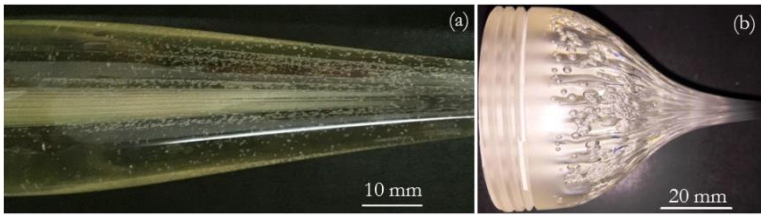

Figure 3.4 Bubbles arose in (a) PMMA secondary preform (b) PC primary preform when drawn before they were annealed.

Table 3.2 Glass transition temperature and water absorption capability of the polymers and the corresponding adapted preforms annealing temperature and time.

Polymer materials	**T_g (°C)**	**Water absorption (saturation value) at 23 °C**	**Preform annealing temperature (°C)**	**Annealing time (hour)**
PMMA	106	2.1 %	80	48
PC	145	0.3 %	125	48
Zeonex	134	< 0.01 %	120	48
Topas	138	< 0.01 %	115	48

3.2 Fibres Characterisation

Once the fibres are fabricated they were cleaved with homemade POFs cleaver [109] and inspected with optical microscope (Axioskop 40, Zeiss). Table 3.3 summarises the applied cleaving temperature to cleave the fibres and also the dimensions of the fibres measured afterward with the optical microscope.

Table 3.3 The fibres cleaving temperature and specifications as measured with the optical microscope.

Fibres	**Blade and fibre temperature (° C)**	**Fibre core (µm)**	**Fibre diameter (µm)**	**Hole to pitch ratio**
PMMA mPOF	73	~8.5	~150	~0.4
PC mPOF	80	~10	~125	~0.4
Zeonex mPOF	76	~8.8	~150	~0.4
Topas-Zeonex SIPOF	76	~4.8	~150	V=2.38 @850 nm

The hole to pitch ratio of the fabricated mPOFs was 0.4 which means that the fibres are endlessly single mode (ESM) [35]–[37]. The fibres facet images taken with the optical microscope are shown in Figure 3.5.

The transmission losses of the fibres were then measured with a cut back method. Several cuts have been made during the measurements in order to minimise any uncertainties arising from power fluctuations, cleave quality, coupling instabilities and so on. Detailed information about loss measurement is reported in Paper 3, 5 and 6. The measured transmission losses for the fibres are plotted in the Figure 3.6.

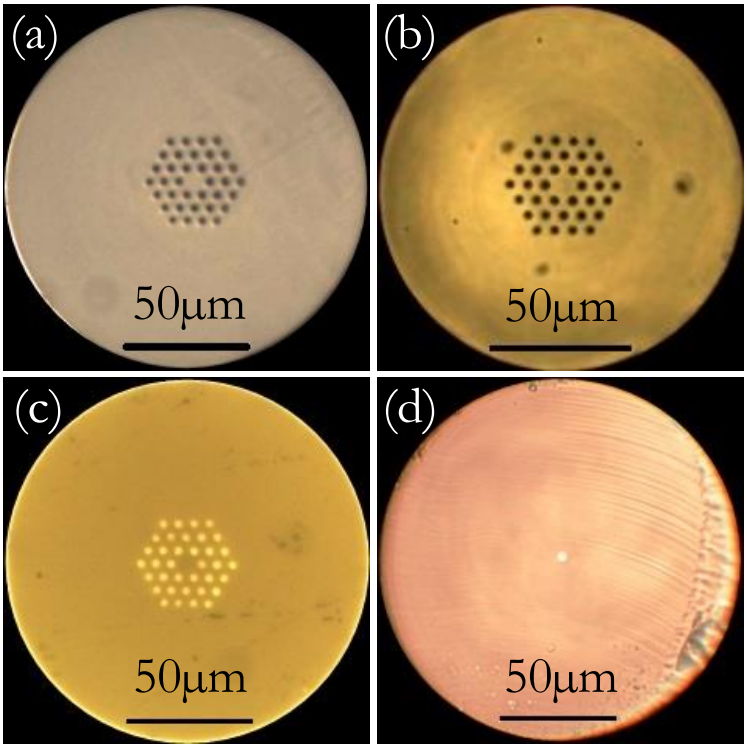

Figure 3.5 Optical microscope facet image of (a) PMMA ESM mPOF (b)PC ESM mPOF (Paper 4) (c) Zeonex ESM mPOF (Paper 6) (d) Topas-Zeonex single mode SIPOF (Paper 5).

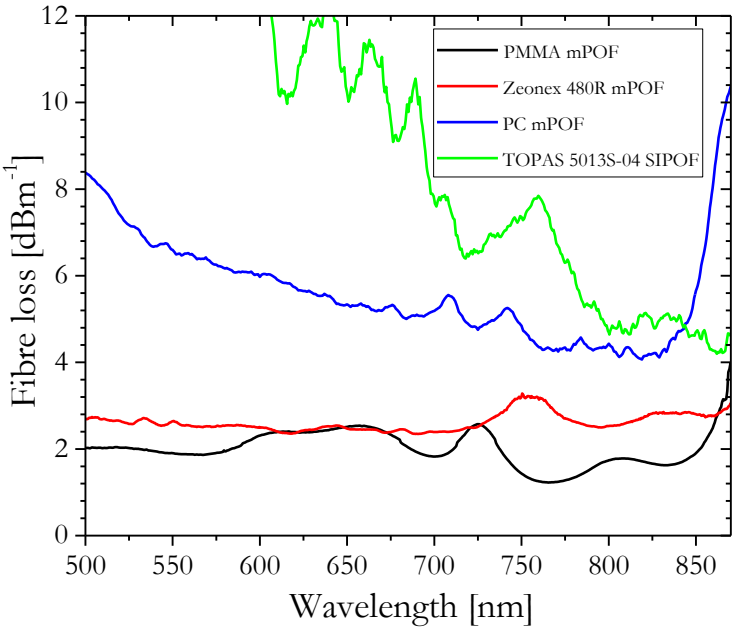

Figure 3.6 The measured transmission loss of PMMA ESM mPOF (black), Zeonex ESM mPOFs (red) (Paper 6), PC ESM mPOFs (blue) (Paper 4) and Topas-Zeonex single mode SIPOF (green) (Paper 5).

3.3 Grating Fabrication

FBGs have been inscribed in the fabricated fibres in order to investigate their potential for sensing applications. The gratings were fabricated with a phase mask technique. The phase mask (Ibsen Photonics) used has a 572.4 nm uniform period and the inscription laser was a 325 nm 50 mW He-Cd UV laser (IK5751I-G, Kimmon). The implemented inscription setup is depicted in Figure 3.7. The interrogation setup composed of supercontinuum source (SuperK Extreme, NKT Photonics), wide band 50:50 split fibre optic coupler (TW805R5A2, Thorlabs) operating in the 850 nm region and CCD spectrometer (CCS175 - Compact Spectrometer, Thorlabs). Once the grating has been inscribed and saturated the reflection spectrum was measured and recorded with optical spectrum analyser (Ando AQ6315A, Yokogawa Electric Corporation).

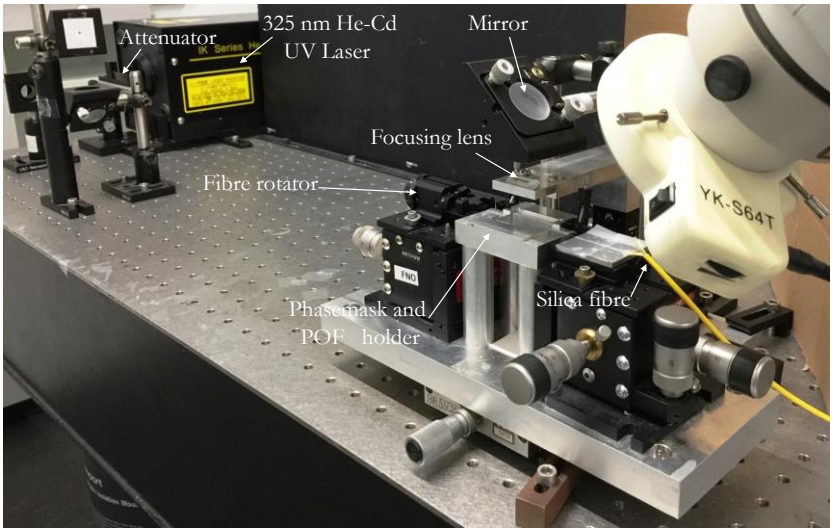

Figure 3.7 DTU Fotonik FBG inscription setup.

One of the most important experimental observations during the grating inscriptions was, the amount of laser power required to write grating in POFs fabricated of different polymer was different. Therefore, for each case the amount of inscription power was optimised. This was done using an optical attenuator (NDL-25C-2, Thorlabs) mounted before the first mirror in the grating setup system as shown in Figure 3.7. When the inscription power was higher than the optimal one low quality gratings resulted in; which means weak grating and peak splitting, and also damaged the fibre gradually. On the other hand, when the inscription power was lower than the optimal one, longer inscription time was observed without any improvement in the FBG strength. A grating may not be obtained at all if the power is too low than the optimal one. Therefore, the power selection should be balanced, taking into account the writing time as well as the strength of the grating. Table 3.4 summarises the optimal inscription power used and the corresponding inscription time and grating strength in the reflection for the fibres (paper 2, 3, 5 and 6). The reflection spectrums of the inscribed grating are depicted in paper 1 for PMMA mPOF, paper 2 and 3 for PC mPOF, paper 6 for Zeonex mPOF and paper 5 for Topas-Zeonex SIPOF.

Table 3.4 He-Cd UV laser power utilised for the grating inscription in the fibres and the corresponding inscription time and reflected grating strength.

Fibres	**Inscription power (mW)**	**Inscription time (minutes)**	**Average Grating strength in reflection (dBm)**	**Bragg wave-length (nm)**
PMMA mPOF	~20	~6	~32	~848
PC mPOF	~4	~6	~28	~892
Zeonex mPOF	~5.5	~5	~30	~865
Topas-Zeonex SIPOF	~6	~4	~30	~870

3.4 Fibre Connectorisation

Before the gratings went through the characterisation step, the fibres were first connectorised with standard single mode FC/APC connectors (30126A9, Thorlabs). As the connectors bore diameter is 126 µm, the fibres were first etched down to 125 µm from their original 150 µm diameter. Acetone (laboratory reagent, $\geq$ 99.5%, Sigma-Aldrich) was used to etch PMMA fibres and cyclohexane (Spectronorm, VWR) was used to etch Zeonex fibres. The PC mPOF was fabricated to be 125 µm because by the time the experiment was performed, the right chemical to etch PC was not found. After the fibre was etched, it was inserted into the bore of the ferrule and pulled gently from the tip of the ferrule until it gets tight in it. Then the fibre out of the ferrule was cut by razor blade and polished with fibre micro polishing machine (REV™, Krelltech) as shown in Figure 3.8. Polishing connectorised POFs had three phases: first the polishing was performed 3 times with 6 µm diamond film under pressure 4, then 3 times with 1 µm diamond film under pressure 3 and

finally twice with extra fine diamond film under pressure 2. This technique of POFs connectorisation and polishing enabled to reuse the connectors as gluing was not required unlike it was previously demonstrated by Abang *et al* [110].

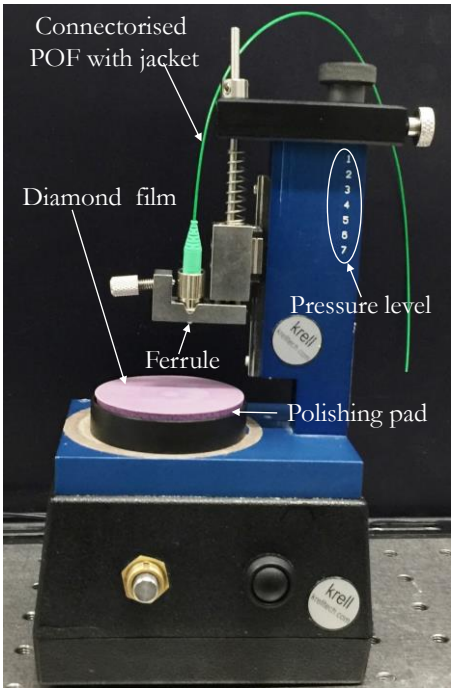

Figure 3.8 Micro fibre polishing machine.

3.5 Grating Characterisation

In order to investigate the fabricated fibres and gratings performance they were characterised for axial strain, temperature and humidity. The strain responses of the POFBGs were studied by mechanically elongating the gratings and monitoring its reflection spectrum. The fibres were first clamped and glued to two 3-axis stage (MBT616D/M, Thorlabs), each being few centimeters away from the grating. One of the stages was used to apply axial strain to the gratings manually. Every time a new strain was loaded or unloaded to the

grating, 10 minutes were given to it to get stable. The fibre was longitudinally strained up to 3 % with steps of 0.5 %.

The temperature and humidity measurements of the POFBGs were performed in a climate chamber (CLIMACELL, MMM Group). The employed characterisation setup is depicted in Figure 3.9. A supercontinuum source (SuperK Extreme, NKT Photonics) was used as a light source and a spectrometer (CCS175-Compact Spectrometer, Thorlabs) was used to continuously track the grating during strain, temperature and humidity measurements. The strain, temperature and humidity responses of the gratings are presented in the next section. It is important to mention here is that before the grating characterization the fibres were annealed and the annealing methods and adapted annealing parameters for each type for fibres are described in the following sections.

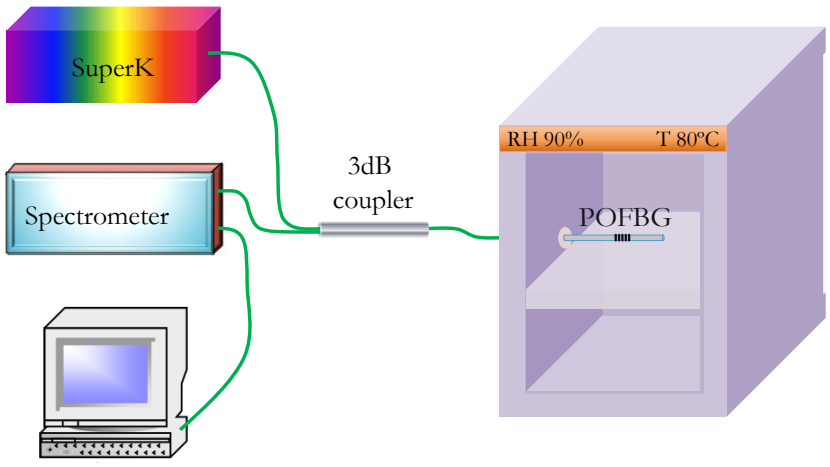

Figure 3.9 POFBGs annealing, temperature and humidity characterisation setup.

3.6 Annealing of Polymer Optical Fibres

During the fabrication of POFs, the fibres are drawn under certain levels of drawing tension. This drawing stress aligns the molecular chain of the polymers along the fibre axis leaving thus some residual stress. The alignment level

depends on the amount of drawing tension applied in the course of fabrication [111]. When POFs are heated at a temperature close but below their T_g, the polymer chains starts to relax from their orientation formed during drawing. The amount of temperature that causes the relaxation highly depends on the amount of stress applied when the fibre was fabricated and the thermal history of the preform from which the fibre was made. In addition, the extent of UV exposure experienced by the fibre also affects the relaxation process [103], [112], [113]. As the fibre is heated up it shrinks, which causes a decrease in the length of the fibre and an increase in its diameter. This process is called annealing and leads to an irreversible change in the fibre dimensions. As POFBGs are annealed, the period of the Bragg grating decreases as the fibre shrinks and thus the Bragg wavelength experiences a permanent blue-shift. The annealing of POFs either before or after inscription of a grating is an integral and vital step in the development of high performance POFBGs sensors. Prior works before this project only use thermal annealing, which involved only annealing the fibre in a conventional oven, to improve the sensor performance [47], [103]. However, during this PhD it had been discovered that only thermal annealing was not sufficient enough in order to develop stable, repeatable and hysteresis free POFBGs sensors. It is found that the amount of RH in the vicinity of the fibre under annealing has an essential role not only in the annealing process but also in the final sensor performance. In this section, different methods of annealing of POFs or POFBGs proposed during the PhD and what advantages they can offer in the realm of POFBGs sensors are presented.

3.6.1 Humidity Assisted Thermal Annealing

Traditionally, annealing of PMMA POFs performed using conventional oven or simple heating elements [47], [66], [103]. In this type of heating devices humidity is not controlled thus as the temperature of these heating elements increases, the corresponding ambient RH considerably decrease as plotted in the Figure 3.10.

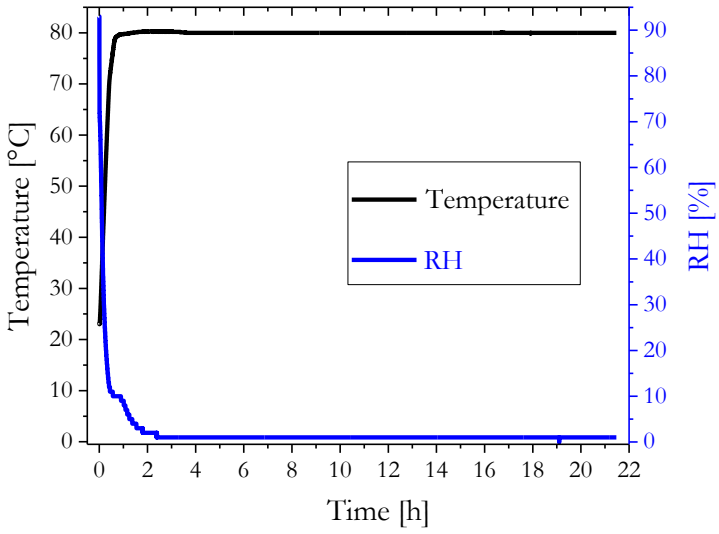

Figure 3.10 The RH response of an oven as the temperature is ramping up to the annealing temperature.

One of the investigations that have been done during the PhD was the combined effect of humidity and temperature on the annealing of POFs (paper1). A systematic investigation has been carried out using an environmental climate chamber and PMMA mPOFBGs inscribed from the same fibre draw. The annealing has been done at 80 °C and different RH levels ranging from 10 – 90 %. The thorough investigation revealed that, RH has a considerable impact on the annealing of PMMA mPOFBGs. The effect seen was seen both in the magnitude and rate of Bragg wavelength shift. For instance, for PMMA mPOFBGs annealed at 90 % RH not only the rate of the blue-shift in the Bragg wavelength was faster but also the amount of the shift was larger as compared to the one annealed 30 % RH level. This phenomenon was due the fact that PMMA has a high water absorption capability and water acts as a plasticiser for PMMA and hence decreased its T_g [114]. Table 3.5 provided a summary of the amount of blue-shifts measured when PMMA mPOFBGs from the same fibre draw annealed up to different RH levels. More elaborative figures can be seen in the attached paper 1.

Table 3.5 Summary of the amount of blue-shift in the Bragg wavelength of PMMA mPOFBGs annealed at 80 °C and up to a different levels of RH.

Annealed up to RH (%)	Total amount of blue-shift (nm)
10	~63.56
30	~74.75
50	~97.43
70	~134.99
90	~231.59

This investigation discovered for the first time that, it is possible to tune the Bragg wavelength of PMMA POFBGs by a relatively huge amount (more than 200 nm) by assisting the thermal annealing with humidity without compromising the grating strength. The largest irreversible blue-shift reported with only thermal annealing was 18 nm [66]. The effect of humidity assisted annealing on the response of PMMA POFBGs is reported in section 3.7.

3.6.2 Solution Assisted Annealing at Room Temperature

PMMA based fibres annealing methods discussed in the previous section is activated thermally. It is the temperature that allows for the polymer chains to relax from their frozen in stresses state and humidity facilitate the process as it lower the $T_{g.}$ As the goal of annealing POFs is to relax the frozen polymer chains for later stable operation of the grating sensors, the question that may rise is, are there any other possible low cost annealing techniques with no need of ovens or climate chambers? Is it possible to anneal POFs at room temperature? One of the findings during this project was that, the realisation of annealing of PMMA POFs at room temperature in methanol-water solutions (paper 2). This was based on early studies by Williams *et al.*, which showed the effect of the presence of methanol on the T_g of PMMA, which revealed that for methanol-equilibrated PMMA systems the T_g is around room temperature [115].

The investigation was carried out using different methanol-water concentration solutions and PMMA mPOFBGs inscribed from the same fibre draw. The gratings were immersed in the solution and their Bragg wavelength was monitored throughout the experiments. When the gratings were in the solutions, swelling and relaxation due to absorption of the solution were observed, while once the gratings were removed from the solution, fibre shrinkage and relaxation due to evaporation of the solution was noticed. The relaxation of the fibres resulted in the fibres to shrink thus the pitch of the grating decreased, leading to an irreversible blue-shift in the Bragg wavelength. The larger the concentration of the methanol, the larger and the faster the relaxation of the fibre was which resembles thermal annealing at high humidity levels.

Table 3.6 The amount of blue-shift in the Bragg wavelength of PMMA mPOFBGs immersed into different menthol-water concentration at room temperature.

Methanol/water v/v [%]	**Total amount of blue-shift (nm)**
50/50	~50
60/40	~80.3
70/30	~111.6

The total amount of Bragg wavelength shifts for the gratings immersed in three different menthol-water concentrations is presented in Table 3.6. This investigation shown that, the real T_g of PMMA was decreased during the experiments to an extent that depends on the methanol concentration and the method was repeatable. The main advantage of this annealing method is that it is cheap compared to the previously mentioned technique of annealing as it does not require expensive climate chamber.

The aforementioned annealing techniques of PMMA POFBGs have several advantages and are a crucial phase of POFBGs sensor development process. By these annealing methods it is possible to fabricate a number of FBGs in a single fibre with a single phase mask for WDM FBG sensor system. Therefore,

the requirement of several phase masks for the development of multiplexed PMMA POFBG sensors could be avoided. In addition, it allows production of gratings at short wavelengths (due to large blue-shifts) where POFs have lower loss but the phase mask technique poses limitations in terms of efficiency and cost. More importantly, these annealing techniques provided an improved performance PMMA mPOFBGs humidity sensors than those annealed in a traditional way as it is presented in the next section.

Table 3.7 The applied annealing temperature and RH to anneal PMMA, PC, and Zeonex mPOFBGs and Topas-Zeonex SIPOFBGs and the corresponding annealing time and the resulted blue-shift in the Bragg wavelengths under the defined annealing stopping criteria.

Fibres	**Annealing temperature (°C)**	**Annealing RH (%)**	**Annealing time (hour)**	**Amount of blue -shift (nm)**	**Annealing stopping criterion (nm/hour)**
PMMA mPOF	80	90	~24	~230	<0.3
PC mPOF	125	-	~36	~12	<0.23
Zeonex mPOF	120	-	~36	~34	<0.2
Topas-Zeonex SIPOF	110	-	~24	~17	<0.35

The annealing of Topas and Zeonex POFs were not affected by humidity. This was due to the fact that they have a very small affinity to water hence their T_g were not decreased by the ambient humidity unlike PMMA consequently they were annealed in a conventional oven. Annealing of PC mPOFs was also took place in a conventional oven despite PC has the ability to absorb water to some extent but lower than PMMA. PC mPOFBG that was annealed in a conventional oven at 125 °C for 36 hours did not show any per-

manent blue-shift when it was further annealed in a climate chamber at 100 °C (maximum stable operating temperature of the chamber) and 90% RH (maximum stable operating RH of the chamber) as discussed in paper 4. This could be due to this temperature level was not energetic enough to activate further annealing as the T_g of PC is 45 °C higher that the annealing temperature despite the ambient RH level was 90%. Table 3.7 summarises the annealing parameters employed to anneal fibres made of different polymers.

3.7 Highly Sensitive and Hysteresis free POFBGs Humidity Sensors

Due to the highly moisture absorbing capability of PMMA, it has been used to develop grating based humidity sensors [99], [100], [116]. Nevertheless, previous researches on PMMA POFBGs humidity sensors have reported not only different sensitivity value to humidity but also shown a strong dependence of the humidity sensitivity on the operating temperature. In addition, the reports indicated that very low sensitivity and high nonlinear response to humidity at temperature particularly beyond 50 °C [100], [116]. However, it is very important to develop POFBGs humidity sensors with a better performance in humidity responsivity: high sensitivity to humidity with no dependence on temperature, hysteresis free and stable operation.

In a quest of this, during the PhD a detail investigation has been performed in order to develop POFBGs humidity sensors that fought back the drawbacks of the previously developed POFBGs humidity sensors. The investigation evidenced that to achieve stable and hysteresis free response to this measurand, the fibre before or after inscription has to be annealed not only at temperature close to the T_g of the polymer but also at high RH (paper 1). For instance, for PMMA based fibres to operate in the RH range 10 - 90 % up to 75 °C with high stability, the annealing should be performed at 80 °C and 90 % RH. Annealing PMMA POFBGs at these conditions not only assisted to develop humidity sensors with no hysteresis but also to obtain consistent sensitivity up to 75 °C operating temperature. PMMA mPOFBGs that have not been annealed or annealed at low RH, for instance in a conventional oven, responded

to have low sensitivity to humidity, highly temperature dependent sensitivity to humidity and highly nonlinear response to humidity, particularly at temperature close to the annealing temperature. Table 3.8 provided the humidity sensitivity of PMMA mPOFBGs that have been annealed at 80 °C and various levels of RH. A detail results can be obtained in paper 1.

Table 3.8 The humidity sensitivity of PMMA mPOFBGs that have been annealed at 80 °C and 10, 30, 50, 70 and 90 % RH levels.

Annealing at 80 °C and RH of	**Humidity sensitivity (pm/%RH)**					
	Operated at 25 °C		**Operated at 50 °C**		**Operated at 75 °C**	
	Absorption	**Desorp sorption**	**Absorption**	**Desorption**	**Absorption**	**Desorption**
10 %	~28.39	~29.12	~27.42	~28.31	Not functional	
30 %	~30.46	~30.89	~29.79	~30.38	Not functional	
50 %	~33.39	~33.61	~33.01	~33.33	Not functional	
70 %	~34.76	~34.86	~34.55	~34.7	Not functional	
90 %	~35.43	~35.49	~35.33	~35.42	~35.19	~35.32

As it can be seen from Table 3.8, was only the grating that was annealed up to 90 % RH and at 80 °C exhibited the most stable response to humidity in the range 10-90 %RH up to 75 °C. In contrast, other gratings annealed at lower RH levels showed smaller sensitivities with hysteresis even at low temperature level such as 25 °C and 50 °C and were not functional when they are operated at 75 °C. At this operating temperature they showed fast, highly nonlinear and permanent decrease in the Bragg wavelength when the RH was raised just above the annealing RH level (see Figure 3.11).

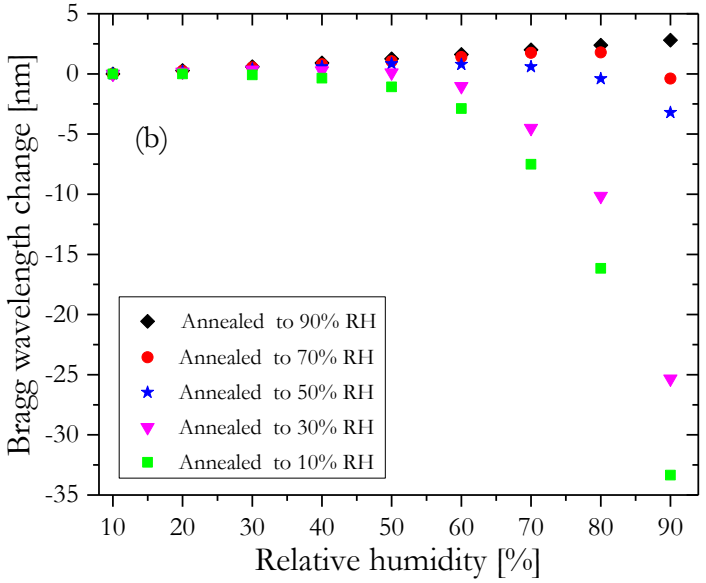

Figure 3.11 Humidity responsivity at 75 °C of PMMA mPOFBGs annealed up to 90%, 70%, 50%, 30%, and 10% RH.

The sensitivity to humidity for PMMA mPOFBG annealed up to 90 % RH at 80 °C was around 35.31 ± 2.49 pm/% RH for the whole range of operated temperature at a Bragg wavelength of around 600 nm. It is possible to obtain a larger sensitivity value if the Bragg wavelength is within a longer wavelength range yet still low loss region, such as the 850 nm region. To achieve this, rather than annealing the fibres after grating inscriptions which causes shifting the Bragg wavelengths to shorter wavelengths, the fibres can be annealed before inscriptions. Figure 3.12 shows the humidity response of a PMMA mPOFBGs inscribed in a fibre that was annealed at 80 °C and 90 % RH for 24 hours before grating inscriptions. The humidity sensitivity of the grating at 850 nm was 10 pm/ % RH larger than the one measured at 600 nm.

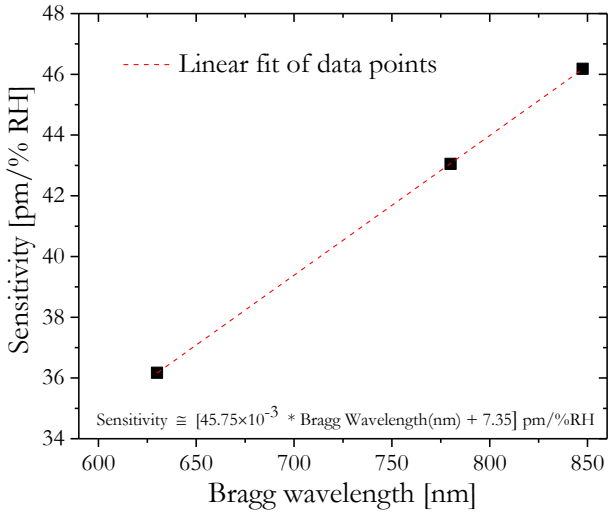

Figure 3.12 (a) Bragg wavelengths versus humidity sensitivity of PMMA mPOFBGs for gratings inscribed at three different wavelength in a fibre annealed at 80 °C and 90 % RH for 24 hours before the grating inscription.

Although PMMA based mPOFBGs have high sensitivity to humidity, they operate with no hysteresis in the range 10-90% RH at maximum limiting temperature of 75 °C. At 90% RH and temperature beyond 80 °C, the grating is experiencing a significant degradation and it is unable to operate. Therefore, PMMA based POFBGs can operate beyond 75 °C but 15-20 °C below its T_g , provided the corresponding ambient RH level is much lower than 90%. Considering this limitation and there are application areas that require humidity measurements at temperatures beyond PMMA mPOFBGs can operate, humidity sensor was developed from a fibre made of different polymer. The criteria to choose the new polymer was: its transparency, moisture absorption ability and its T_g, and PC satisfied the aforementioned criteria. Topas and Zeonex were not a suitable material for humidity sensor development because their water absorption capability is very small although their T_g is higher than that of PMMA.

PC mPOFBGs was then demonstrated to be able to measure RH in the range from 10 to 90 % up to 100 °C (paper 4). It is possible to operate PC

mPOFBG beyond this temperature level as the T_g of PC is 145 °C but the climate chamber used for calibration can only operates up to 100 °C. The measured humidity sensitivity of PC mPOFBGs was 7.25 ± 0.08 pm/% RH in the range 10-90 % RH up to 100 °C operating temperature. This figure indicates that the RH sensitivity of PC mPOFBGs is indeed 7 times smaller than that of PMMA mPOFBGs but can operate well beyond PMMA mPOFBGs could reach. Despite the low moisture absorption property of PC as compared to PMMA considered as a limitation, this turns out to be an advantage when PC mPOFBG was used to as temperature sensor. For instance, for a climate chamber that has RH precision of 1 %, when PMMA mPOFBGs were characterised for temperature response, a 1 % of RH fluctuation in the chamber causes the temperature measurement to be difficult and unreadable.

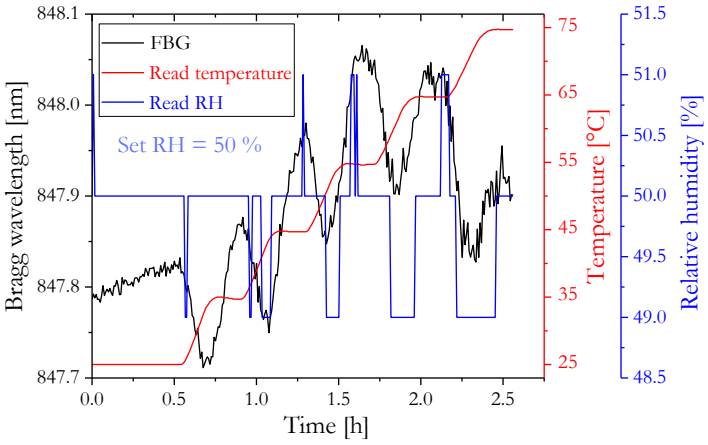

Figure 3.13 Temperature responses of PMMA mPOFBGs at 50 % RH (set value). The fibre was annealed at 80 °C and 90 % RH for 24 hours before the grating inscription.

This is due the fact that PMMA mPOFBGs have high sensitive to humidity and small sensitivity to temperature. Figure 3.13 plots the temperature response of PMMA mPOFBGs at 50 % RH (set value). As it can be seen from this figure, it is hardly possible to get accurate temperature measurement due to 1 % RH fluctuation in the chamber. However, this problem was not seen when temperature characterisation was performed for PC mPOFBG (paper 4).

This is as a result of PC has smaller moisture absorption capability but high sensitivity to temperature as compared to PMMA such that 1 % RH fluctuation in the chamber does not affect the temperature response of the PC grating. Therefore, high resolution climate chamber is not required to calibrate both the temperature and humidity responses of PC mPOFBGs. The temperature response of the PC mPOFG can be seen from Figure 3.14. The temperature sensitivity of PC mPOFGs was measured to be around - 25.86 ± 0.63 pm/ °C in the range 20 -100 °C up to 90 %RH.

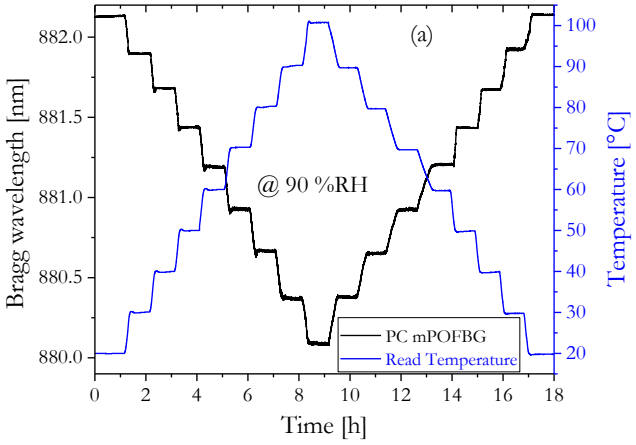

Figure 3.14 Measured temperature response of PC mPOFBG at 90 % RH.

3.8 Humidity Insensitive and Stable POFBGs High Temperature Sensors

As described in the previous section PMMA POFBGs are highly sensitive to humidity and the temperature response of these gratings is considerably affected by a very small fluctuation in the ambient RH. Therefore, they are not ideal for the development of temperature sensors. One of a promising solution to develop POFBGs temperature sensors which are resilient to humidity variations is using POFs made of polymers which have low affinity to water. In a quest of this, mPOFBGs made of cyclo-olefin copolymers, such as Topas 8007F-04 [50], [78] and [51] have been proposed and realised for humidity

insensitive temperature measurement as this class of polymers have very low affinity to water. During the PhD project new fibres, Topas-Zeonex SIPOF (paper 5) and Zeonex mPOF (paper 6), based grating have also been demonstrated for humidity insensitive temperature measurements. The reasons why these new fibres types were necessarily developed is discussed in the following paragraphs.

In general, the polymer Topas and Zeonex share several properties [107][108][117]:

- are optical thermoplastics that have good chemical inertness to bases and acids, and many polar solvents as compared to PMMA;
- very low moisture uptake;
- low birefringence and superior mouldability;
- almost the same glass transition temperature and high temperature resistance, this makes them preferable for high operating temperature POFBGs strain sensor development unlike Topas grade 8007F-04;
- very close refractive indices, where the refractive index of Topas is higher than that of Zeonex.

Even though these two polymers have the abovementioned several common properties, they have a fundamental difference regarding their chemical structures. Topas is a class of cyclic-olefin copolymer, which is an amorphous ethylene-norbornene copolymer with a high percentage of norbornene. However, Zeonex is a class of cyclo-olefin homopolymer, which is an amorphous norbornene homopolymer. In addition, the weight-average molecular weight (M_w) of Zeonex is six times larger than that of Topas [118], [119]. For thermoplastic materials the melt flow index defined as the flowability, decreases with increasing M_w [120]. Therefore, Zeonex preforms tend to flow slower than Topas under similar fibre drawing conditions, thereby ensuring a highly controllable and stable fibre draw process, which makes Zeonex much better than Topas for manufacturing of mPOFs (paper 6). This advantage of Zeonex polymer enabled to transfer the microstructured from the preform to the final fibre stage more efficiently in the Zeonex mPOFs fabrication process. For ex-

ample, it was possible to draw Zeonex mPOFs with the cladding holes that are uniform and symmetrical compared to Topas mPOFs (see Figure 3.15). Due to the better stability of Zeonex mPOFs drawing process, fluctuations in the fibre diameter were also reduced. Nevertheless, it should be noted that either too high or too low values of M_w can make the fibre drawing very challenging or even unfeasible. The M_w of Zeonex is sufficiently low to avoid this potential problem. Therefore, Zeonex mPOF showed its superior drawability over Topas mPOFs (paper 6).

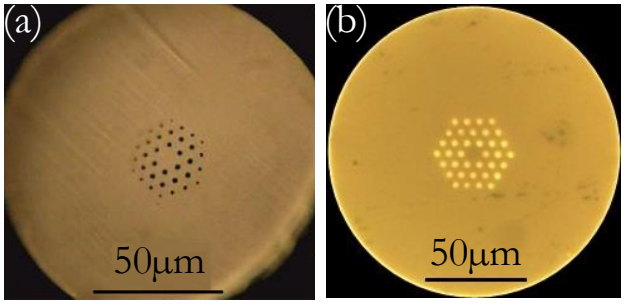

Figure 3.15 Optical microscope facet image of (a) Topas mPOF [51] (b) Zeonex mPOFs.

Thus using this important advantage of Zeonex, during the PhD an ESM Zeonex mPOF was fabricated and grating sensors based on this fibre was realised for the first time (paper 6). In addition to the merits mentioned above, Zeonex also demonstrated better transmittance than Topas mPOFs. Moreover, Zeonex mPOFBGs provided higher sensitivity to temperature than Topas mPOFBGs. Furthermore, Zeonex showed a very good compatibility with PMMA for co-drawing applications [121] and this property allowed to develop multi-parameter mPOFBGs sensors during the project and it is described in section 3.10.

Although Topas polymer was not an ideal candidate for the fabrication of mPOFs, it was proposed for step index fibre production. This is because step index fibres do not pose complexity during drawing as there are no microstructured holes. Basically, step index fibres are sometimes preferable than

microstructured as they reducing or even avoiding transmission loss caused by scattering from the microstructured air-holes and impurities getting into holes. In addition, step index fibres reducing FBG inscription time as there are no holes which block the inscription laser from reaching the core of the fibre. Further, handling of SIPOFs such as cleaving, connectorising and splicing is easier compared to mPOFs. Nonetheless, although step SIPOFs have these merits, realising SIPOFs for single mode guidance is not as an easy as ESM mPOFs. This is due to the fact that during the polymerisation of monomers in the preform making process, it is difficult to control dopant diffusion from core to cladding hence to maintain the refractive index profile of SIPOFs to ensure single mode operation. In the realisation of single mode SIPOFs, another constraint may also raise due to the inverse relation between the wavelength and the core size of an optical fibre for single mode operation. As POFs have low loss in the visible region, to realise SIPOFs for single mode operation in this wavelength region the core size should be small. And it is known that small core size fibres increases scattering losses and also make connectorisation difficult. In addition to the aforementioned challenges, conventional methods used to fabricate SIPOFs such as interfacial-gel polymerisation, batch extrusion and continuous extrusion, centrifugation and chemical vapor deposition are time consuming and complex [53]. And these are the main reason why the development of single mode SIPOFs has lagged behind silica optical fibres [45].

In order to mitigate the above mentioned problems and challenges, during PhD project a new method of fabricating step index preform was developed by exploiting the common advantages of Topas and Zeonex polymers. Casting, drilling and injection moulding technique have been used to fabricate the step index preform. (paper 5). Topas and Zeonex were used as a core and cladding material, respectively, thus no doping was required. In the preform preparation stage, first the Zeonex cladding was cast and a hole was drilled at the centre of the preform and then Topas was injection moulded in the drilled hole. The main advantage of the injection moulding technique is that, it is a fast, flexible and cost effective way of preparing step index fibre preforms. Two steps of heat drawing have been used for fibre fabrication. First a cane

was drawn and then sleeved with a Zeonex tube and drawn to a fibre. The final fibre had a core and cladding dimeter of 4.8 µm and 150 µm, respectively. The normalized frequency was 2.38 at 850 nm. This fibre is the first humidity insensitive single mode SIPOF. The FBG inscription time of the fabricated single mode SIPOF was only 4 minutes and the optimum inscription laser power for this fibre was only 6 mW (see Table 3.4). Despite this small power was used, the writing time was shorter than the shortest writing time of 7 minutes reported for PMMA mPOF [79] and it was much shorter than the writing time of 338 minutes reported for Topas based mPOF [78], both inscribed with a 30 mW CW He-Cd laser. In addition, the fabricated fibre is compatible in core dimension with a standard single mode silica fibre in the 850 nm region. The fabrication and characterisation of this fibre is described in detail in paper 5. However, the comparison of the humidity and temperature sensitivity of the fibre with the other mPOFBGs is reported in Table 3.9.

Table 3.9 Humidity and temperature response of gratings inscribed in PMMA, PC, and Zeonex mPOFs and Topas-Zeonex SIPOF. Before characterisation the fibres were annealed as reported in Table 3.7.

Fibres	Bragg wavelength (nm)	Operated RH range (%)	Operated temperature range (°C)	RH sensitivity (pm/% RH)	Temperature sensitivity (pm/ °C)
PMMA mPOF	~847.51	10-90	25-75	~46.18	-
PC mPOF	~875.70	10-90	20-100	~7.31	~ -25.86
Zeonex mPOF	~831.57	10-90	20-100	~0.75	~ -24.01
Topas-Zeonex SIPOF	~852.12	10-90	20-105	~0.45	~ -17.57

3.9 Large Dynamic Range and Hysteresis Free POFBGs Strain Sensors

The strain responses to gratings fabricated in PMMA, PC and Zeonex mPOFs and Topas-Zeonex SIPOF were also measured (paper 3, 5 and 6). All the gratings were annealed as described in section 3.6. There was no significant difference observed in strain response of the gratings fabricated in the fibres. All measured strain in the range 0-3% without hysteresis and an average sensitivity of 7.4 nm/ % strain. The gratings strength attenuates only by 0.25 % when the strain level was 3%. Strain level more than 3% resulted in a rapid degradation in the grating. Table 3.10 summarises the strain response of gratings inscribed in the fibres.

Table 3.10 Strain responsivity of gratings inscribed in a PMMA, PC, and Zeonex mPOFs and Topas-Zeonex SIPOF. Before strain measurements the fibres were annealed as stated in Table 3.7.

Fibres	**Bragg wavelength (nm)**	**Measured strain range (%)**	**Strain sensitivity (nm/ % strain)**	**Ambient temperature and RH**
PMMA mPOF	847.51	0-3	7.3	Room
PC mPOF	875.70	0-3	7.9	Room
Zeonex mPOF	831.57	0-3	7.7	Room
Topas-Zeonex SIPOF	852.12	0-3	7.6	Room

3.10 Microstructured POFBGs thermo-hygrometer

In the realm of POFBGs sensors, several single parameter grating based sensors have been developed including those developed during this PhD project. However, only a little work has been done towards the development of multi-parameter POFBGs sensors. Bhowmik *et al.* demonstrated a sensing configuration for simultaneous measurement of strain and temperature based on a FBG pair with one grating being inscribed in the etched and the other in unetched POF region [122]. Zhang *et al.* fabricated a sensor for simultaneous measurement of temperature and humidity by cascading silica and PMMA FBGs [102]. Despite the cascaded sensor configuration provided a well-conditioned response, the mechanical stability of the sensor is in question as the two fibres were glued as a means of connectorisation. In addition, the glue could not withstand relatively high temperature and humidity which limit the range of operation of the sensor. Recently Oliver *et al.* also demonstrated POF strain, temperature, humidity and refractive index sensor based on multimode interference in combination with FBG [123]. In the sensor configuration the grating was inscribed in a highly multimode fibre which is not suitable for high precision grating sensors. This is because it is difficult to accurately track the response of multimode gratings and hence these sensing devices suffer from low accuracy and resolution. Considering these limitations and also there are only a few investigations on multi-parameter POFBG sensors, during the PhD research the first thermo-hygrometer purely made of mPOFBGs has been demonstrated.

A new fibre design has been used to realise the thermo-hygrometer. The fibre involved an over cladding in addition to core and cladding (see Figure 3.16). Zeonex formed the core and the cladding, and PMMA the over cladding (paper 7). The sensing probe is based on two separate in-line FBGs inscribed in the fabricated mPOF. To inscribe the two grating, which were both spatially and temporally apart, only a single phase mask was used in combination with thermal annealing technique. In a piece of the fabricated fibre, at one end, the PMMA over cladding was etched out for few centimeters and the first grating was inscribed and then the grating was annealed to shift the Bragg

wavelength by few nanometers. The second grating was then inscribed in the unetched section of the fibre few centimeters away from the first grating.

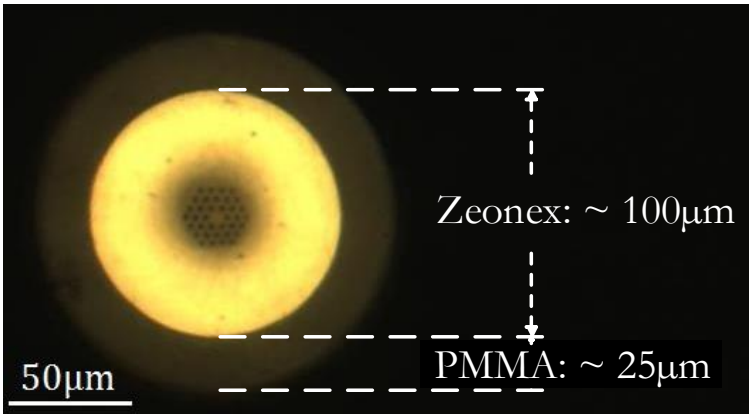

Figure 3.16 Optical microscope image of the fabricated Zeonex - PMMA mPOF.

The basic principle behind humidity measurement with the PMMA over cladding Zeonex mPOF relies on the swelling effect caused by PMMA. When PMMA absorbs moisture it induces strain on the grating inscribed in the Zeonex core thus effectively leading to a shift in the Bragg wavelength. In the range 10 to 90 % RH and 20 to 80 °C, a root mean square deviation of 0.8 % RH and 0.6 °C was found. The potential advantages of the developed device are being easy to fabricate, low cost, compact, all polymer based and mechanically stable. In addition, it has also multiplexing capability as the two gratings are temporally close.

Here it worth mentioning that the PMMA over cladding thickness is the one which control the humidity sensitivity of the thermo-hygrometer. The thicker the PMMA over cladding, the higher the humidity sensitivity would be. However, as the thickness of the PMMA over cladding increases, the corresponding sensor response time is also increasing. Therefore, the optimal thickness should be found which compromise both the humidity sensitivity and the response time of the device. In the development process of the multi-parameter mPOFBGs based sensors several attempts were made with different fibre

types and methods before achieving the above described result. The attempts made are also described in detail in the attached paper 7.

Chapter 4 -Conclusions

This dissertation reported the fabrications and characterisations of POFs and POFBGs for sensing applications to mature the technology which leads to commercialisation. In this chapter, a brief summary of the keys achievements and recommendations for future works are given.

4.1 Conclusion

During the PhD study several polymers, namely PMMA, PC, Zeonex and Topas, were explored for POFs fabrications pertaining to gratings based sensors development. The fabricated fibres were of both microstructured and step index in type. All the fabricated fibres were characterised and gratings were inscribed to investigate their potentials for sensing applications. To this end, optimisation in the writing parameters of a grating have been made for each fabricated fibres in order to achieve high quality gratings. The optimisations result revealed that each polymer prefer a certain level of average power to realise a grating in them.

Considering the requirement for the development of high performance reliable POFBG sensors, methods for efficient ways of annealing were proposed and experimentally demonstrated. The proposed annealing methodologies were humidity assisted and solution mediated annealing scheme. Both methods were an effective way of annealing while the latter was cost effective. Using these methods of annealing a temperature independent, highly sensitive, and hysteresis free PMMA mPOFBGs humidity sensor was developed. In addition, these annealing techniques served as method to tune a PMMA mPOFBGs Bragg wavelength by more than 200 nm without affecting the characteristics of the gratings significantly. This provided an alternative way to produce grating at short wavelength where the loss of POFs is low and fabricating phase masks and grating is difficult.

It has also been demonstrated that PMMA POFBGs humidity sensors cannot operate beyond 75 °C when they are operated up to 90 %RH. In view of this, a humidity sensor which can operate up to 100 °C was developed using PC mPOFBG for application areas which required RH measurement at high temperature. In addition to this, due to the high T_g of PC, grating made of it enabled to measure temperature up to 125 °C at room RH and this is the record temperature level measured among the currently existing POFBGs.

Seeing the difficulty of drawing Topas based mPOFs with uniform microstructured holes, a new polymer, called Zeonex which is fabrication friendly was explored and a high quality microstructured fibre was drawn from it. Zeonex mPOF showed high transparency and grating fabricated from it demonstrated higher temperature sensitivity compared to Topas mPOFs. Despite Topas was not suitable to draw mPOFs, in light of the unavailability and the high demand of single mode SIPOFs commercially for sensing applications, single mode SIPOF was developed using Topas as a core material. The fibre preform was developed using a combination of casting, drilling and injection moulding techniques and the fibre was drawn using heat and draw method. This method fabrication was easy, flexible and very efficient as compared to other methods of SIPOFs production techniques and no dopant was introduced to increase the refractive index of the core. This fibre presented a grating inscription time much shorter than the microstructured Topas fibres. Grating made of Topas and Zeonex fibres showed very small sensitivity to humidity. This property makes them a good materials for the development of grating based temperature and strain sensors as the humidity cross sensitivity is avoided.

Wide dynamic range and hysteresis free POFBGs strain sensors have been also developed from PMMA, PC and Zeonex ESM mPOFs and Topas-Zeonex single mode SIPOF gratings. All gratings demonstrated the same strain response both in sensitivity and dynamic range regardless the materials for where the fibre was fabricated.

In light of the importance and the high demand of monitoring the two most environmental monitored measurands, temperature and humidity, in agriculture, medical and food industries, a fully polymeric thermo-hygrometer has been developed. The sensor was operated in the range 10 to 90 % RH and 20 to 80 °C with a root mean square deviation of 0.8 % RH and 0.6 °C. The great advantages of the device are: easy to fabricate, low cost, compact, mechanically stable, and all polymer based.

To summarise, during the PhD project the followings have been achieved for the first time:

- Humidity assisted thermal annealing and solution assisted annealing at room temperature of POFBGs were proposed and investigated, and their potential impacts on POFBGs sensors development were thoroughly studied;
- Tuning of PMMA POFBG by more than 200 nm was achieved with humidity assisted thermal annealing,
- Temperature independent sensitivity, hysteresis free, and stable PMMA and PC mPOFBG humidity sensor were developed;
- Solid core PC and Zeonex mPOFs was realised;
- Grating in PC and Zeonex mPOFs realised;
- Humidity insensitive single mode Topas core and Zeonex cladding SIPOF was developed;
- The record temperature measurement, up to 125 °C, achieved with PC mPOFBGs;
- Humidity sensor that can operate up to 100 °C was developed with PC POFBGs;
- Fully polymeric low cost and mechanically stable thermo-hygrometer was developed;

4.2 Outlook

One of the most common limitations of POFs is the high transmission loss. Although it is possible to use a few meters of POFs as a part of the sensor

system, the inherent high attenuation hinder from developing a fully POFs based grating sensor systems particularly for a wide territorial area using multiplex technique. The main contribution to the loss of POFs is the intrinsic loss. Thus a dedicated research must be carried out to reduce this loss mechanism. The extrinsic loss which may resulted from fibre fabrication can be avoided and it has been realised a fibre which has an attenuation equivalent to the material loss [31].

By optimising the grating inscription setup and laser power, grating inscription time of POFs have been shortened significantly down to few minutes from where it was in hours using the phase mask inscription technique and the 325 nm He-Cd UV laser. Recent research in the grating inscription achieved inscription time in less than 30 sec in a PMMA mPOFs using KrF laser by optimising the characteristics of this laser to be suitable to write grating in PMMA POFs [80]. This inscription time is a reliable indication to produce POFBGs commercially. A shorter inscription time should be achieved also for POFs made of other materials such as PC, Topas and Zeonex on the road to the commercialising phase. Investigation on this is currently undergoing.

The other most important thing that needs a dedicated research is reduction of POFBGs sensors response time particularly humidity sensors. Currently the humidity response time of these types of sensors is in the order of several 10 minutes and this is uncompetitive compared to electronic based humidity sensors which have response of a few seconds or even less than a second. The main reason behind the long humidity response time of POFBGs is due to the slow diffusion of moisture in the fibres. One proposed solution to reduce humidity response time of POFBGs sensors is to use small diameter fibres. In a quest of this, so far researchers proposed some method such as etching the fibre to a smaller dimeter [124] and laser micro-machining the side of the fibre where the FBG is located [125]. Even using these methods it was not possible to reduce the humidity response significantly. There, a new method is required shorten the response time considerably such as by using different microstructured fibre designs.

Appendices

Appendix A - Collection of Papers

Paper 1

Temperature insensitive hysteresis free highly sensitive polymer optical fibre Bragg grating humidity sensor

G.Woyessa, K.Nielsen, A.Stefani, C.Markos and O.Bang

Optics Express 24(2), 1206-1213 (2016)

Temperature insensitive hysteresis free highly sensitive polymer optical fiber Bragg grating humidity sensor

Getinet Woyessa,[1,*] Kristian Nielsen,[1] Alessio Stefani,[1,2] Christos Markos,[1,3] and Ole Bang[1]

[1] *Department of Photonics Engineering, Technical University of Denmark, DK-2800 Kgs. Lyngby, Denmark*
[2] *Institute of Photonics and Optical Science (IPOS), School of Physics, The University of Sydney, NSW 2006, Australia*
[3] *CREOL, The College of Optics & Photonics, University of Central Florida, 4000 Central Florida Blvd., Orlando, FL 32816, USA*
[*] *gewoy@fotonik.dtu.dk*

Abstract: The effect of humidity on annealing of poly (methyl methacrylate) (PMMA) based microstructured polymer optical fiber Bragg gratings (mPOFBGs) and the resulting humidity responsivity are investigated. Typically annealing of PMMA POFs is done in an oven without humidity control around 80°C and therefore at low humidity. We demonstrate that annealing at high humidity and high temperature improves the performances of mPOFBGs in terms of stability and sensitivity to humidity. PMMA POFBGs that are not annealed or annealed at low humidity level will have a low and highly temperature dependent sensitivity and a high hysteresis in the humidity response, in particular when operated at high temperature. PMMA mPOFBGs annealed at high humidity show higher and more linear humidity sensitivity with negligible hysteresis. We also report how annealing at high humidity can blue-shift the FBG wavelength more than 230 nm without loss in the grating strength.

OCIS codes: (130.5460) Polymer waveguides, (060.3735) Fiber Bragg gratings, (060.2370) Fiber optics sensors.

References and links

1. K. Peters, "Polymer optical fiber sensors - A review," Smart Mater. Struct. **20**(1), 013002 (2011).
2. D. J. Webb, "Fiber Bragg grating sensors in polymer optical fibers," Meas. Sci. Technol. **26**(9), 092004 (2015).
3. H. Dobb, D. J. Webb, K. Kalli, A. Argyros, M. C. J. Large, and M. A. van Eijkelenborg, "Continuous wave ultraviolet light-induced fiber Bragg gratings in few- and single-mode microstructured polymer optical fibers," Opt. Lett. **30**(24), 3296–3298 (2005).
4. Z. Xiong, G. D. Peng, B. Wu, and P. L. Chu, "Highly tunable Bragg gratings in single-mode polymer optical fibers," IEEE Photonics Technol. Lett. **11**(3), 352–354 (1999).
5. A. Stefani, S. Andresen, W. Yuan, N. Herholdt-Rasmussen, and O. Bang, "High sensitivity polymer optical fiber-Bragg-grating-based accelerometer," IEEE Photonics Technol. Lett. **24**(9), 763–765 (2012).
6. J. Jensen, P. Hoiby, G. Emiliyanov, O. Bang, L. Pedersen, and A. Bjarklev, "Selective detection of antibodies in microstructured polymer optical fibers," Opt. Express **13**(15), 5883–5889 (2005).
7. G. Emiliyanov, J. B. Jensen, O. Bang, P. E. Hoiby, L. H. Pedersen, E. M. Kjaer, and L. Lindvold, "Localized biosensing with Topas microstructured polymer optical fiber," Opt. Lett. **32**(5), 460–462 (2007).
8. C. Markos, W. Yuan, K. Vlachos, G. E. Town, and O. Bang, "Label-free biosensing with high sensitivity in dual-core microstructured polymer optical fibers," Opt. Express **19**(8), 7790–7798 (2011).
9. N. G. Harbach, "Fiber Bragg gratings in polymer optical fibers," PhD Thesis, Lausanne, EPFL (2008).
10. C. Zhang, X. Chen, D. J. Webb, and G. D. Peng, "Water detection in jet fuel using a polymer optical fiber Bragg grating," Proc. SPIE **7503**, 750380 (2009).
11. C. Zhang, W. Zhang, D. J. Webb, and G. D. Peng, "Optical fiber temperature and humidity sensor," Electron. Lett. **46**(9), 643–644 (2010).
12. W. Yuan, L. Khan, D. J. Webb, K. Kalli, H. K. Rasmussen, A. Stefani, and O. Bang, "Humidity insensitive TOPAS polymer fiber Bragg grating sensor," Opt. Express **19**(20), 19731–19739 (2011).

#253345 Received 5 Nov 2015; revised 30 Dec 2015; accepted 4 Jan 2016; published 14 Jan 2016

Corrected: 11 February 2016

13. C. Markos, A. Stefani, K. Nielsen, H. K. Rasmussen, W. Yuan, and O. Bang, "High-Tg TOPAS microstructured polymer optical fiber for fiber Bragg grating strain sensing at 110 degrees," Opt. Express **21**(4), 4758–4765 (2013).
14. Z. F. Zhang and X. M. Tao, "Synergetic effects of humidity and temperature on PMMA based fiber Bragg gratings," J. Lightwave Technol. **30**(6), 841–845 (2012).
15. W. Zhang and D. J. Webb, "Humidity responsivity of poly(methyl methacrylate)-based optical fiber Bragg grating sensors," Opt. Lett. **39**(10), 3026–3029 (2014).
16. W. Yuan, A. Stefani, M. Bache, T. Jacobsen, B. Rose, N. Herholdt-Rasmussen, F. K. Nielsen, S. Andresen, O. B. Sørensen, K. S. Hansen, and O. Bang, "Improved thermal and strain performance of annealed polymer optical fiber Bragg gratings," Opt. Commun. **284**(1), 176–182 (2011).
17. B. T. Kuhlmey, R. C. McPhedran, and C. Martijn de Sterke, "Modal cutoff in microstructured optical fibers," Opt. Lett. **27**(19), 1684–1686 (2002).
18. T. A. Birks, J. C. Knight, and P. S. Russell, "Endlessly single-mode photonic crystal fiber," Opt. Lett. **22**(13), 961–963 (1997).
19. A. Stefani, K. Nielsen, H. K. Rasmussen, and O. Bang, "Cleaving of TOPAS and PMMA microstructured polymer optical fibers: Core-shift and statistical quality optimization," Opt. Commun. **285**(7), 1825–1833 (2012).
20. A. Abang and D. J. Webb, "Demountable connection for polymer optical fiber grating sensors," Opt. Eng. **51**(8), 080503 (2012).
21. I. P. Johnson, D. J. Webb, K. Kalli, M. C. J. Large, and A. Argyros, "Multiplexed FBG sensor recorded in multimode microstructured polymer optical fiber," Proc. SPIE **7714**, 77140D (2010).

1. Introduction

The interest in polymer optical fibers (POFs) in sensing is steadily increasing because of their low processing temperature, high flexibility in bending, high fracture toughness, ease of handling, and non-brittle nature, which are properties that glass fibers do not have [1,2]. In addition, POFs are biocompatible and have a high elastic strain limit and low Young's modulus, which makes them advantageous for fiber Bragg grating (FBG) based strain and bio-sensing applications [3–8]. Some polymers, such as PMMA, are humidity sensitive and strongly absorb water [9–11], while other polymers, such as TOPAS, were shown to be insensitive to humidity [12,13]. Due to the moisture absorbing capability of PMMA based POFs, which leads to a change in the refractive index and size of the fiber, both of which contribute to a change in Bragg wavelength [9], they are used for developing humidity sensors [10,11]. Papers on PMMA POFBGs humidity sensors have so far reported different sensitivities to humidity and shown a strong dependence of the humidity sensitivity on the operating temperature and very low sensitivity at high temperature [14,15].

It is important to develop POFBG humidity sensors with a high sensitivity to humidity, no hysteresis in the humidity response and no cross-sensitivity to temperature. Likewise it is important to have a detailed knowledge of the humidity responsivity when designing all other types of POFBG sensors, in order to eliminate the cross-sensitivity to humidity. Here we address this issue by thorough characterization of PMMA mPOFBGs in a controlled environment in a climate chamber. It is well-known that prior annealing at a temperature close to, but below the glass transition temperature of the polymer, is important for stable and hysteresis free temperature and strain sensing with PMMA POFBGs [16]. Typically the recommended annealing temperature for PMMA POFBGs is around 80°C for more than 12 hours. At this temperature in a standard oven the relative humidity is very low, usually less than 10%. In prior investigations the humidity was thus low and not controlled during annealing. In this work, we demonstrate that humidity control during the annealing process of PMMA POFBGs plays a significant role in achieving high-quality humidity sensors that fulfil the above listed criteria and that in fact the relative humidity (RH) level during annealing should be high, preferable more than 90%.

2. Experiments and Results

To investigate the effect of humidity on annealing of PMMA mPOFs and the resulting humidity responsivity we prepared five identical 850 nm mPOFBGs using the phase mask technique. The fibers used in these experiments are PMMA mPOFs, from the same drawing,

#253345 Received 5 Nov 2015; revised 30 Dec 2015; accepted 4 Jan 2016; published 14 Jan 2016

fabricated at DTU Fotonik. The diameter of the fibers is 150 μm and the hole diameter and the pitch size are 1.5 μm and 4.2 μm, respectively. The hole to pitch ratio is 0.36 ensuring that the fiber is endlessly single mode [17,18]. A microscope image of the mPOF end facet, which was cleaved with a custom made cleaver at a temperature of 73°C of both blade and fiber [19], is shown as in Fig. 1.

We have conducted 5 series of experiments. In all experiments the PMMA mPOFBG was first connectorized with a single mode silica patch cable [20] and then placed in a climate chamber (CLIMACELL, MMM Group). A supercontinuum source (SuperK Compact, NKT Photonics) has been used as a light source and a spectrometer (CCS175 - Compact Spectrometer, Thorlabs) has been used to continuously track the peak of the grating during annealing in the climate chamber. Figure 1 shows the experimental setup for the humidity controlled annealing of PMMA mPOFBGs.

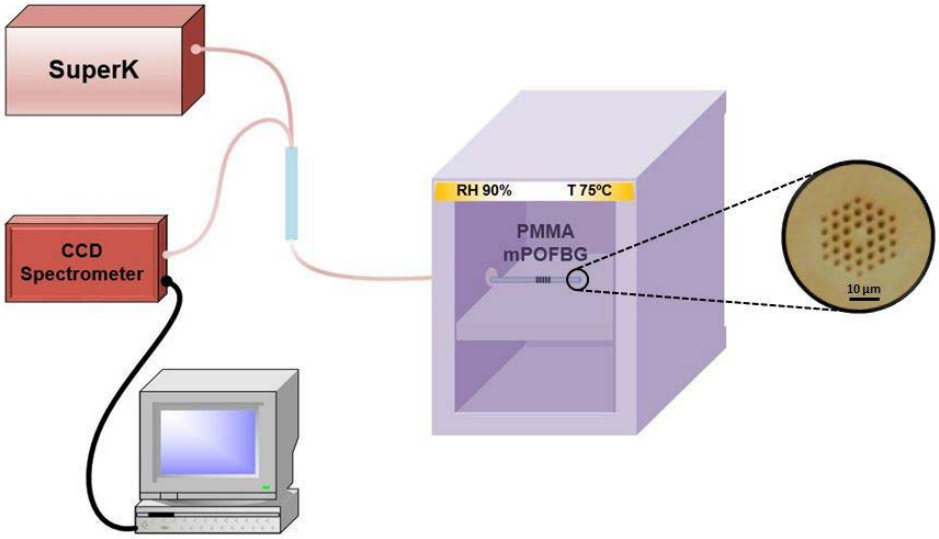

Fig. 1. Experimental setup for annealing and humidity response measurement of PMMA mPOFBGs. Inset: microscope image of the end facet of PMMA mPOF.

For all 5 experiments we first took the climate chamber to the ambient conditions, defined as 25°C and 50% RH and then carried out three annealing phases: pre-annealing, annealing and post-annealing. The pre-annealing phase consisted of 2 steps, in which the temperature and relative humidity were first kept at the ambient condition for two hours, after which the relative humidity was decreased to 10% at a fixed temperature of 25°C and kept there for three hours. The annealing phase always involved taking the temperature to 80°C and keeping it fixed at 80°C it during a pre-determined relative humidity sequence. The post-annealing phase always consisted of taking the temperature and the relative humidity back to the ambient condition and keeping them there for 10 hours. Thus, for all 5 experiments, the annealing process was started and ended at ambient conditions. This precise control of initial and final state of the mPOFBG is extremely important in order to determine and compare the amount of blue-shift introduced by the five series of experiments without ambiguity. It is also very important that the post-annealing phase, after which sensitivity measurements were performed, always brought the mPOFBG to the same stable ambient condition (therefore the rather long post-annealing time of 10 hours), in order to be able to compare the relative humidity sensitivities measured in the five experiments.

For the first experiment the annealing phase was as follows: the temperature of the chamber was increased to 80°C, keeping the relative humidity at 10%. When the rate of blue-shift of the mPOFBG became less than 0.3 nm/hour, which we defined as mPOFBG

#253345 Received 5 Nov 2015; revised 30 Dec 2015; accepted 4 Jan 2016; published 14 Jan 2016

equilibrium condition, the RH of the chamber was increased to 30%. When the rate of blue-shift of the mPOFBG again became less than 0.3 nm/hour the RH of the chamber was increased to 50%, then to 70%, and 90%, each time when the mPOFBG reached equilibrium condition. The exact same experiment was then repeated with a new identical mPOFBG, but stopping the annealing phase at 70%, 50%, 30% and 10% RH, respectively. The results of the five humidity controlled annealing experiments are reported in Fig. 2.

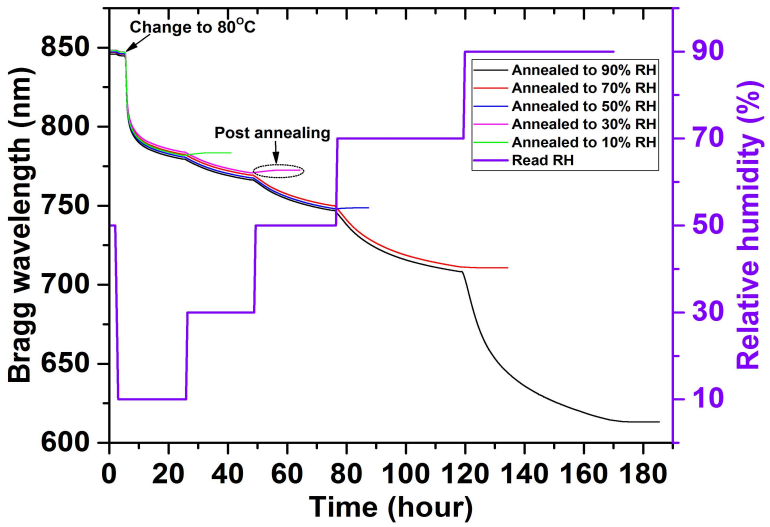

Fig. 2. Complete annealing process of PMMA mPOFBGs annealed at 80°C and up to a relative humidity of 90% (black), 70% (red), 50% (blue), 30% (pink) and 10% (green). The relative humidity sequence is shown only for the pre-annealing and annealing phases.

As it can be seen from Fig. 2, during the annealing phase the first rapid blue-shift is due to the temperature being increased from 25°C to 80°C (at fixed RH of 10%). This shows that initially the fiber was releasing the frozen-in stress induced during the fabrication process very fast. After 20 hours the blue-shift rate had decreased to 0.3nm/hour for all cases and the humidity was increased to 30% for the first four cases. It can be seen that as the RH was increased by 20%, the rate of blue-shift abruptly increased. This abrupt increase became higher the higher the RH level was and led to very large blue-shifts. Thus, for the higher RH levels, such as 70% and 90%, not only the rate of the blue-shift was faster but also the amount of the shift was larger. The total blue-shift for the mPOFBG annealed up to 90% was more than 230nm.

After each series of annealing experiment the humidity response of the mPOFBG sensor has been measured at three different temperatures: 25°C, 50°C and 75°C, in the interval of 10-90% RH, where the environmental chamber had greatest stability with a precision less than 0.3°C and 1% RH. For each temperature level, the humidity measurement has been done first by increasing the RH from 10% to 90%, with steps of 10% and then decreasing it from 90% to 10% with 10% steps. For both cases, the chamber was programmed to change the RH gradually over 30 mins and then to maintain the environmental conditions stable for 60 mins. Hence, the total time allowed before increasing or decreasing the relative humidity by 10% was 90mins. The response of the PMMA mPOFBG annealed to 90% RH for both increasing and decreasing relative humidity at 25°C is shown in Fig. 3(a). Figure 3(b) shows the comparison between humidity measurement at 25°C of the stabilized PMMA mPOFBGs that have been annealed to 90% and 10% RH.

#253345 Received 5 Nov 2015; revised 30 Dec 2015; accepted 4 Jan 2016; published 14 Jan 2016

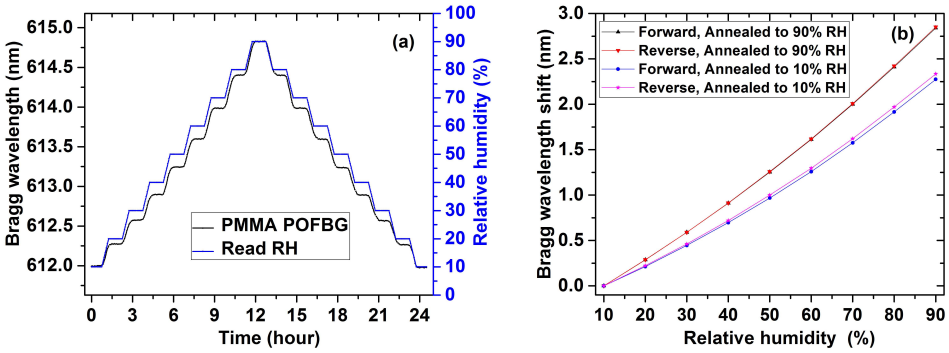

Fig. 3. (a) Measured humidity response at 25°C of PMMA mPOFBG annealed up to 90% RH versus time and humidity. The steps are defined in the text. (b) Corresponding stabilized response of the PMMA mPOFBGs annealed up to 90% and 10%.

The humidity sensitivity calculated by linear regression for the above humidity measurements are summarized in Fig. 4 for both increasing (circles) and decreasing (squares) humidity. The PMMA mPOFBG annealed up to 90% RH demonstrated the largest sensitivity to humidity, at all three temperature levels, while the one annealed only up to 10% RH had the lowest sensitivity.

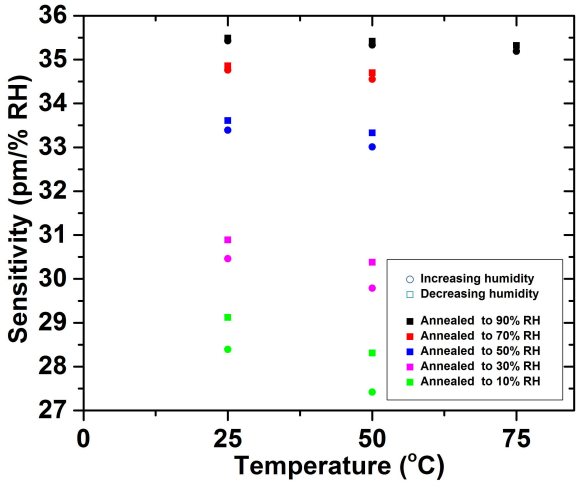

Fig. 4. Humidity sensitivity at 25°C and 50°C for PMMA mPOFBGs annealed to 90%, 70%, 50%, 30% and 10% RH and at 75°C for PMMA mPOFBG annealed to 90%.

The PMMA mPOFBG annealed up to 90% RH not only had the largest sensitivity, but also the lowest level of hysteresis, i.e., the smallest difference in sensitivity to humidity between the forward and reverse experiments. Importantly, the humidity sensitivity of the 90% mPOFBG is also to a good approximation temperature independent over the range of 25-75°C. From Fig. 4 it is important to notice that the hysteresis is considerably increased for mPOFBGs that have been annealed at lower levels of humidity. In addition these mPOFBGs annealed at low humidity also display a non-stable humidity response with a hysteresis that increases with operation temperature and a sensitivity that decreases with temperature.

At 75°C the PMMA mPOFBG annealed up to 90% measured a sensitivity of 35.19 ± 2.46 and 35.32 ± 2.54 pm/% RH, for increasing and decreasing humidity, respectively. Even at this

#253345 Received 5 Nov 2015; revised 30 Dec 2015; accepted 4 Jan 2016; published 14 Jan 2016

temperature the response thus to a good approximation hysteresis free. In contrast the other PMMA mPOFBGs annealed at a lower humidity showed a strong nonlinear decrease in the Bragg wavelength when the RH reached just above the annealing RH level as can be seen in Fig. 5. This showed that mPOFBGs annealed at low humidity or non-annealed mPOFBGs cannot be used for humidity sensing above a certain temperature level. Even if they were used only at low temperatures, their sensitivity to humidity is low, as seen in Fig. 4.

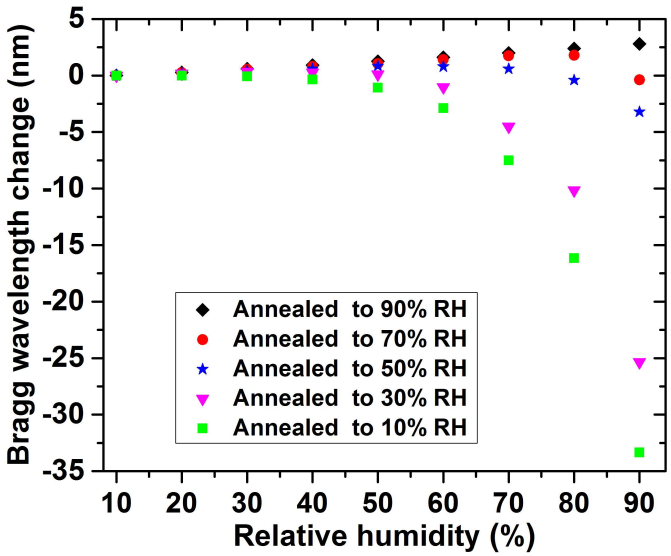

Fig. 5. Humidity responsivity at 75°C of PMMA POFBGs annealed up to 90%, 70%, 50%, 30%, and 10% RH.

In the above investigation and comparison between the performances of mPOFBGs annealed at different levels of humidity, we identified the mPOFBG annealed up to 90% RH as the one having the by far superior performance, i.e., the largest humidity sensitivity, the highest operation temperature, and the smallest hysteresis. The total annealing phase time of that mPOFBG was over 150 hours. Of course this can be shortened significantly by just directly annealing the mPOFBG at 90% RH and 80°C.

To demonstrate this we have done a sixth experiment. A new PMMA mPOFBG was inscribed at 850 nm in the same fiber type used for the above 5 series of experiments and annealed at constant 90% RH and 80°C, while tracking the Bragg wavelength. From Fig. 6(a) we see that the Bragg wavelength blue-shifted rapidly and took only about 24 hours to reach an equilibrium condition, which we defined earlier as when the rate of blue-shift has decreased to 0.3 nm/hour. It should be noticed that also in this case, coherently with the first experiment, the mPOFBG showed a permanent 235 nm blue-shift (in 24hours only), which is a record tuning of a POFBG without compromising the grating strength [21]. Figure 6(b) shows the amount of permanent blue-shift and strength of the PMMA mPOFBG recorded at ambient conditions before and after annealing at 80°C and 90% RH. This method of annealing at high humidity can therefore also be used to produce stable and strong gratings at short wavelengths where phase masks become more inefficient and expensive.

#253345 Received 5 Nov 2015; revised 30 Dec 2015; accepted 4 Jan 2016; published 14 Jan 2016

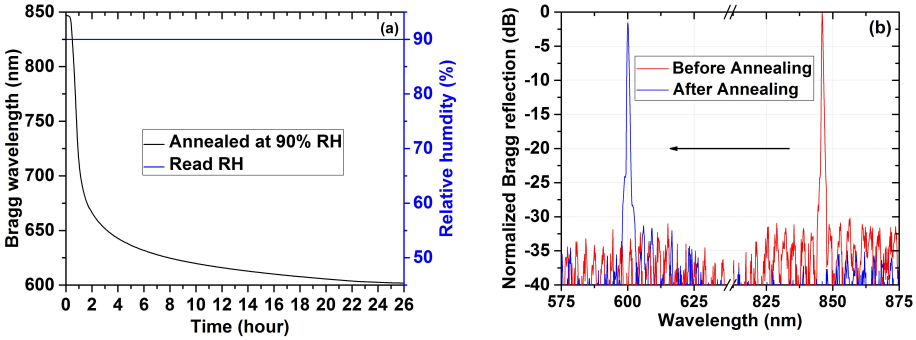

Fig. 6. (a) Annealing history of PMMA mPOFBGs annealed at 80°C and 90% RH. (b) Bragg reflection of PMMA mPOFBG before and after annealing at 80°C and at 90% RH both normalized to the non-annealed grating.

To test the responsivity of the annealed sensor humidity measurement has also been performed for this PMMA mPOFBG with the same procedure as used previously. For this PMMA mPOFBG the sensitivities returned by linear regression at 25°C, 50°C, and 75°C are 35.45 ± 2.58, 35.31 ± 2.49, and 35.17 ± 2.51 pm/%RH for increasing humidity and 35.50 ± 2.58, 35.43 ± 2.50, 35.28 ± 2.52 pm/%RH for decreasing humidity, respectively. These figures show that the humidity responsivities are in agreement with the mPOFBG annealed up to 90%RH in the early experiment. Therefore, by annealing a POFBG at fixed 90% RH and 80°C for only 24 hours it is possible to develop a stable humidity sensor that is able to operate between 25 and 75 °C in the range of 10-90% RH. The specific Bragg wavelength change versus increasing relative humidity at the three temperatures is plotted in Fig. 7.

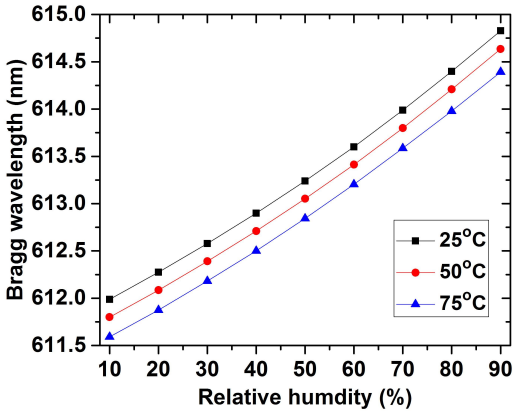

Fig. 7. Bragg wavelength change versus increasing in relative humidity at 25°C, 50°C and 75°C.

3. Conclusion

Our controlled annealing experiments have shown that when PMMA POFBGs are annealed at a given temperature and humidity the FBG wavelength shifts to the blue. The shift rate continuously decreases and eventually the shift stops. However, we have shown that when the humidity is again increased the blue-shift starts again at a higher rate than before and giving a larger total blue-shift. The rate increase and the total shift become larger with increasing

#253345 Received 5 Nov 2015; revised 30 Dec 2015; accepted 4 Jan 2016; published 14 Jan 2016

humidity. This shows that a high humidity level is very important in facilitating the annealing process.

PMMA POFBGs that are not annealed or annealed at a low humidity level have been shown to have low sensitivity to humidity and high hysteresis, particularly when operated at high temperature. PMMA POFBGs annealed at low humidity or not annealed therefore cannot be used for humidity sensing above a certain temperature level. Even if they are used at low temperature, they have a small sensitivity to humidity and high hysteresis. On the other hand, PMMA POFBGs annealed at high humidity (90% RH) have been demonstrated to have a superior response with a very low hysteresis, an improved sensitivity, and an increased stable operation temperature. PMMA POFBGs annealed at 80°C and 90% RH gave the same sensitivity, 35 pm/%RH, at 25, 50 and 75°C.

Finally, we have demonstrated that by annealing PMMA POFBGs for 24 hours at 80°C and 90% RH it is possible to tune the FBG wavelength, without loss in the grating strength, by a huge amount. This allows production of gratings at short wavelengths where POFs show lower loss but where the phase mask technique poses limitations in terms of efficiency and costs.

Acknowledgments

The research leading to these results has received funding from the People Programme (Marie Curie Actions) of the European Union's Seventh Framework Programme FP7/2007-2013/ under REA grant agreement n° 608382. The authors also acknowledge financial support from Innovation Fund Denmark for the project ShapeOCT (J. No. 4107-00011A), the Eugen Lommel Stipend for financial support and Danish Council for Independent Research (FTP Case No. 4184-00359B).

#253345 Received 5 Nov 2015; revised 30 Dec 2015; accepted 4 Jan 2016; published 14 Jan 2016

Paper 2

Solution-mediated annealing of polymer optical fiber Bragg gratings at room temperature

A.Fasano, G.Woyessa, J. Janting, Henrik K. Rasmussen, and O.Bang

IEEE Photonics Technology Letters 29(8), 687-690 (2017)

Solution-Mediated Annealing of Polymer Optical Fiber Bragg Gratings at Room Temperature

Andrea Fasano, Getinet Woyessa, Jakob Janting, Henrik K. Rasmussen, and Ole Bang

***Abstract*— In this letter, we investigate the response of poly(methylmethacrylate) (PMMA) microstructured polymer optical fiber Bragg gratings (POFBGs) after immersion in methanol/water solutions at room temperature. As the glass transition temperature of solution-equilibrated PMMA differs from the one of solvent-free PMMA, different concentrations of methanol and water lead to various degrees of frozen-in stress relaxation in the fiber. After solvent evaporation, we observe a permanent blue-shift in the grating resonance wavelength. The main contribution in the resonance wavelength shift arises from a permanent change in the size of the fiber. The results are compared with conventional annealing. The proposed methodology is cost-effective as it does not require a climate chamber. Furthermore, it enables an easy-to-control tuning of the resonance wavelength of POFBGs.**

***Index Terms*— Annealing, plastic optical fiber, optical fiber sensors, Bragg gratings, polymers, absorption.**

I. Introduction

SENSING devices such as fiber Bragg gratings (FBGs) based on polymer optical fibers (POFs) bring about various advantages over their counterparts made of silica. They offer an increased sensitivity to stress due to a considerably lower Young's modulus and a wider range of strains available [1], [2]. Also, polymer optical fibers are ideal candidates for *in-vivo* biosensing applications [3]–[5] due to their non-brittle nature, flexibility in bending and biocompatibility. Further advantages are ease of handling, low densities, and low processing temperatures, as well as flexibility in the production process (choice of functional group, polymerization method, etc.) [1], [2]. Poly(methyl methacrylate) (PMMA) is the most common material for polymer optical fiber Bragg gratings (POFBGs) [6]–[8]. However, for more specific purposes, such as humidity insensitivity, low attenuation, and high-temperature resistance, TOPAS (COC, cyclic olefin copolymer) [9], CYTOP (an amorphous fluoropolymer) [10], and polycarbonate (PC) [11] POFBGs, respectively, have been developed.

Manuscript received December 14, 2016; revised February 12, 2017; accepted February 23, 2017. Date of publication March 6, 2017; date of current version March 23, 2017. This work was supported by the People Programme (Marie Curie Actions) of the European Union's Seventh Framework Programme FP7/2007-2013/ under REA Grant Agreement 608382.

A. Fasano and H. K. Rasmussen are with the Department of Mechanical Engineering, Technical University of Denmark, DK-2800 Kongens Lyngby, Denmark (e-mail: andfas@mek.dtu.dk; hkra@mek.dtu.dk).

G. Woyessa, J. Janting, and O. Bang are with the Department of Photonics Engineering, Technical University of Denmark, DK-2800 Kongens Lyngby, Denmark (e-mail: gewoy@fotonik.dtu.dk; jajant@fotonik.dtu.dk; oban@fotonik.dtu.dk).

Digital Object Identifier 10.1109/LPT.2017.2678481

One particular problem associated with the use of POFBGs is their limited thermal stability at temperatures even much lower than their glass transition temperature (T_g) [12]. To overcome this problem, proper annealing is typically required. Annealing of POFs and POFBGs has recently been the subject of an increasing number of studies [12]–[16]. This process has proved well in enhancing the thermal stability and widening the range of linear temperature response of POFBGs [12], [13]. The recently published papers by Woyessa *et al.* [15] and Stajanca *et al.* [16] focus on how the particular value of relative humidity (RH) at which annealing is carried out can in fact affect the properties of PMMA POFs and POFBGs. The RH effect is due to the fact that water acts as a plasticizer for PMMA and lowers its T_g [16], [17]. Such investigations consider the effect of RH when the annealing temperature is itself particularly high, about 80-90 °C. This effect is huge because of the elevated annealing temperature [15], [16]. Zhang *et al.* [8] also studied the effect of RH on the wavelength drift of PMMA-based POFBGs, but this mechanism was caused by the optical absorption increasing with RH, which led to an increase in internal temperature due to photothermal effect.

Early investigations showed that, when PMMA is at equilibrium with water, the T_g of the polymer is lowered by approximately 20 °C compared to the dry one [17]. Given that the T_g of PMMA is typically 105-115 °C [14], [16], its minimum actual T_g at saturation ranges between 85 °C and 95 °C. Similar considerations apply to several other polymer-solvent combinations. Indeed, the T_g of a polymeric material equilibrated with one or more solvents may be different from that of the pure polymer. To an extent that depends on the specific way polymer and solvent/solution interact. For instance, if a swelling agent for PMMA is used, such as methanol, the actual T_g of the polymer-solution system at equilibrium can go down to room temperature [18].

The present work is based on the following idea: why not to generate an effect equivalent to conventional annealing simply by lowering the actual T_g of the polymer to such an extent that room temperature 'matters' energetically? In other words, immersing a PMMA fiber in methanol/water solutions at room temperature may have an effect akin to annealing a solvent-free fiber at high temperature and controlled humidity. Therefore, instead of increasing the local temperature to approach T_g in a climate chamber at controlled RH, here we want to observe a comparable effect by using a suitable T_g–lowering solution. In particular, the specific aim of this work is to investigate the relaxation of PMMA microstructured polymer

optical fiber Bragg gratings (mPOFBGs) when immersed in methanol/water solutions. As a consequence of the solution concentration dependence of the T_g, varying methanol/water ratio implies changing the T_g of the PMMA fiber when equilibrated with the solution, which results in different degrees of frozen-in draw stress relaxation. The solution-based annealing is cost-effective as it does not require a climate chamber. It would reduce the overall cost of POFBG sensor development and it is also better suited for large-scale production processes than annealing in a climate chamber.

II. Solution-Mediated Annealing Method

Early studies by Williams *et al.* focused on the effect of the presence of methanol on the T_g of PMMA [18]. Depending on the weight-average molecular weight (M_w), for methanol-equilibrated PMMA systems they found a T_g ranging from 20 °C ($M_w = 23500$ g/mol) to 30 °C ($M_w = 550000$ g/mol). The weight-average molecular weight can be thought of as an average polymer chain length. Since PMMA polymers optimal for the fiber draw process have an M_w being within this range [14], [19], the T_g of a PMMA-based optical fiber equilibrated in methanol corresponds to room temperature. When heated up close to its actual T_g, a polymer fiber tends to relax frozen-in draw stresses. This can affect the dimensional stability of the fiber and therefore limit its operating temperature to values well below the theoretical ones. Heating up an unannealed fiber to even modest temperatures during operation can yield a permanent blue-shift in the resonance wavelength of Bragg gratings [12]. Furthermore, their optical and mechanical properties may also be affected [14], [16]. As a result of the polymer fiber draw process, polymer chains are aligned along the drawing direction, which leads to the formation of frozen-in stress in the fiber. Such degree of alignment depends on the draw stress applied to the preform (1-stage drawing) or both preform and cane (2-stage drawing) [14], [16], [19]. After drawing, polymer chains are in a non-equilibrium configuration and have the tendency to move back toward the original state as soon as they are provided with enough energy to do so. The higher the temperature, the greater the rearrangement of the polymer chains relaxing the frozen-in draw stresses. The relaxation is typically accompanied by a change in dimension of the fiber, i.e. shrinkage in the axial direction as well as an increase in diameter [12], [14], [16]. Considering that the relaxation occurs when the local temperature approaches T_g, we can theoretically obtain an effect similar to annealing if we simply lower the T_g of a PMMA fiber by immersing it in a methanol-based solution at room temperature. The literature reports the use of methanol to facilitate the doping of PMMA canes for fiber drawing with various compounds, e.g. benzyl dimethyl ketal (BDK) [20] and rhodamine 6G [21]. However, pure methanol cannot be directly used for fibers, since the very low T_g would lead to an excessive draw stress relaxation in PMMA mPOFBGs. This effect is much less pronounced at the cane level, as at this stage the polymer canes are thicker and the polymer chains are less oriented than in the final fiber.

The best way to obtain a sufficiently low T_g but not too close to room temperature is to use a proper diluent, similarly to what is done in annealing using a climate chamber where the temperature is high but lower than T_g [15], [16]. Water represents a good candidate in this regard, as it is miscible with methanol and, as already mentioned, the T_g of water-saturated PMMA is known from the literature to be about 20 °C lower than that of the pure polymer [17]. As a result, the addition of water to a methanol-based solution is expected to increase the T_g of PMMA fibers equilibrated with the solution.

TABLE I
Initial Bragg Wavelength for the Different Experiments

Methanol/water v/v [%]	Initial Bragg wavelength [nm]
50/50	847.3 (grating 1); 845.5 (grating 2)
60/40	846.2 (grating 1); 846.6 (grating 2)
70/30	847.3 (grating 1); 847.4 (grating 2)

III. Experiments And Results

An in-house made 2-ring PMMA mPOF was used in the experiments. The microstructured fiber was manufactured at DTU Fotonik from GEHR PMMA rods (glass transition of the bulk material being 106 °C) by using the drill-and-draw technique [19]. It had an average diameter of approximately 150 μm and an 8-μm core. The average draw temperature and draw stress were 190 °C and 10 MPa, respectively. The hole diameter and pitch size were 2 μm and 5 μm, respectively. The resulting hole to pitch ratio of 40% ensured that the fiber was endlessly single mode [22]. Bragg gratings were inscribed into the fiber by using a CW HeCd laser operating at 325 nm (IK5751I-G, Kimmon). We used the phase mask method for grating writing and an inscription setup being the same as the one reported in Bundalo *et al.* [23]. For inscription, a laser power of 20 mW and a custom-made phase mask by Ibsen Photonics A/S, optimized for writing at 325 nm and having a uniform period of 572.4 nm, were used. Six FBGs were inscribed in six PMMA mPOFs from the same fiber draw and tested in solutions at three different volumetric concentrations (v/v) of methanol/water, 50:50%, 60:40%, and 70:30% (uncertainty of 1% v/v). The grating behavior in each solution was tested with two different FBGs. The initial resonance wavelength of the gratings used in the experiments is reported in Table I. Note, the small differences in initial Bragg wavelength are due to the slightly different pre-strain levels applied during the grating inscription. CHROMASOLV methanol (Sigma-Aldrich, purity $\geq$ 99.9% by weight) and Milli-Q water were used. In both cases, 10 ml solutions were prepared in 10 ml graduated cylinders that were sealed at the top with Parafilm to avoid evaporation during the measurements. We used a supercontinuum source (SuperK Compact, NKT Photonics) as the light source and a spectrometer (CCS175 – Compact Spectrometer, Thorlabs) to track the reflection peak continuously throughout the experiments. The FBGs were immersed and kept in the respective solutions as long as the relaxation continued. Fig. 1 shows an example of a Bragg grating peak monitored during the experiments. Three different phenomena were expected to occur: solution absorption (red-shift) and frozen-in stress relaxation (blue-shift) while the grating was immersed in the solution, and desorption (blue-shift) as well as some residual relaxation (blue-shift)

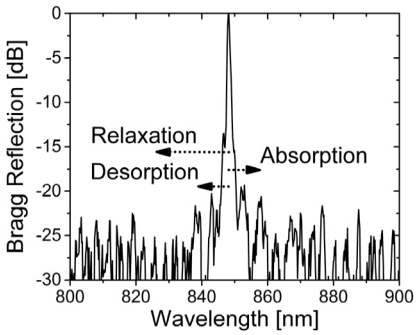

Fig. 1. Normalized Bragg reflection spectrum monitored throughout the experiments at room temperature. Stress relaxation and solution absorption-desorption phenomena interplay and contribute to the observed overall shift.

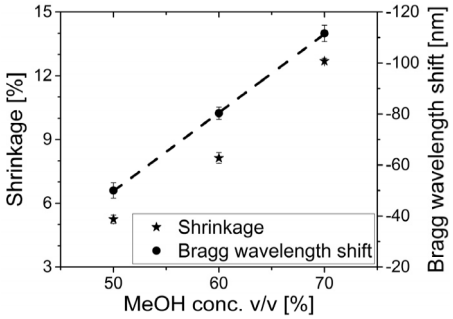

Fig. 3. Shrinkage and Bragg wavelength shift versus MeOH concentration. The fibers and gratings were checked after one week and both shrinkage and resonance wavelength shift were permanent. The dotted line represents the trend of the rate of Bragg wavelength shift within the range 50-70% v/v.

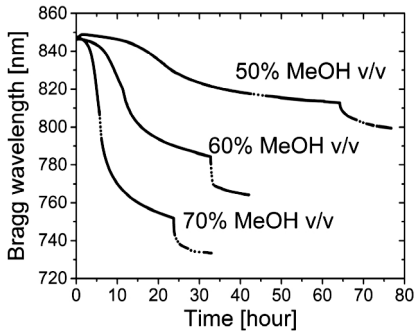

Fig. 2. Fiber Bragg grating wavelength versus methanol (MeOH) volumetric concentration. Note, a few experimental data were missing due to high reflection noise and were recovered by fitting (represented by dotted lines).

once the fiber was removed from the solution. The FBGs were taken out of the solution once the rate of Bragg reflection wavelength blue-shift was $\sim$ 0.4 nm/hour (absolute value), after which the desorption-evaporation of the solution was monitored.

Fig. 2 shows an example of the Bragg grating wavelength as a function of time for a PMMA mPOFBG immersed in a solution of methanol and water 50:50% for 64 hours (stopping criterion met), after which the grating was removed from the solution and monitored for further 13 hours to study the grating response during solvent evaporation. In this experiment the overall resonance wavelength shift obtained after solvent evaporation was -50.0 ± 3.0 nm (error expressed in terms of standard deviation). The absorption of the methanol/water solution changed both refractive index and fiber size. Since the shift was large and permanent (same value after one week), the observed behavior must be due mainly to a permanent change in the size of the fiber, as already seen in high-temperature annealing of polymer optical fibers and sensors [12], [14], [16]. An initial red-shift in Bragg wavelength was observed, with a maximum of 1.5 ± 0.1 nm after approximately 100 minutes, because of the swelling dominating the chain alignment relaxation at the beginning of the experiment. This was the result of a temporary positive balance between red-shift due to solution-mediated swelling and blue-shift caused by chain alignment relaxation. However, after about 8 hours the total shift referred to the initial Bragg wavelength became constantly negative. This corresponded to the tendency towards relaxation becoming stronger and stronger after an initial lag phase due to the initial diffusion of the solution into the fiber. However, the real contribution due to absorption-swelling, which would lead to a much greater red-shift than the observed one, was hidden by the incipient relaxation (blue-shift). This can easily be seen in Fig. 2, where the rapid solvent evaporation upon FBG removal from the solution corresponds to a sudden and sharp blue-shift of the resonance wavelength. The fast evaporation process was facilitated by the small diameter of the fiber. The further down-shift occurred after removal of the Bragg grating from the solution was measured to be -15.0 ± 1.6 nm at the end of the experiment. The shift was toward blue as the evaporation implied further fiber shrinkage. The mild decrease observed after the sharp downward jump in resonance wavelength was due to solvent evaporation and some residual relaxation becoming less and less important as the evaporation went on.

To obtain a measurement of the corresponding fiber shrinkage, we repeated the in-solution annealing experiments applying similar conditions to four PMMA mPOFs from the same draw. Fig. 3 shows the permanent values of both shrinkage (stars) and Bragg wavelength shift (circles). At 50% v/v of methanol the average fiber shrinkage was $5.25\pm0.20\%$.

Fig. 2 further shows the Bragg grating wavelength as a function of time for two PMMA mPOFBGs being immersed in a solution methanol/water 60:40% v/v and 70:30% v/v for 33 hours and 24 hours, respectively, and further monitored for 9 hours during desorption-evaporation of the solution once the gratings were removed from the solution. Three main differences with respect to the case 50:50% can be noticed. First, the relaxation process was clearly faster than in the previous case due to the higher concentration of methanol, since methanol is a stronger swelling agent for PMMA than water. In particular, the relaxation speed increased with methanol concentration. Second, as expected the overall Bragg wavelength shifts were considerably higher in absolute value, being -80.3 ± 2.4 nm and -111.6 ± 3.2 nm for 60% and 70% v/v of methanol, respectively (Fig. 3). The dispersion in the data can be due to the uncertainty in solution concentration as well as to fluctuations in room temperature and fiber diameter. Fig. 3 shows that also the fiber shrinkage increased with methanol concentration, being $8.13\pm0.25\%$ and $12.69\pm0.13\%$ for the experiments at 60% and 70% v/v, respectively. Third, probably because of the relaxation occurring very fast, in these

TABLE II
IMPROVED THERMAL STABILITY OF IN-SOLUTION ANNEALED PMMA mPOFs

Methanol/water v/v [%]	Fiber shrinkage [%]
Unannealed	8.13±0.32
50/50	5.41±0.27
60/40	4.29±0.13
70/30	3.08±0.14

two cases only a slight initial red-shift in Bragg wavelength was observed, although the desorption curves during solvent evaporation were steeper, as can be easily seen in Fig. 2. Note, the final Bragg wavelength shifts obtained in the cases 60% and 70% v/v are comparable with the ones obtained by annealing at 80 °C in a climate chamber at 30% RH (−76.2 nm [15]) and 70% RH (−136.5 nm [15]), respectively. Also, similarly to conventional annealing [15], in all the three cases (50%, 60% and 70% v/v of methanol) there was no significant loss in grating strength, as it was lowered by 2 dB at the most.

In Fig. 3 it can also be seen that a decrease in resonance wavelength by about 3 nm can be expected if we run the experiment with a methanol concentration being increased by 1% within the range 50%-70% v/v (dotted line). This value can be used to calculate the solution concentration approximately required to tune the resonance wavelength of PMMA POFBGs down to a specific spectral region of interest.

We further tested the previously treated fibers together with four PMMA mPOFs from the same draw in a climate chamber (CLIMACELL, MMM Group) at 80 °C and 50% RH for 48 hours. The length of each fiber was measured before and after the experiment. The results are reported in terms of shrinkage in Table II. The shrinkage was significantly lower for the fibers annealed in solution compared to unannealed fibers, and it decreased with increasing methanol/water ratio used for the in-solution treatment. This shows that the proposed method can lead to enhancing the thermal stability of PMMA fibers.

IV. CONCLUSION

The possibility of relaxing stresses frozen in the PMMA fibers by using methanol/water solutions was demonstrated. By immersing two-ring PMMA mPOFBGs in solutions at various concentrations of methanol and water, it was possible to obtain significant and permanent Bragg wavelength blue-shifts at room temperature. The thermal stability of the PMMA mPOFs was seen to be improved as a consequence of the solution-mediated annealing. This technique does not require the use of a climate chamber, and it is easy to control and implement. In addition, if an appropriate combination of solvents is used, the solution-based annealing method may also be applied to other polymers such as TOPAS and PC.

REFERENCES

[1] D. J. Webb, "Polymer fiber Bragg grating sensors and their applications," in *Optical Fiber Sensors Advanced Techniques and Applications*, G. Rajan Ed. Boca Raton, FL, USA: CRC Press, 2015, pp. 257–276.

[2] K. Peters, "Polymer optical fiber sensors—A review," *Smart Mater. Struct.*, vol. 20, no. 1, p. 013002, 2011.

[3] J. B. Jensen, P. E. Hoiby, G. Emiliyanov, O. Bang, L. H. Pedersen, and A. Bjarklev, "Selective detection of antibodies in microstructured polymer optical fibers," *Opt. Exp.*, vol. 13, no. 15, pp. 5883–5889, 2005.

[4] G. Emiliyanov, P. E. Høiby, L. H. Pedersen, and O. Bang, "Selective serial multi-antibody biosensing with TOPAS microstructured polymer optical fibers," *Sensors*, vol. 13, no. 3, pp. 3242–3251, Mar. 2013.

[5] H. U. Hassan, K. Nielsen, S. Aasmul, and O. Bang, "Polymer optical fiber compound parabolic concentrator tip for enhanced coupling efficiency for fluorescence based glucose sensors," *Biomed. Opt. Exp.*, vol. 6, no. 12, pp. 5008–5020, 2015.

[6] G. D. Peng, Z. Xiong, and P. L. Chu, "Photosensitivity and gratings in dye-doped polymer optical fibers," *Opt. Fiber Technol.*, vol. 5, no. 2, pp. 242–251, Apr. 1999.

[7] Z. Xiong, G.-D. Peng, B. Wu, and P. L. Chu, "Highly tunable Bragg gratings in single-mode polymer optical fibers," *IEEE Photon. Technol. Lett.*, vol. 11, no. 3, pp. 352–354, Mar. 1999.

[8] W. Zhang, A. Abang, D. J. Webb, and G. D. Peng, "Wavelength drift of PMMA-based optical fiber Bragg grating induced by optical absorption," *IEEE Photon. Technol. Lett.*, vol. 27, no. 4, pp. 336–339, Feb. 15, 2015.

[9] I. P. Johnson *et al.*, "Optical fibre Bragg grating recorded in TOPAS cyclic olefin copolymer," *Electron. Lett.*, vol. 47, no. 4, pp. 271–272, Apr. 2011.

[10] A. Lacraz, M. Polis, A. Theodosiou, C. Koutsides, and K. Kalli, "Femtosecond laser inscribed Bragg gratings in low loss CYTOP polymer optical fiber," *IEEE Photon. Technol. Lett.*, vol. 27, no. 7, pp. 693–696, Apr. 1, 2015.

[11] A. Fasano *et al.*, "Fabrication and characterization of polycarbonate microstructured polymer optical fibers for high-temperature-resistant fiber Bragg grating strain sensors," *Opt. Mater. Exp.*, vol. 6, no. 2, pp. 649–659, 2016.

[12] K. E. Carroll, C. Zhang, D. J. Webb, K. Kalli, A. Argyros, and M. C. J. Large, "Thermal response of Bragg gratings in PMMA microstructured optical fibers," *Opt. Exp.*, vol. 15, no. 14, pp. 8844–8850, Jul. 2007.

[13] W. Yuan *et al.*, "Improved thermal and strain performance of annealed polymer optical fiber Bragg gratings," *Opt. Commun.*, vol. 284, no. 1, pp. 176–182, 2011.

[14] C. Jiang, M. G. Kuzyk, J.-L. Ding, W. E. Johns, and D. J. Welker, "Fabrication and mechanical behavior of dye-doped polymer optical fiber," *J. Appl. Phys.*, vol. 92, no. 1, pp. 4–12, 2002.

[15] G. Woyessa, K. Nielsen, A. Stefani, C. Markos, and O. Bang, "Temperature insensitive hysteresis free highly sensitive polymer optical fiber Bragg grating humidity sensor," *Opt. Exp.*, vol. 24, no. 2, pp. 1206–1213, 2016.

[16] P. Stajanca, O. Cetinkaya, M. Schukar, and K. Krebber, "Molecular alignment relaxation in polymer optical fibers for sensing applications," *Opt. Fiber Technol.*, vol. 28, pp. 11–17, 2016.

[17] L. S. A. Smith and V. Schmitz, "The effect of water on the glass transition temperature of poly(methyl methacrylate)," *Polymer*, vol. 29, no. 10, pp. 1871–1878, 1988.

[18] D. R. G. Williams, P. E. M. Allen, and V. T. Truong, "Glass transition temperature and stress relaxation of methanol equilibrated poly (methyl methacrylate)," *Eur. Polym. J.*, vol. 22, no. 11, pp. 911–919, 1986.

[19] M. C. J. Large, G. W. Barton, L. Poladian, and M. A. van Eijkelenborg, *Microstructured Polymer Optical Fibres*. New York, NY, USA: Springer, 2008.

[20] D. Sáez-Rodríguez, K. Nielsen, H. K. Rasmussen, O. Bang, and D. J. Webb, "Highly photosensitive polymethyl methacrylate microstructured polymer optical fiber with doped core," *Opt. Lett.*, vol. 38, no. 19, pp. 3769–3772, 2013.

[21] M. C. J. Large, S. Ponrathnam, A. Argyros, N. S. Pujari, and F. Cox, "Solution doping of microstructured polymer optical fibres," *Opt. Exp.*, vol. 12, no. 9, pp. 1966–1971, 2004.

[22] B. Kuhlmey, R. C. McPhedran, and C. M. de Sterke, "Modal cutoff in microstructured optical fibers," *Opt. Lett.*, vol. 27, no. 19, pp. 1684–1686, 2002.

[23] I.-L. Bundalo, K. Nielsen, C. Markos, and O. Bang, "Bragg grating writing in PMMA microstructured polymer optical fibers in less than 7 minutes," *Opt. Exp.*, vol. 22, no. 5, pp. 5270–5276, 2014.

Paper 3

Fabrication and characterization of polycarbonate microstructured polymer optical fibers for high-temperature-resistant fiber Bragg grating strain sensors

A.Fasano, G.Woyessa, P.Stajanca, C. Markos, A.Stefani, K.Nielsen, H. K. Rasmussen, K. Krebber, and O. Bang

Optical Materials Express 6(2), 649-659 (2016).

Fabrication and characterization of polycarbonate microstructured polymer optical fibers for high-temperature-resistant fiber Bragg grating strain sensors

Andrea Fasano,[1] Getinet Woyessa,[2] Pavol Stajanca,[3] Christos Markos,[2,4] Alessio Stefani,[2,5] Kristian Nielsen,[2] Henrik K. Rasmussen,[1] Katerina Krebber,[3] and Ole Bang[2,*]

[1] *DTU Mekanik, Department of Mechanical Engineering, Technical University of Denmark, 2800 Kgs. Lyngby, Denmark*

[2] *DTU Fotonik, Department of Photonics Engineering, Technical University of Denmark, 2800 Kgs. Lyngby, Denmark*

[3] *Division 8.6 "Optical and Fibre Optic Methods", BAM Federal Institute for Materials Research and Testing, 12205 Berlin, Germany*

[4] *CREOL, The College of Optics & Photonics, University of Central Florida, 4000 Central Florida Blvd., Orlando, FL 32816, USA*

[5] *Institute of Photonics and Optical Science (IPOS), School of Physics, The University of Sydney, NSW 2006, Australia*

[*] *oban@fotonik.dtu.dk*

Abstract: Here we present the fabrication of a solid-core microstructured polymer optical fiber (mPOF) made of polycarbonate (PC), and report the first experimental demonstration of a fiber Bragg grating (FBG) written in a PC optical fiber. The PC used in this work has a glass transition temperature of 145°C. We also characterize the mPOF optically and mechanically, and further test the sensitivity of the PC FBG to strain and temperature. We demonstrate that the PC FBG can bear temperatures as high as 125°C without malfunctioning. In contrast, polymethyl methacrylate-based FBG technology is generally limited to temperatures below 90°C.

OCIS codes: (060.2370) Fiber optics sensors; (060.3735) Fiber Bragg gratings; (060.4005) Microstructured fibers; (060.2270) Fiber characterization; (160.5470) Polymers.

References and links

1. D. J. Webb, "Polymer Fiber Bragg Grating Sensors and Their Applications," in *Optical Fiber Sensors: Advanced Techniques and Applications*, G. Rajan, ed. (CRC Press, 2015).
2. K. Peters, "Polymer optical fiber sensors — a review," Smart Mater. Struct. **20**(1), 013002 (2011).
3. Cambridge University Engineering Department, *Materials Data Book*, (Cambridge University Engineering Department, 2003), http://www-mdp.eng.cam.ac.uk/web/library/enginfo/cueddatabooks/materials.pdf.
4. J. Jensen, P. Hoiby, G. Emiliyanov, O. Bang, L. Pedersen, and A. Bjarklev, "Selective detection of antibodies in microstructured polymer optical fibers," Opt. Express **13**(15), 5883–5889 (2005).
5. G. Emiliyanov, J. B. Jensen, O. Bang, P. E. Hoiby, L. H. Pedersen, E. M. Kjaer, and L. Lindvold, "Localized biosensing with Topas microstructured polymer optical fiber," Opt. Lett. **32**(5), 460–462 (2007).
6. G. Emiliyanov, P. E. Høiby, L. H. Pedersen, and O. Bang, "Selective serial multi-antibody biosensing with TOPAS microstructured polymer optical fibers," Sensors (Basel) **13**(3), 3242–3251 (2013).
7. H. U. Hassan, K. Nielsen, S. Aasmul, and O. Bang, "Polymer optical fiber compound parabolic concentrator tip for enhanced coupling efficiency for fluorescence based glucose sensors," Biomed. Opt. Express **6**(12), 5008–5020 (2015).
8. G. D. Peng, Z. Xiong, and P. L. Chu, "Photosensitivity and gratings in dye-doped polymer optical fibers," Opt. Fiber Technol. **5**(2), 242–251 (1999).
9. Z. Xiong, G. D. Peng, B. Wu, and P. L. Chu, "Highly tunable Bragg gratings in single-mode polymer optical fibers," IEEE Photonics Technol. Lett. **11**(3), 352–354 (1999).
10. W. Zhang, A. Abang, D. J. Webb, and G.-D. Peng, "Wavelength Drift of PMMA-Based Optical Fiber Bragg Grating Induced by Optical Absorption," IEEE Photonics Technol. Lett. **27**(4), 336–339 (2015).
11. A. Lacraz, M. Polis, A. Theodosiou, C. Koutsides, and K. Kalli, "Femtosecond Laser Inscribed Bragg Gratings in Low Loss CYTOP Polymer Optical Fiber," IEEE Photonic. Tech. L. **27**(7), 693–696 (2015).

#255045 Received 3 Dec 2015; revised 15 Jan 2016; accepted 17 Jan 2016; published 27 Jan 2016

12. I. P. Johnson, W. Yuan, A. Stefani, K. Nielsen, H. K. Rasmussen, L. Khan, D. J. Webb, K. Kalli, and O. Bang, "Optical fibre Bragg grating recorded in TOPAS cyclic olefin copolymer," Electron. Lett. **47**(4), 271–272 (2011).
13. W. Yuan, L. Khan, D. J. Webb, K. Kalli, H. K. Rasmussen, A. Stefani, and O. Bang, "Humidity insensitive TOPAS polymer fiber Bragg grating sensor," Opt. Express **19**(20), 19731–19739 (2011).
14. C. Markos, A. Stefani, K. Nielsen, H. K. Rasmussen, W. Yuan, and O. Bang, "High-Tg TOPAS microstructured polymer optical fiber for fiber Bragg grating strain sensing at 110 degrees," Opt. Express **21**(4), 4758–4765 (2013).
15. M. van Eijkelenborg, M. Large, A. Argyros, J. Zagari, S. Manos, N. Issa, I. Bassett, S. Fleming, R. McPhedran, C. M. de Sterke, and N. A. P. Nicorovici, "Microstructured polymer optical fibre," Opt. Express **9**(7), 319–327 (2001).
16. J. C. Knight, T. A. Birks, P. S. J. Russell, and D. M. Atkin, "All-silica single-mode optical fiber with photonic crystal cladding," Opt. Lett. **21**(19), 1547–1549 (1996).
17. M. C. J. Large, L. Poladian, G. W. Barton, and M. A. van Eijkelenborg, *Microstructured Polymer Optical Fibres* (Springer, 2008).
18. A. Argyros, "Microstructures in Polymer Fibres for Optical Fibres, THz Waveguide, and Fibre-Based Metamaterials," ISRN Optics. 785162 (2013).
19. M. A. van Eijkelenborg, A. Argyros, and S. G. Leon-Saval, "Polycarbonate hollow-core microstructured optical fiber," Opt. Lett. **33**(21), 2446–2448 (2008).
20. J. Harrington, R. George, P. Pedersen, and E. Mueller, "Hollow polycarbonate waveguides with inner Cu coatings for delivery of terahertz radiation," Opt. Express **12**(21), 5263–5268 (2004).
21. G. T. T. Gibson, R. D. Wright, and R. D. Oleschuk, "Multiple electrosprays generated from a single polycarbonate microstructured fibre," J. Mass Spectrom. **47**(3), 271–276 (2012).
22. Y. Gao, N. Guo, B. Gauvreau, M. Rajabian, O. Skorobogata, E. Pone, O. Zabeida, L. Martinu, C. Dubois, and M. Skorobogatiy, "Consecutive Solvent Evaporation and Co-Rolling Techniques for Polymer Multilayer Hollow Fiber Preform Fabrication," J. Mater. Res. **21**(9), 2246–2254 (2006).
23. T. R. Woliński, M. Tefelska, K. Mileńko, A. Siarkowska, D. Budaszewski, A. W. Domański, S. Ertman, K. Orzechowski, K. Rutkowska, M. Sierakowski, E. Nowinowski-Kruszelnicki, R. Dąbrowski, and P. Mergo, "Photonic Liquid Crystal Fibers with Polymers," Acta Phys. Pol. A **124**(3), 613–616 (2013).
24. Y. Koike, T. Ishigure, and E. Nihei, "High-Bandwidth Graded-Index Polymer Optical Fiber," J. Lightwave Technol. **13**(7), 1475–1489 (1995).
25. A. Tanaka, H. Sawada, T. Takoshima, and N. Wakatsuki, "New plastic optical fiber using polycarbonate core and fluorescence-doped fiber for high temperature use," Fiber Integr. Opt. **7**(2), 139–158 (1988).
26. S. Irie and M. Nishiguchi, "Development of the heat resistant plastic optical fiber," in *Proceedings of the Third International Conference on Plastic Optical Fibres & Applications*, (Yokohama, Japan, 1994), pp. 88–91.
27. O. Ziemman, J. Krauser, P. E. Zamzow, and W. Daum, *POF Handbook. Optical Short Range Transmission Systems* (Springer, 2008), Chap. 2.
28. D. G. Legrand and J. T. Bendler, *Handbook of Polycarbonate Science and Technology* (Marcel Dekker, 2000).
29. Bayer MaterialScience AG, "Optical properties of Makrolon and Apec for non-imaging optics," (Bayer MaterialScience AG, 2014), http://www.plastics.covestro.com/Products/~/media/B6555362438341FF9804F21A253E5B23.ashx?la=en.
30. M. D. Migahed and H. M. Zidan, "Influence of UV-irradiation on the structure and optical properties of polycarbonate films," Curr. Appl. Phys. **6**(1), 91–96 (2006).
31. K. Hareesh, A. K. Pandey, Y. Sangappa, R. Bhat, A. Venkataraman, and G. Sanjeev, "Changes in the properties of Lexan polycarbonate by UV irradiation," Nucl. Instrum. Methods Phys. Res. B **295**, 61–68 (2013).
32. J. Liu, S. Wang, M. Lv, and X. Zeng, "Surface modification of bisphenol A polycarbonate material by ultraviolet Nd:YVO_4 laser high-speed microprocessing technology," J. Micromech. Microeng. **24**(8), 085002 (2014).
33. A. Mockutė, R. Tomašiūnas, R. Petruškevičius, and D. Jucius, "Formation technology of planar polymer waveguide structure," Lith. J. Phys. **47**(4), 411–414 (2007).
34. K. E. Carroll, C. Zhang, D. J. Webb, K. Kalli, A. Argyros, and M. C. J. Large, "Thermal response of Bragg gratings in PMMA microstructured optical fibers," Opt. Express **15**(14), 8844–8850 (2007).
35. A. Son, A. Alizadeh, and H. Marand, "On the multiple melting behavior of bisphenol-A polycarbonate," Polymer (Guildf.) **41**(25), 8879–8886 (2000).
36. B. T. Kuhlmey, R. C. McPhedran, and C. Martijn de Sterke, "Modal cutoff in microstructured optical fibers," Opt. Lett. **27**(19), 1684–1686 (2002).
37. N. Sultanova, S. Kasarova, and I. Nikolov, "Dispersion Properties of Optical Polymers," Acta Phys. Pol. A **116**(4), 585–587 (2009).
38. T. Yamashita and K. Kamada, "Intrinsic Transmission Loss of Polycarbonate Core Optical Fiber," Jpn. J. Appl. Phys. **32**(Part 1, No. 6A), 2681–2686 (1993).
39. T. B. Gorczyca and M.-Y. Shih, "Photo-defined Polymeric Photonic Materials and Processes," Proc. SPIE **5179**, 97–104 (2003).
40. A. Stefani, K. Nielsen, H. K. Rasmussen, and O. Bang, "Cleaving of TOPAS and PMMA microstructured polymer optical fibers: Core-shift and statistical quality optimization," Opt. Commun. **285**(7), 1825–1833 (2012).
41. A. Argyros, R. Lwin, S. G. Leon-Saval, J. Poulin, L. Poladian, and M. C. J. Large, "Low loss and temperature stable microstructured polymer optical fibers," J. Lightwave Technol. **30**(1), 192–197 (2012).

#255045 Received 3 Dec 2015; revised 15 Jan 2016; accepted 17 Jan 2016; published 27 Jan 2016

42. M. A. van Eijkelenborg, A. Argyros, A. Bachmann, G. Barton, M. C. J. Large, G. Henry, N. A. Issa, K. F. Klein, H. Poisel, W. Pok, L. Poladian, S. Manos, and J. Zagari, "Bandwidth and loss measurements of graded-index microstructured polymer optical," Electron. Lett. **40**(10), 592–593 (2004).
43. I.-L. Bundalo, K. Nielsen, C. Markos, and O. Bang, "Bragg grating writing in PMMA microstructured polymer optical fibers in less than 7 minutes," Opt. Express **22**(5), 5270–5276 (2014).
44. T. Wang, Q. Wang, Y. Luo, W. Qiu, G.-D. Peng, B. Zhu, Z. Hu, G. Zou, and Q. Zhang, "Enhancing photosensitivity in near UV/vis band by doping 9-vinylanthracene in polymer optical fiber," Opt. Commun. **307**, 5–8 (2013).
45. D. Sáez-Rodríguez, K. Nielsen, H. K. Rasmussen, O. Bang, and D. J. Webb, "Highly photosensitive polymethyl methacrylate microstructured polymer optical fiber with doped core," Opt. Lett. **38**(19), 3769–3772 (2013).
46. R. Oliveira, L. Bilro, and R. Nogueira, "Bragg gratings in a few mode microstructured polymer optical fiber in less than 30 seconds," Opt. Express **23**(8), 10181–10187 (2015).
47. W. Yuan, A. Stefani, M. Bache, T. Jacobsen, B. Rose, N. Herholdt-Rasmussen, F. K. Nielsen, S. Andresen, O. B. Sørensen, K. S. Hansen, and O. Bang, "Improved thermal and strain performance of annealed polymer optical fiber Bragg gratings," Opt. Commun. **284**(1), 176–182 (2011).
48. C. Jiang, M. G. Kuzyk, J.-L. Ding, W. E. Johns, and D. J. Welker, "Fabrication and mechanical behavior of dye-doped polymer optical fiber," J. Appl. Phys. **92**(1), 4–12 (2002).
49. A. Stefani, W. Yuan, C. Markos, and O. Bang, "Narrow Bandwidth 850-nm Fiber Bragg Gratings in Few-Mode Polymer Optical Fibers," IEEE Photonics Technol. Lett. **23**(10), 660–662 (2011).
50. I. P. Johnson, K. Kalli, and D. J. Webb, "827nm Bragg grating sensor in multimode microstructured polymer optical fibre," Electron. Lett. **46**(17), 1217–1218 (2010).
51. K. Kalli and D. J. Webb, "Polymer Optical Fiber-Based Sensors," in *Advanced Fiber Optics: Concepts and Technology*, L. Thévenaz, ed. (EPFL Press, 2011).
52. B. Crist, "Yield processes in glassy polymers," in *The Physics of Glassy Polymers*, R. N. Haward and R. J. Young, ed. (Springer Science & Business Media, 1997).
53. N. G. McCrum, C. P. Buckley, and C. B. Bucknall, *Principles of Polymer Engineering* (Oxford University Press, 1997), Chap. 5.
54. GEHR GmbH, "Technical Data Sheet – GEHR PMMA ," (GEHR GmbH, 2013), http://www.gehrplastics.com/images/upload/downloads/tech_datenblaetter/acrylic/PMMA_en.pdf.
55. TOPAS Advanced Polymers Inc, "Data Sheet - TOPAS 8007S-04," (TOPAS Advanced Polymers Inc., 2014), http://www.topas.com/sites/default/files/TDS_8007S-04_english%20units_2.pdf.
56. A. Stefani, S. Andresen, W. Yuan, N. Herholdt-Rasmussen, and O. Bang, "High Sensitivity Polymer Optical Fiber-Bragg-Grating-Based Accelerometer," IEEE Photonics Technol. Lett. **24**(9), 763–765 (2012).

1. Introduction

Polymer optical fiber (POF) sensors offer several advantages over their silica-based counterpart. First of all, POFs have a larger strain range available and an increased sensitivity to stress due to a considerably lower Young's modulus [1,2]. Young's modulus is in the range 68-74 GPa for silica glass, 2.2-3.8 GPa for polymethyl methacrylate (PMMA), and 2.0-2.4 GPa for polycarbonate (PC) [3]. Because of their biocompatibility, flexibility in bending, and non-brittle nature, POFs represent ideal candidates for in-vivo biosensing applications [4–7]. Another attractive characteristic of POFs lies in the possibility to detect different chemical and biochemical species by changing functional groups, polymerization process, and additives, since they are made of organic compounds [1]. In addition, polymers have lower density than silica glass [3], which is in general desirable, as it is often necessary to minimize the total weight of a device. The aforementioned characteristics come in handy especially in fiber Bragg grating (FBG) sensors, for some applications of which, materials alternative to silica are incessantly sought for. To date, the most widespread material for polymer-based FBGs is PMMA [1,2,8–10], although the use of some alternative plastics, such as CYTOP (amorphous fluoropolymer) [11] and TOPAS (cyclic olefin copolymer) [12–14], has recently been investigated.

Microstructured polymer optical fibers (mPOFs) have drawn increasing attention since 2001 [15], within the framework of the research on photonic crystal fibers starting in the 1990s [16], due to the large variety of optical effects obtainable simply by changing internal microstructure [17,18]. In this class of fibers, the ability to guide light is based on a patterning of microscopic holes running along the length of a fiber [15–18]. Only a few journal papers on mPOFs made of PC have been published to date. None of those papers, however, have demonstrated light propagation in a solid-core microstructured PC fiber. Van Eijkelenborg et al. [19] fabricated and characterized a hollow-core PC mPOF fiber, where the polymer preform was produced via capillary stacking technique. Hollow-core PC waveguides with

#255045 Received 3 Dec 2015; revised 15 Jan 2016; accepted 17 Jan 2016; published 27 Jan 2016

inner Cu coatings were employed in [20] for terahertz transmission, while Gibson et al. [21] made use of solid-core PC mPOFs to fabricate multichannel electrospray emitters. Moreover, PC was studied in combination with polyvinyl difluoride (PVDF) for the manufacturing of mPOFs from multilayered all-polymer hollow preforms prepared by solvent evaporation and co-rolling methods [22]. A PC mPOF was further reported in [23], where, however, localized light propagation in the core could not be achieved (the light source was a 633-nm laser).

Polycarbonate optical fibers were introduced by Fujitsu in 1986 (the core was made of PC, with a polyolefin-based material as the cladding) [24] and have been extensively studied and used since then [25–27]. Polycarbonate is an engineering plastic that exhibits excellent clarity and impact strength [28]. The main advantage of using this material for optical fiber fabrication indeed lies in the well-balanced combination of its optical and mechanical properties. Firstly, it is transparent to visible light [29] and for this reason can be considered as a natural alternative to PMMA. Secondly, PC usually yields and breaks at elevated values of strain [29], and is highly flexible in bending. In addition, its glass transition temperature (T_g) is one of the highest among transparent plastics, thereby resulting in a larger available temperature range. These properties make PC fibers particularly attractive for those applications requiring high-temperature-resistant polymer sensors, as long as the specific application does not involve long-term exposure to a high-humidity environment at high temperature. Early investigations indeed seem to indicate that humid heat may cause premature aging of PC POFs [27].

The change of properties in PC due to UV irradiation has been the subject of several studies [30–32]. In particular, photosensitivity studies on PC [30] showed that the refractive index profile of PC films was affected by UV irradiation, suggesting a potential applicability of the photo-irradiation dependency for optical devices. Nevertheless, to the best of our knowledge, no FBG in PC optical fibers has been demonstrated yet. Literature only reports the inscription of Bragg gratings into a PC-based planar waveguide via an ablation process [33]. Here we present the first experimental demonstration of an endlessly single-mode solid-core PC mPOF. The microstructured fiber, fabricated via mechanical casting from plastic granulates, is also characterized both optically and mechanically. We further write an FBG into the optical fiber (which is dopant-free) by using a UV laser and demonstrate strain sensing up to 3%, and a linear response to temperature up to the record of 125°C with neither malfunctioning nor any significant hysteresis in the cooling phase. Microstructured polymer optical fiber Bragg gratings (mPOFBGs) made of a high-T_g grade of TOPAS (5013) were previously tested up to 110°C [14], whilst the maximum operation temperature of PMMA was reported to be 92°C in [34]. We consider the present work as a further step towards enabling high-temperature-resistant POFBG technology.

2. Experimental results

2.1 Fabrication of the solid-core PC mPOF

The solid-core PC mPOF was fabricated by using a drill-and-draw technique starting from casting of plastic granulates. The material used for casting was Makrolon LED2245 from Bayer MaterialScience AG with a T_g of 145°C. This material grade shows an extremely low tendency towards yellowing, even at temperatures as high as 120 °C [29]. Being hygroscopic, the PC granulates needed to be dried before casting to avoid bubble formation, which would otherwise increase the transmission loss and degrade the mechanical properties of the final fiber. A strict control of timing, temperature, and pressure was also required during the casting in order to obtain a good-quality solid rod. In particular, relatively high temperatures were applied as PC might contain polymer crystals at temperatures even higher than 220°C [35]. The presence of residual crystals in the PC preform would lead to both considerably poorer optical performance and inhomogeneities in the fiber.

The cast polymer rod was then machined and the desired hole pattern, which consisted of three rings of air holes in a hexagonal arrangement, was drilled into it. The preform was finally drawn to an intermediate cane, which was then sleeved with an in-house fabricated PC

#255045 Received 3 Dec 2015; revised 15 Jan 2016; accepted 17 Jan 2016; published 27 Jan 2016

tube and drawn down to fiber. A complete description of the experimental methodologies involved in the drill-and-draw technique can be found in [17]. The diameter of the final fiber was about 150 µm, whereas the core diameter was 7 µm. The average air hole diameter (d) and pitch between air holes (Λ) were 1.75 µm and 4.375 µm, respectively. The ratio d/Λ of 0.40 ensured that the mPOF was endlessly single-moded [36].

2.2 Characterization of the cast bulk PC material

The refractive index (RI) of the PC material used in our experiments was measured by using a commercially available ellipsometer VASE (J.A. Woollam), which covers a wavelength range of 210-1690 nm with a 5-nm resolution for the range 210-1000 nm and a 10-nm resolution for the range 1000-1690 nm. Figure 1(a) shows the measured material dispersion of PC and directly compares our data with other material dispersions reported in the literature. As it can be seen from Fig. 1(a), the measurements performed on PC were relatively close to the other dispersion data, with ours being slightly higher (<0.012) than the RI values from the PC datasheet [29] and Sultanova et. al. [37]. This slight difference in RI can be attributed to different preparation procedures utilized to manufacture the bulk PC material.

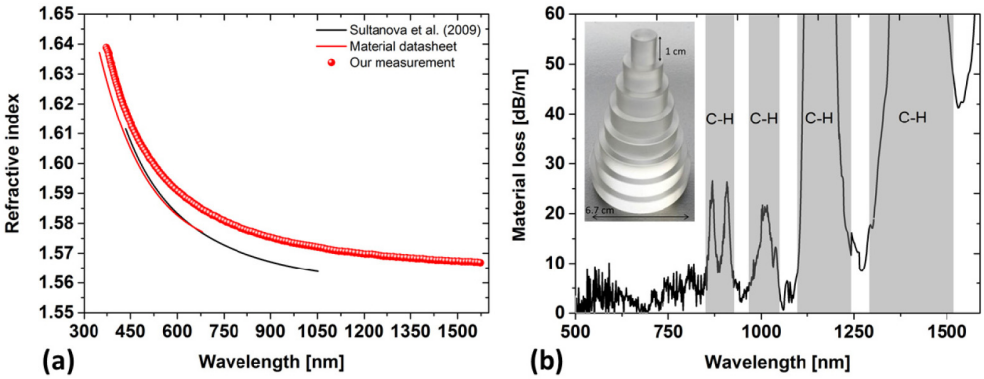

Fig. 1. (a) Material dispersion of PC. Our measurement (circles) is compared with the results of [29] (red curve) and [37] (black curve). (b) Bulk material optical loss of a PC solid rod made via casting from plastic granulates. Note the very high loss at longer wavelengths due to the absorption bands mainly caused by carbon and hydrogen bond (aliphatic and aromatic) vibrations [25,38]. Inset: PC step-like structure fabricated to measure the bulk material propagation loss.

Bulk material propagation loss was also measured within the interval 500-1600 nm based on a modified cut-back technique. A 10 cm long initial cylindrical preform was machined into an 8-step structure, with each step being 1 cm long (inset of Fig. 1(b)). We then determined the propagation loss of the material by using a broadband supercontinuum source and recording the spectrum in each step of the preform. The material loss was relatively low between 500 nm and 853 nm, as shown in Fig. 1(b). Moreover, four further transmission windows (with loss below 15 dB/m) could be detected at the wavelength ranges 876-898 nm, 917-998 nm, 1028-1102 nm, and 1247-1287 nm, respectively. The material transmission loss in the near-IR spectral range was slightly lower than the one reported in [39]. From Fig. 1(b) it may further be noticed that there is a significant amount of noise at short wavelengths. This is because of the lower loss, around a few dB/m, and also due to increasing scattering. A non-perfect surface of the sample introduces surface scattering, which is highly wavelength dependent. This leads to the growth of spectral noise towards shorter wavelengths.

2.3 Characterization of the solid-core PC mPOF

After the characterization of the bulk material we investigated the properties of the drawn mPOF. The fiber transmission loss profile was obtained via cut-back measurement. Cleaving was performed with an in-house made hot blade cleaver equipped with a flat side blade,

#255045 Received 3 Dec 2015; revised 15 Jan 2016; accepted 17 Jan 2016; published 27 Jan 2016

which yields high-quality end facets [40]. Applying the same temperature to blade and fiber, we tested several temperatures in the range 50-80°C (with steps of 5°C) so as to optimize the cleaving process for the PC mPOF. The optimal temperature of both blade and fiber was found to be 80°C. Figure 2(a) shows the transmission loss of the solid-core PC mPOF in the range of wavelengths between 550 nm and 900 nm, while Fig. 2(b) displays a microscope image of the fiber end facet with the desired hexagonal arrangement of air holes. The fiber transmission loss was found to be lower than 10 dB/m within the range 800-840 nm. Specifically, the minimum loss was 8.91 dB/m at 833.5 nm, whereas at the same wavelength the material loss was 4.37 dB/m [Fig. 1(b)]. By comparing Fig. 1(b) with Fig. 2(a) it may be noticed that the fiber loss was considerably higher than the propagation loss measured for the bulk material, especially at shorter wavelengths. This is probably due to the presence of material and geometrical inhomogeneities in the microstructured fiber. In particular, the higher loss of the PC fiber compared to its bulk material loss may arise from scattering. There are many possible sources of scattering due to the way mPOFs are manufactured [17,18,41,42]. The drilling process yields surface roughness within the holes of the polymer preform and this fact increases fiber loss. Even though the fiber drawing has the effect of smoothing the internal surface of the holes, some residual roughness in the final fiber is expected, leading to higher loss. This problem can be limited by adopting larger fiber cores [41]. Furthermore, material impurities introduced throughout the drill-and-draw process, such as dust, as well as the presence of any residual micro-swarfs on the hole surface as a consequence of the preform drilling, increase attenuation. Microbending losses, due to microdeformations in the mPOF producing scattering, are also expected. Particularly for small diameters, as is the case for the fiber characterized here, this source of loss may become important [41]. Overall it is expected that fiber loss can be substantially reduced by improving the whole PC fiber fabrication process.

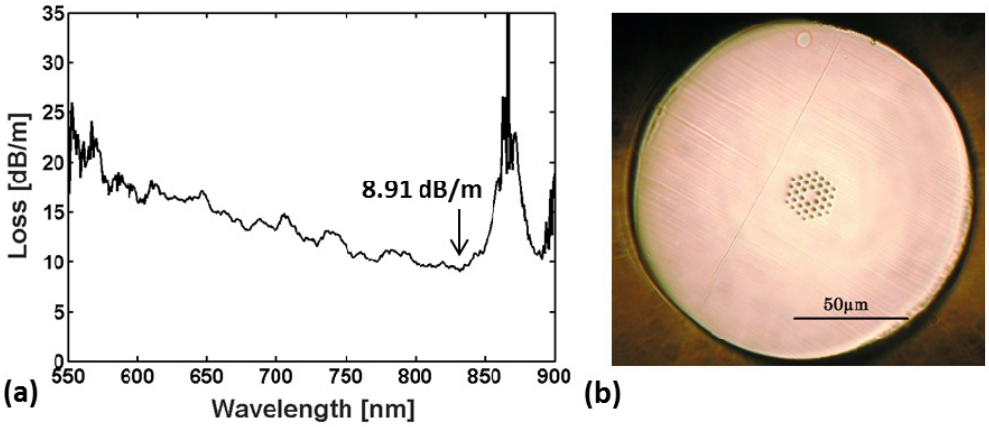

Fig. 2. (a) Transmission loss profile measured from 550 to 900 nm by the cut-back technique. The fiber was cut back from 4 m to 50 cm recording the transmission spectrum over 17 different fiber cuts. (b) Microscope image of the end facet of the solid-core PC mPOF. The fiber diameter was approximately 150 µm.

2.4 FBG inscription into the PC mPOF

The writing of the fiber Bragg grating in the polycarbonate mPOF was carried out with a 50 mW CW HeCd laser operating at 325 nm (IK5751I-G, Kimmon). For grating inscription we used the phase mask technique. The configuration of the inscription setup was the same as described in [43]. The phase mask was custom-made by Ibsen Photonics A/S. It is optimized for inscription with a HeCd laser (325 nm) and has a uniform period of 572.4 nm. The laser power was attenuated to 4 mW. The Bragg wavelength for the PC mPOF fiber was centered at 892.4 nm (with a FWHM of 0.46 nm) and the strength of the reflected peak was 25 dB, as

#255045 Received 3 Dec 2015; revised 15 Jan 2016; accepted 17 Jan 2016; published 27 Jan 2016

shown in Fig. 3. By using the RI from the material, the theoretical effective refractive index was calculated to be 1.5652 at 895.9 nm. For a pitch of 572.4 nm this gives a Bragg wavelength of 895.9 nm, which is close to the experimental value of 892.4 nm. The difference between theoretical and experimental value is due to the fact that we assumed an idealized geometry and neglected the effect of fabrication on RI in the calculation. In addition, the fiber was slightly pre-strained during the inscription process, which may lead to a mild down-shift of the FBG resonance wavelength upon release of the fiber from the inscription setup. The successful inscription of the FBG demonstrates that PC is photosensitive at typical Bragg grating writing conditions. The fiber loss at the Bragg grating wavelength (892.4 nm) was 11.37 dB/m [Fig. 2(a)]. However, transmission loss did not represent a critical factor in our experiments as only short lengths of the fiber were used. Although the laser power was only 4 mW, the FBG writing took just a few minutes. The inscription process was fast considering that the fiber was dopant-free. In particular, without the use of dopants the fastest writing time in PMMA mPOFs by means of a HeCd laser was shown to be slightly below 7 minutes in [43] (the laser power was 30 mW). For PC mPOFBGs, the average inscription time with a HeCd laser is about 6 minutes at a power of 4 mW. Short inscription times are of importance for the stability of a grating. The writing time in PMMA mPOFs can be reduced by either doping the fiber core [8,44,45] or using a different laser [46]. The same should hold true also for PC.

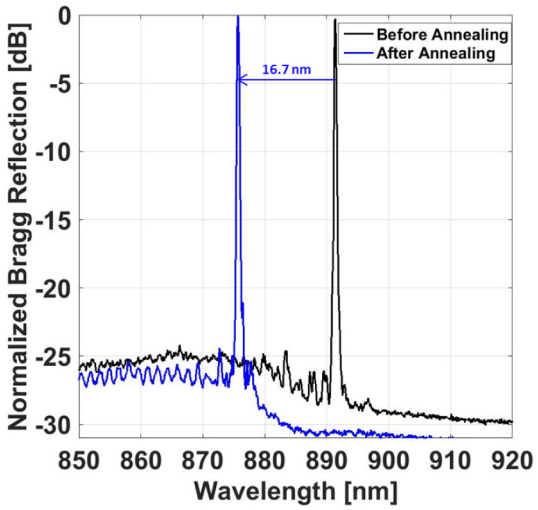

Fig. 3. PC mPOFBG spectrum at room temperature before annealing (black) and after annealing (blue).

The fiber was then annealed in order to improve the stability of the strain sensing [34,47]. Specifically, the annealing was done in two phases. First at 120°C for 24h, after which the resonance wavelength was 881.7 nm (10.7 nm lower than that of the un-annealed FBG). Then at 130°C for 12 h, which further blue-shifted it by 6.0 nm. After annealing the new Bragg wavelength was thus centered at 875.7 nm, with a total blue-shift of 16.7 nm (Fig. 3). The shift in the resonance wavelength was probably caused by fiber shrinkage [34], due to (at least partial) relaxation of the polymer chains as a consequence of the annealing process [48].

2.5. Strain and temperature sensing with the PC mPOFBG

The FBG was characterized in terms of sensitivity to strain and temperature by using a fiber coupler, a supercontinuum source (SuperK Compact by NKT Photonics A/S) and an optical spectrum analyzer (OSA, Ando AQ6315A). The two ends of the PC mPOF were glued to two micro-translation stages, one of which being fixed and the other one free to move according to the applied axial strain. The fixed end was butt-coupled to a silica step-index fiber through

#255045 Received 3 Dec 2015; revised 15 Jan 2016; accepted 17 Jan 2016; published 27 Jan 2016

which light was launched into the fiber. The axial strain values were calculated as the ratio (expressed in %) of the change in the length between the two gluing points ΔL to the original length of the fiber L_0 (4 cm). To minimize time-dependency in the mechanical behavior, the FBG reflection spectrum was read after approximately 10 minutes each time the axial strain was varied. The fiber was gradually stretched up to 3% (loading phase, "forward") and then the strain was slowly decreased until the original dimension was recovered (unloading phase, "reverse"). Figure 4(a) displays the results from the strain tuning of the PC FBG in forward and reverse straining. The Bragg wavelength exhibited a linear response over the strain range 0-3%, with a sensitivity of 0.701 ± 0.003pm/με calculated by linear regression. This sensitivity is very close to the value of 0.71 pm/με reported for PMMA 3-ring mPOFBGs at 850nm [49] and 827nm [50], and similar to that of 0.64 pm/με measured for a TOPAS 2-ring mPOFBG at 870 nm [13]. Moreover, the fiber did not show any hysteresis in the unloading phase, since the forward and reverse curves were perfectly overlapped, as shown in Fig. 4(a). Indeed, the strain sensitivity in the reverse phase was calculated to be still the same as the forward one (namely, 0.701 ± 0.003pm/με).

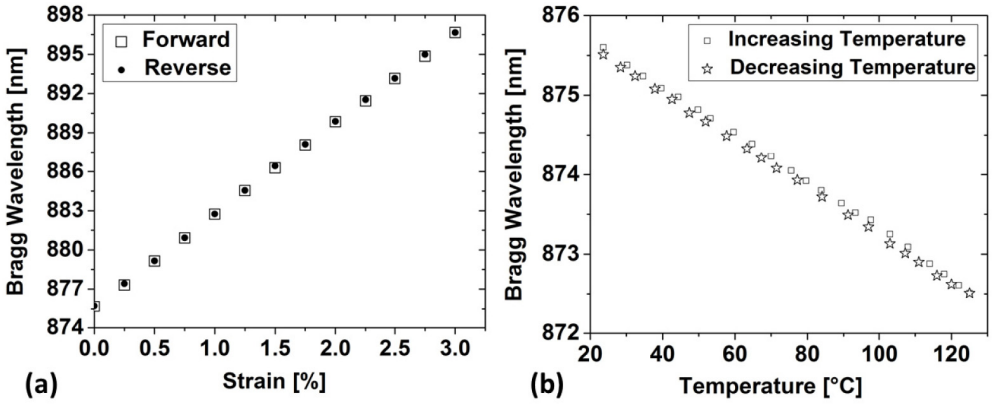

Fig. 4. (a) Strain response of the PC mPOFBG at room temperature. (b) Temperature response of the unstrained PC mPOFBG.

The temperature response of the solid-core PC mPOFBG was also investigated. The setup was similar to the one used for strain measurements, except for the Bragg grating now being placed on a resistive hot stage so as to control its temperature. A thermocouple with an uncertainty of around 0.3°C was placed as close as possible to the PC mPOF. Several layers of lens paper were used to cover it and therefore obtain a more uniform temperature. Each Bragg grating wavelength was recorded after 15 minutes once a new temperature value was set. Figure 4(b) shows the temperature tuning of the PC mPOFBG performed in a forward-backward test. The PC mPOFBG displayed a linear response between room temperature (23.6°C) and 125°C, showing a negative Bragg wavelength shift with increasing temperature. No malfunctioning was observed even at the highest temperatures. Note that in a study of the temperature response of FBGs inscribed in a PMMA 4-ring mPOF [34] with a similar diameter as the one of our PC fiber, a time interval of 10 minutes before readings were taken at each measurement step was sufficient to observe a markedly non-linear response when the elevated temperature region was approached.

The maximum temperature applied in our characterization of the PC grating (125°C) was greater than the one previously demonstrated by using a high-T_g TOPAS mPOFBG (110°C) [14], and well above the maximum operational temperature of PMMA (92 °C) reported in [34]. Furthermore, the PC mPOFBG response was seen to be linear in the cooling-down test. From a linear regression over the whole temperature range, the sensitivity of the FBG was calculated to be equal to −29.99 ± 0.17 pm/°C in the forward test and to −29.78 ± 0.09 pm/°C in the backward test. No significant hysteresis was observed as the temperature was ramped down, as also confirmed by the almost unaltered sensitivities. The stability of the fiber was

#255045 Received 3 Dec 2015; revised 15 Jan 2016; accepted 17 Jan 2016; published 27 Jan 2016

expected mainly for two reasons. The first one was that the T_g of the PC used in the present study is 20°C higher than the maximum operational temperature demonstrated here. This margin can be thought of as the minimum one to ensure long-term stability of a POFBG [14]. Secondly, the combination of two distinct annealing phases at 120°C and 130°C was likely to have significant impact in this regard, as early investigations showed the annealing process to considerably contribute to enhancing the thermal stability of polymeric FBGs and extending the linearity in their response to temperature [34,47]. The particular temperature of 125°C makes PC POFBGs applicable to certain areas of automation technology and automotive engineering. For instance, in the engine compartment of a vehicle, temperatures can go up to 125°C [27]. Polycarbonates make this area now accessible to polymer-based FBGs for the first time to our knowledge. In addition, PC can be sterilized with steam autoclaving [28], though for limited reuse applications. Autoclaves for sterilization typically work at 121°C for 15-20 minutes. No previous POFBG could withstand such conditions. The latter characteristic can be of great importance from a biomedical perspective.

It should also be mentioned that PC is not humidity-insensitive. An example of polymers used for manufacturing humidity-insensitive mPOFBGs is TOPAS [13]. As a reference, the percent water absorption of PC is 0.12% in air at 23°C and 50% relative humidity (RH) (generally measured after 24 h), whereas this value increases up to 0.3% (at saturation) when the PC is immersed in distilled water at 23°C [29]. Since the PC mPOFBG characterization was carried out in the open laboratory, its response to temperature could have been affected by cross-sensitivity to humidity. The true temperature and humidity responses of the PC mPOFBG, as assessed in a humidity-controlled environment (i.e., by using a climate chamber), are out of the scope of this paper.

2.6 Mechanical testing of the PC mPOF

The datasheet by the manufacturer of the used PC reports a tensile modulus of 2.35 GPa, a strain at break >50%, and yield stress and strain of 63 MPa and 6.0% [29], respectively. The tensile strain (%) is defined as $\varepsilon = 100\cdot(l-l_0)/l_0$, where l_0 represents the initial length of the sample and l denotes the instantaneous length of the sample being stretched. All the data presented here are based on the engineering stress defined as $\sigma = F/A_0$, with A_0 being the initial cross sectional area of the sample and F the stretching force. Note that the structuring of the polymer in the direction of the drawing due to the specific drawing conditions applied in the fiber fabrication process can affect the strain-stress behavior [48,51]. Moreover, tensile test results may also depend on the test temperature [52] and applied strain rate [2,48], as well as on the specific RH value (as water can act as a plasticizer of polymer materials), where the latter factor is expected not to be important for humidity-insensitive fibers, such as TOPAS. We carried out a tensile test on an un-annealed PC 3-ring microstructured optical fiber using an in-house built tensile testing machine. Five fiber samples were tested at a constant straining rate of 66%/min in a monitored open environment (T = 21.9-23.7°C, RH = 34.0-48.1%). The average diameter of the fiber samples was 146 ± 4 μm. The diameter measurements were performed with a micrometer screw gauge and cross-checked by means of an optical microscope. Both methods led to values in reasonable agreement. The cross-sectional area of the air holes in the microstructured region was neglected, as it accounted only for about 0.5% of the whole fiber cross section. Figure 5 shows a typical engineering stress-strain curve of the tested PC fiber samples. This kind of representation is useful as it contains more information than that presented in the datasheet. It may indeed be seen from Fig. 5 that our PC mPOF did not show a distinct yield point based on the Considere's construction method [53], as $d\sigma/d\varepsilon$ continued to be positive, although its value became considerably low at strains around 5%. After a further 10% elongation region at nearly constant stress, the fiber exhibited significant strain hardening at high strains (>15%) where the molecular alignment stiffened the drawn polymer.

Figures 6(a) and 6(b) summarize the results expressed in terms of Young's modulus (E) and break point, respectively. We calculated the Young's modulus using linear regression of the stress-strain data within the strain region of 0.05%-0.25%, as recommended in ISO 527-

#255045 Received 3 Dec 2015; revised 15 Jan 2016; accepted 17 Jan 2016; published 27 Jan 2016

1:1996 for plastics in tension. The Young's modulus of the PC mPOF was estimated to be equal to 3.03 ± 0.10 GPa. This is approximately 35% larger than the value reported in the bulk material datasheet [29]. Notice that thermal annealing commonly has the effect of lowering E and increasing ductility [48,51]. The curve shape is also likely to change as a result of the annealing process [48].

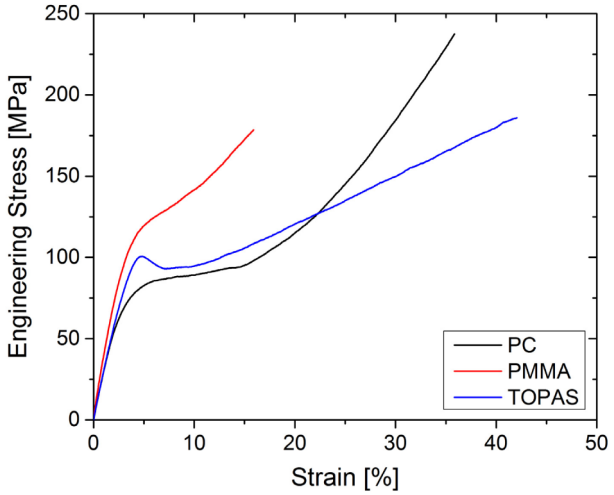

Fig. 5. Typical stress-strain curves of 3-ring solid-core PC, PMMA, and TOPAS mPOFs with an average diameter 146 ± 4 µm, 141 ± 5 µm, and 133 ± 4 µm, respectively. Average diameter estimation for 5 samples of each fiber was performed by adopting a confidence interval (CI) of 95%.

Figures 5, 6(a), and 6(b) further include the data from the experiments carried out on un-annealed GEHR PMMA [54] and TOPAS 8007S-04 [55] 3-ring mPOFs, which were tested in extension for comparison. The average diameters of the PMMA and TOPAS fibers were 141 ± 5 µm and 133 ± 4 µm, respectively. Similar drawing conditions as for the PC mPOF were also applied.

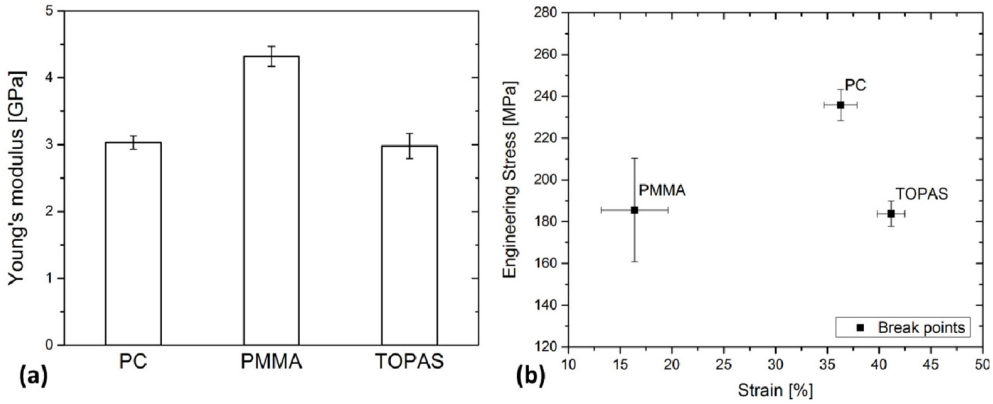

Fig. 6. (a) Average Young's moduli calculated on the whole statistical group (5 samples of each fiber). The bars represent a CI of 95%. (b) Average break points (the bars indicate a CI = 95%).

The stress-strain curves measured for the TOPAS mPOF exhibited a drop in the stress (usually identified as the yield point [53]) after the quasi-linear region, whereas the PMMA mPOF did not. These measurements displayed a similar increase in Young's modulus as the PC fiber compared to the data reported by the respective manufacturers. Indeed, the average E

#255045 Received 3 Dec 2015; revised 15 Jan 2016; accepted 17 Jan 2016; published 27 Jan 2016

values of PMMA and TOPAS were found to be 4.32 ± 0.15 GPa (34% greater than in [54]) and 2.98 ± 0.19 GPa (+ 15% compared to the company's datasheet [55]), respectively. The PC tensile strain at break was 36.3 ± 1.6%, slightly lower than TOPAS (41.2 ± 1.3%) but more than twice as much as PMMA (16.4 ± 3.2%). Note that a higher strain at break basically means a larger strain range available before failure. In addition, as a result of the higher degree of strain hardening, the PC mPOF could bear an average tensile stress at break of 235.9 ± 7.4 MPa, which is considerably greater than those measured for PMMA (185.5 ± 24.8 MPa) and TOPAS (183.8 ± 6.1 MPa).

A replacement of PMMA with PC-based mPOFBGs in strain sensing would increase the maximum operative temperature from 90°C to at least 125°C. Moreover, the lower Young's modulus of PC compared to PMMA is likely to increase the sensitivity of PC-based mPOFs in vibration sensors and accelerometers [56].

3. Conclusion

In this paper we have presented the fabrication of an FBG sensor in a PC mPOF manufactured through a multistage process starting from plastic granulates. The solid-core PC mPOF was characterized optically as well as mechanically. We observed fiber loss below 10 dB/m within the wavelength range 800-840 nm, with a minimum of 8.91 dB/m at 833.5 nm. In the mechanical characterization, the solid-core PC mPOF showed a pseudo-yield point after being strained by about 5%, and had relatively low Young's modulus and high strain at break compared to PMMA.

Furthermore, we reported for the first time that an FBG can be UV-written in a PC fiber. The FBG was inscribed in only a few minutes at a power of 4 mW. This inscription time was extremely fast considering that the fiber was undoped. Most importantly, we have demonstrated strain sensing up to 3% in a PC FBG, and a linear response of the grating to temperature up to 125°C, which is, to our knowledge, the currently highest reported operating temperature for a POFBG. We do think that PC FBGs represent a step towards the development of a reliable high-temperature-resistant polymer-based FBG technology.

Acknowledgments

The research leading to these results has received funding from the People Programme (Marie Curie Actions) of the European Union's Seventh Framework Programme FP7/2007-2013/ under REA grant agreement n° 608382. The authors also acknowledge Financial support from Innovation Fund Denmark for the project ShapeOCT (J. No. 4107-00011A). C.M. acknowledges support from Danish Council for Independent Research (FTP Case No. 4184-00359B). A.S. acknowledges the Eugen Lommel Stipend for financial support.

#255045 Received 3 Dec 2015; revised 15 Jan 2016; accepted 17 Jan 2016; published 27 Jan 2016

Paper 4

Low loss polycarbonate polymer optical fiber for high temperature FBG humidity sensing

G. Woyessa, A. Fasano, C. Markos, H.K. Rasmussen, and O. Bang

IEEE Photonics Technology Letters 29(7), 575-578 (2017).

Low Loss Polycarbonate Polymer Optical Fiber for High Temperature FBG Humidity Sensing

Getinet Woyessa, Andrea Fasano, Christos Markos, Henrik K. Rasmussen, and Ole Bang

***Abstract*— We report the fabrication and characterization of a polycarbonate (PC) microstructured polymer optical fiber (mPOF) Bragg grating (FBG) humidity sensor that can operate beyond 100°C. The PC preform, from which the fiber was drawn, was produced using an improved casting approach to reduce the attenuation of the fiber. The fiber loss was found reduced by a factor of two compared to the latest reported PC mPOF [20], holding the low loss record in PC based fibers. PC mPOFBG was characterized to humidity and temperature, and a relative humidity (RH) sensitivity of 7.31±0.13 pm/% RH in the range 10–90% RH at 100°C and a temperature sensitivity of 25.86±0.63 pm/°C in the range 20–100 °C at 90% RH were measured.**

***Index Terms*— Annealing, Fiber gratings, Humidity measurement, Optical fiber sensors, Plastic optical fiber, Temperature measurement.**

I. Introduction

THE interest in polymer optical fiber (POF) sensors is steadily increasing because of their low processing temperature, high flexibility in bending, high fracture toughness, ease of handling, and non-brittle nature, which are properties that glass fibers do not have [1]. In addition, POFs have a high elastic strain limit with low Young's modulus and they are biocompatible, which makes them advantageous for a range of strain and bio-sensing applications [2]–[11]. Some polymers, such as PMMA, are humidity sensitive and strongly absorb water [12]–[15], while others, such as Topas and Zeonex, have been reported to be insensitive to humidity [16]–[19]. Therefore, one of the key characteristics of PMMA based POFs is their ability to highly absorb moisture. The moisture absorption leads to a change in the refractive index and size of the fiber, which consequently change the Bragg wavelength [12]. Therefore, PMMA based fiber Bragg gratings (FBGs) are considered as potential candidates for developing humidity sensors [12]–[13].

Manuscript received November 12, 2016; revised February 1, 2017; accepted February 10, 2017. Date of publication February 13, 2017; date of current version March 9, 2017. This work was supported by People Programme of the European Union's Seventh Framework Programme under Grant 608382, in part by Danish Research Council FTP under Grant 4184-00359B, in part by Carslberg Foundation under Grant CF14-0825 and in part by the Innovation Fund Denmark ShapeOCT under Grant 4107-00011A.

G. Woyessa, C. Markos, and O. Bang are with the Department of Photonics Engineering, Technical University of Denmark, Lyngby 2800 Kgs, Denmark (e-mail: gewoy@fotonik.dtu.dk; chmar@fotonik.dtu.dk; ban@fotonik.dtu.dk).

A. Fasano and H. K. Rasmussen are with the Department of Mechanical Engineering, Technical University of Denmark, Lyngby 2800 Kgs, Denmark (e-mail: andfas@mek.dtu.dk; hkra@mek.dtu.dk).

Color versions of one or more of the figures in this letter are available online at http://ieeexplore.ieee.org.

Digital Object Identifier 10.1109/LPT.2017.2668524

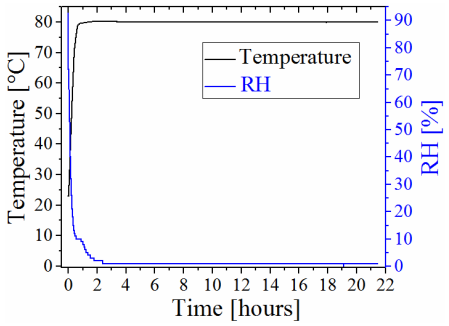

Fig. 1. The humidity response of an oven as the temperature is increasing.

The temperature and relative humidity (RH) operational limits and stability of polymer optical fiber Bragg gratings (POFBGs) strongly dependent on two parameters: the glass transition temperature (T_g) and moisture absorbing capability of the fiber material. The temperature operational limit of POFBGs produced from humidity insensitive polymers, such as Topas and Zeonex, relies exclusively upon their T_g and thus they can reliably operate 15-20 °C below their T_g regardless of the surrounding RH level [16]–[19]. However, this is not the case for other polymers such as PMMA which have high affinity to water. The temperature operational limit of PMMA POFBGs is strongly dependent on the surrounding RH level and vice versa. At ambient or lower RH level, they can operate 15-20 °C below their T_g. It has been reported that PMMA POFBGs can operate up to 90 °C at ambient RH [20]. However, when the surrounding RH is higher than the ambient RH, the temperature operational limit decreases significantly. For instance, when PMMA POFBGs humidity sensors are operated up to 90% RH, the maximum operational temperature is 75 °C [15]. This is attributed to the fact that glass transition temperature of PMMA decreases with increasing humidity [21]. So far, characterization for temperature measurement of POFBGs has been carried out using a hot plate or a conventional oven with no control on relative humidity [20], [22]. It is known that as the temperature of the hot plate or oven increases the corresponding surrounding relative humidity decreases dramatically. To verify this behavior we performed a systematic investigation using an environmental controlled chamber. The chamber was first programmed to have a fixed RH of 90% and ambient temperature. Releasing the RH of the chamber and by increasing the temperature up to 80 °C, it can be clearly seen from Fig. 1 how the RH of the chamber significantly and rapidly decreases and reaching an equilibrium at 1% RH in less than 3 hours. Based on this response, we can conclude that similar behavior occurs in a

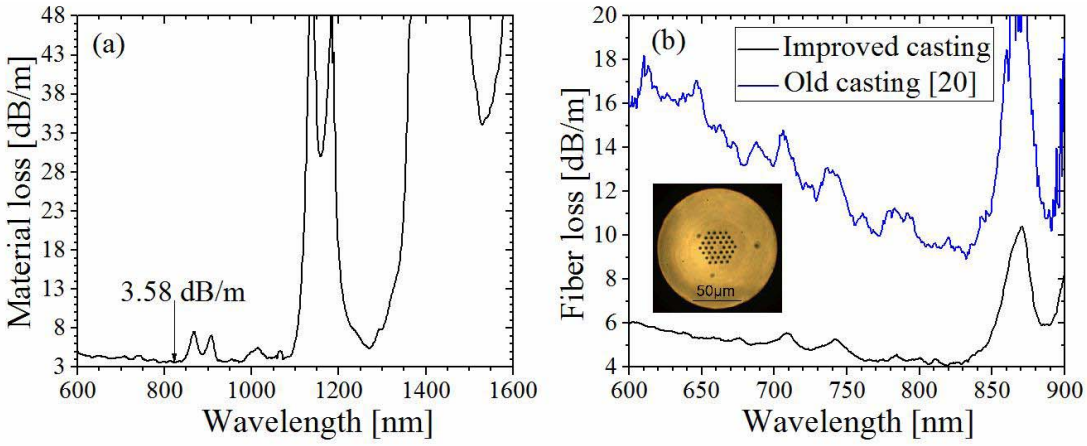

Fig. 2. (a) Bulk material optical loss for the improved PC solid rod. (b) Measured transmission loss of PC mPOF from both old and improved casting methods. Inset: Optical microscope image of the fabricated PC mPOF.

TABLE I

POLYMERS GLASS TRANSITION TEMPERATURE AND WATER ABSORPTION (SATURATION VALUE) AT 23 °C

Polymer types	Glass transition temperature	Water absorption (saturation value) at 23ºC
PMMA [24]	106ºC	2.1%
PC [25]	145ºC	0.3%
TOPAS5013S-04 [26]	134ºC	<0.01%
Zeonex 480R [27]	138ºC	<0.01%

humidity uncontrolled environment such as for example in an open space hot element or oven. At 1% RH, T_g of PMMA is expected to be higher than the one at ambient relative humidity as the water uptake capability will be lower and water acts as a plasticizer for PMMA [21]. Therefore, humidity is a limiting factor in the maximum operating temperature of POFBGs which have strong affinity to water. Similarly, when PMMA POFBGs are used as humidity sensors, the range of operation is highly dependent on the environmental temperature. PMMA mPOFBGs have been operated in the range 10-90% RH at maximum limiting temperature of 75 °C with no hysteresis [15]. At 90% RH and temperature beyond 80°C, the grating is experiencing a significant degradation and it is unable to operate. Therefore, PMMA based POFBGs can operate beyond 75 °C provided the corresponding RH level is lower than 90%.

Thus, it is extremely important for different applications to develop POFBG humidity sensors which can fulfill and operate at both high temperatures beyond the operational limit of PMMA POFBGs, and also wide range of relative humidity operation. In this work, we demonstrate for the first time a record low loss mPOFBGs humidity sensor that can operate beyond 90% RH and 100 °C using PC as the fiber material. Recently, it has been demonstrated that PC mPOFBG can operate up to 125 °C at ambient relative humidity [23]. The glass transition temperature and water absorption (saturation value) at 23°C for different polymer used for the fabrication of mPOFs is listed in Table I.

II. EXPERIMENTS AND RESULTS

The microstructured fiber used in this report was fabricated in-house at DTU Fotonik using a drill and draw method described in [23]. However, to reduce the loss of the fiber we used an improved casting approach for the preform production. One of the most crucial factors which define the final fiber loss is perhaps the quality of the cast preform. The casting procedure was optimized with regard to two aspects: drying phase and melting phase. A better water removal was achieved by using an oven with enhanced air circulation. This made it easier for the water trapped inside the plastic pellets to diffuse out during the drying, thereby improving the overall quality of the casting process. The melting phase was extended to remove any possible micro-sized residuals of crystals left in the final preform. Indeed, incomplete melting due to insufficient melting time might lead to the presence of micro-crystals in the core of the cast preform, which would result in higher scattering loss. This can be seen in the visible region in Fig. 2(b), where the gap between old and new fiber transmission losses increases with decreasing wavelength.

The bulk material loss of the PC polymer and the PC mPOFs losses are shown in Fig. 2(a) and 2(b), respectively. The minimum fiber propagation loss was found to be ∼4.06 dB/m at 819 nm and at this wavelength the material loss is ∼3.58 dB/m. It should be emphasized that the fiber loss was reduced by a factor of two compared to the first fabricated PC mPOF [23], holding thus the record in PC POFs loss. Both the cane and the fiber have been drawn at 170 °C and 10.5 MPa drawing stress. The final core and cladding diameter of the fabricated fiber are 10 μm and 125 μm, respectively. The average size of the holes diameter and the pitch size are 2.5 μm and 6.25 μm, respectively. The hole to pitch ratio is 0.4 ensuring that the fiber is endlessly single mode [28]. A microscope image of the PC mPOF end facet, which was cleaved with a custom made cleaver at a temperature of 80 °C of both blade and fiber [29], is shown as an inset in Fig. 2(b).

A fiber Bragg grating was first inscribed in the fabricated PC mPOF. The phase mask writing technique was used for the FBG inscription while the detailed experimental setup can be found in [30]. The phase mask used for grating

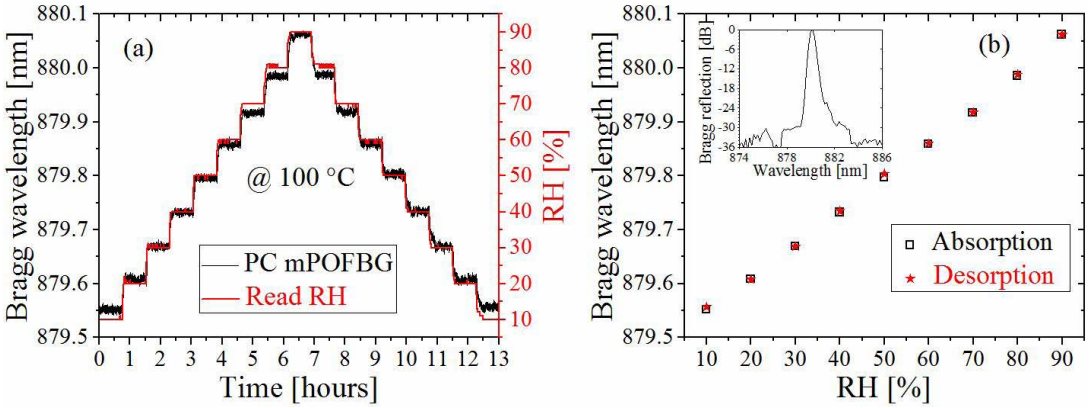

Fig. 3. (a) Measured humidity response at 100 °C of the PC mPOFBG. (b) Corresponding stabilized humidity response of the PC mPOFBGs at 100 °C. Inset: Normalized Bragg reflection spectrum of the PC mPOFBG.

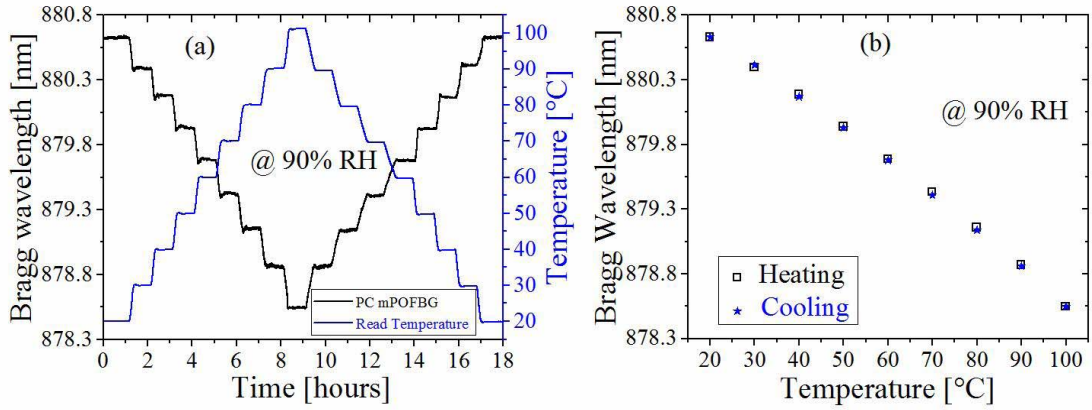

Fig. 4. (a) Measured temperature response at 90 % RH of the PC mPOFBG. (b) Corresponding stabilized temperature response of the PC mPOFBGs at 90 % RH.

inscription has a uniform period of 572.4 nm and the writing laser was a 325 nm HeCd CW UV laser. We used only 5 mW for the inscription of the grating. The grating had a length of 2 mm and the Bragg wavelength was located at 892.24 nm with reflection strength of 30 dB and a full width half maximum of 0.92 nm. The PC mPOFBG was then annealed at 125 °C for 36 hours in a conventional oven without humidity control. The new Bragg wavelength after annealing was blue shifted to 880.19 nm. To be sure that the PC mPOFBG was properly annealed for humidity sensing operation up to 90% RH and at high temperatures, we further annealed it in the climate chamber at 90 % RH and 100 °C for 6 hours, as high humidity has been shown to strongly assist the annealing of PMMA POFBGs [15]. For this, the PC mPOFBG was connectorized [31], and placed in a climate chamber (CLIMACELL, MMM Group). A supercontinuum source (SuperK Compact, NKT Photonics) has been used as the broadband light source and a spectrometer (CCS175 - Compact Spectrometer, Thorlabs) has been used to continuously track and record the grating during annealing in the climate chamber. This additional annealing did not lead to any further permanent blue shift, indicating that the POFBG was indeed properly annealed for operation at temperatures and relative humidity levels of 100 °C and 90% RH, respectively. The normalized Bragg reflection spectrum of the PC mPOFBG at 90 % RH and 100 °C is shown as an inset in Fig. 3(b).

After the annealing process, the humidity response of the PC mPOFBG sensor was measured at three different temperatures: 25 °C, 50 °C and 100 °C, in the interval of 10-90% RH. For each temperature level, the humidity measurement has been done first by increasing the RH from 10% to 90%, with step of 10% and then decreasing it from 90% to 10% with 10% step. For both cases, the chamber was programmed to change the RH in a minute and then to maintain stable the environmental conditions for 45 mins. The response of the PC mPOFBG, for both increasing and decreasing relative humidity at 100°C, is shown in Fig. 3(a). Fig. 3(b) shows the humidity response at 100°C where each measurement point was taken at the end of the 45 mins stabilization period. The humidity sensitivity at 100°C was 7.31±0.13 pm/% RH (R-squared of 0.998), for both increasing and decreasing relative humidity. The corresponding humidity sensitivities at 25 °C and 50 °C were measured to be 7.35±0.05 pm/% RH and 7.19±0.11 pm/% RH, respectively. These sensitivity figures confirm that the humidity response of PC mPOFBG is unaffected by temperature, and this is due to the fact that the grating was adequately annealed.

We have also measured the temperature sensitivity at two different RH levels: 50 % and 90 % RH in the range from 20 to 100 °C. For each RH level, the temperature measurement was first performed from 20 °C up to 100 °C, with a 10 °C step and then decreasing it back to 20 °C with the same step.

For both cases, the chamber was programmed to change the temperature in 10 mins and then to maintain the environmental conditions stable for 45 mins. The response of the PC mPOFBG for both increasing and decreasing temperature at 90% RH is shown in Fig. 4(a). Fig. 4(b) shows the temperature response at 90% RH where each measurement point was taken at the end of the 45 mins for the stabilization period. The temperature sensitivity at 90 % RH was 25.86±0.63 pm/°C. The corresponding sensitivity at 50% RH was 25.62±0.56 pm/°C. No hysteresis was also observed during the temperature characterization, further confirming the fact that the grating was properly annealed.

III. Conclusion

We have developed and characterized a polycarbonate based mPOFBG humidity sensor that can operate beyond 100 °C in the relative humidity range 10-90%. The mPOF preform was made by using an improved casting method and the measured loss was found to be two times smaller than the hitherto. The sensor gave a RH sensitivity of 7.31±0.13 pm/% RH in the range 10-90% RH at 100 °C and a temperature sensitivity of 25.86±0.63 pm/°C in the range 20-100 °C at 90 % RH.

The humidity sensitivities of our PMMA mPOFBGs and TOPAS step index POFBGs at 850nm are 45 pm/%RH and 0.45 pm/%RH, respectively. Thus the humidity sensitivity of PC mPOFBGs is 6 times smaller than PMMA mPOFBG and 16 times larger than TOPAS POFBGs which are basically humidity insensitive. However, PC mPOFBG humidity sensors can operate up to 90 % RH at a temperature 25 °C higher than the maximum operational limit of PMMA mPOFBGs. The temperature sensitivity of PC mPOFBGs is more than a factor of two larger than that of PMMA mPOFBGs. At ambient relative humidity PC mPOFBGs can operate up to 125 °C while PMMA mPOFBG can only be operated up to 90 °C. Thus, PC mPOFBGs humidity sensors can be used in several different applications areas where humidity measurement at high temperature is required such as in industry for ceramic driers, in domestic electric appliance for microwave oven and in agriculture for thermo-hygrostatic chamber [32].

References

[1] D. J. Webb, "Fiber Bragg grating sensors in polymer optical fibers," *Meas. Sci. Technol.*, vol. 26, no. 9, p. 092004, 2015.

[2] H. Dobb, D. J. Webb, K. Kalli, A. Argyros, M. C. J. Large, and M. A. van Eijkelenborg, "Continuous wave ultraviolet light-induced fiber Bragg gratings in few- and single-mode microstructured polymer optical fibers," *Opt. Lett.*, vol. 30, no. 24, pp. 3296–3298, 2005.

[3] I. P. Johnson *et al.*, "Optical fibre Bragg grating recorded in TOPAS cyclic olefin copolymer," *Electron. Lett.*, vol. 47, no. 4, pp. 271–272, 2011.

[4] A. Stefani, S. Andresen, W. Yuan, N. Herholdt-Rasmussen, and O. Bang, "High sensitivity polymer optical fiber-Bragg-grating-based accelerometer," *IEEE Photon. Technol. Lett.*, vol. 24, no. 9, pp. 763–765, May 1, 2012.

[5] R. Oliveira, L. Bilro, and R. Nogueira, "Bragg gratings in a few mode microstructured polymer optical fiber in less than 30 s," *Opt. Exp.*, vol. 23, no. 8, pp. 10181–10187, 2015.

[6] A. Lacraz, M. Polis, A. Theodosiou, C. Koutsides, and K. Kalli, "Femtosecond laser inscribed Bragg gratings in low loss CYTOP polymer optical fiber," *IEEE Photon. Technol. Lett.*, vol. 27, no. 7, pp. 693–696, Apr. 1, 2015.

[7] J. Jensen, P. Hoiby, G. Emiliyanov, O. Bang, L. Pedersen, and A. Bjarklev, "Selective detection of antibodies in microstructured polymer optical fibers," *Opt. Exp.*, vol. 13, no. 15, pp. 5883–5889, 2005.

[8] G. Emiliyanov *et al.*, "Localized biosensing with Topas microstructured polymer optical fiber," *Opt. Lett*, vol. 32, no. 5, pp. 460–462, 2007.

[9] C. Markos, W. Yuan, K. Vlachos, G. E. Town, and O. Bang, "Label free biosensing with high sensitivity in dualcore microstructured polymer optical fibers," *Opt. Exp.*, vol. 19, no. 8, pp. 7790–7798, 2011.

[10] H. U. Hassan, K. Nielsen, S. Aasmul, and O. Bang, "Polymer optical fiber compound parabolic concentrator tip for enhanced coupling efficiency for fluorescence based glucose sensors," *Bio. Opt. Exp.*, vol. 12, no. 2, pp. 5008–5020, 2015.

[11] C. Broadway *et al.*, "Fabry-Perot micro-structured polymer optical fibre sensors for opto-acoustic endoscopy," *Proc. SPIE*, vol. 9531, p. 953116, Jun. 2015.

[12] H. G. Harbach, "Fiber Bragg gratings in polymer optical fibers," Ph.D. dissertation, Faculty Eng. Sci. Technol., École Polytechnique Fédérale de Lausanne, Lausanne, Switzerland, 2008.

[13] C. Zhang, W. Zhang, D. J. Webb, and G. D. Peng, "Optical fibre temperature and humidity sensor," *Electron. Lett.*, vol. 46, no. 9, pp. 643–644, Apr. 2010.

[14] C. Zhang, X. Chen, D. J. Webb, and G.-D. Peng, "Water detection in jet fuel using a polymer optical fibre Bragg grating," *Proc. SPIE*, vol. 7503, p. 750380, Oct. 2009.

[15] G. Woyessa, K. Nielsen, A. Stefani, C. Markos, and O. Bang, "Temperature insensitive hysteresis free highly sensitive polymer optical fiber Bragg grating humidity sensor," *Opt. Exp.*, vol. 24, no. 2, pp. 1206–1213, 2016.

[16] W. Yuan *et al.*, "Humidity insensitive TOPAS polymer fiber Bragg grating sensor," *Opt. Exp.*, vol. 19, no. 20, pp. 19731–19739, 2011.

[17] C. Markos, A. Stefani, K. Nielsen, H. K. Rasmussen, W. Yuan, and O. Bang, "High-T_g TOPAS microstructured polymer optical fiber for fiber Bragg grating strain sensing at 110 degrees," *Opt. Exp.*, vol. 21, no. 4, pp. 4758–4765, 2013.

[18] G. Woyessa *et al.*, "Single mode step-index polymer optical fiber for humidity insensitive high temperature fiber Bragg grating sensors," *Opt. Exp.*, vol. 24, no. 2, pp. 1253–1260, 2016.

[19] G. Woyessa, A. Fasano, C. Markos, A. Stefani, H. K. Rasmussen, and O. Bang, "Zeonex microstructured polymer optical fiber: Fabrication friendly fibers for high temperature and humidity insensitive Bragg grating sensing," *Opt. Mater. Exp.*, vol. 7, no. 1, pp. 286–295, 2017.

[20] K. E. Carroll, C. Zhang, D. J. Webb, K. Kalli, A. Argyros, and M. C. J. Large, "Thermal response of Bragg gratings in PMMA microstructured optical fibers," *Opt. Exp.*, vol. 15, no. 14, pp. 8844–8850, Jul. 2007.

[21] L. S. A. Smith and V. Schmitz, "The effect of water on the glass transition temperature of poly(methyl methacrylate)," *Polymer*, vol. 29, no. 10, pp. 1871–1878, 1988.

[22] H. Y. Liu, G.-D. Peng, and P. L. Chu, "Thermal tuning of polymer optical fiber Bragg gratings," *IEEE Photon. Technol. Lett.*, vol. 13, no. 8, pp. 824–826, Aug. 2001.

[23] A. Fasano *et al.*, "Fabrication and characterization of polycarbonate microstructured polymer optical fibers for high-temperature-resistant fiber Bragg grating strain sensors," *Opt. Mater. Exp.*, vol. 6, no. 2, pp. 649–659, 2016.

[24] *GEHR PMMA (Acrylic)*, accessed on Mar. 27, 2014. [Online]. Avaialable: https://www.gehrplastics.com/pmma-acrylic.html

[25] *Makrolon Polycarbonate*, accessed on Apr. 16, 2014. [Online]. Available: http://www.plastics.covestro.com/en/Products/Makrolon/ProductList/201305212210/Makrolon-LED2245

[26] *Topas Advanced Polymers Topas 5013S-04*, accessed on May 7, 2014. [Online]. Available: http://www.topas.com/sites/default/files/TDS_5013S_04_e_1.pdf

[27] *Zeon Corporation Zeonex*, accessed on May 7, 2014. [Online]. Available: http://www.zeonex.com/optics.aspx

[28] T. A. Birks, J. C. Knight, and P. S. J. Russell, "Endlessly single-mode photonic crystal fiber," *Opt. Lett.*, vol. 22, no. 13, pp. 961–963, Jul. 1997.

[29] A. Stefani, K. Nielsen, H. K. Rasmussen, and O. Bang, "Cleaving of TOPAS and PMMA microstructured polymer optical fibers: Core-shift and statistical quality optimization," *Opt. Commun.*, vol. 285, no. 7, pp. 1825–1833, 2012.

[30] I.-L. Bundalo, K. Nielsen, C. Markos, and O. Bang, "Bragg grating writing in PMMA microstructured polymer optical fibers in less than 7 minutes," *Opt. Exp.*, vol. 22, no. 5, pp. 5270–5276, 2014.

[31] A. Abang and D. J. Webb, "Demountable connection for polymer optical fiber grating sensors," *Opt. Eng.*, vol. 51, no. 8, p. 080503, 2012.

[32] N. Yamazoe and Y. Shimizu, "Humidity sensors: Principles and applications," *Sens. Actuators*, vol. 10, nos. 3–4, pp. 379–398, 1986.

Paper 5

Single mode step-index polymer optical fiber for humidity insensitive high temperature fiber Bragg grating sensors

G.Woyessa, A.Fasano, A. Stefani, C.Markos, K.Nielsen, H.K. Rasmussen and O.Bang

Optics Express 24(2), 1253-1260 (2016)

Single mode step-index polymer optical fiber for humidity insensitive high temperature fiber Bragg grating sensors

Getinet Woyessa,[1,*] Andrea Fasano,[2] Alessio Stefani,[1,3] Christos Markos,[1,4] Kristian Nielsen, [1] Henrik K. Rasmussen,[2] and Ole Bang[1]

[1]*DTU Fotonik, Department of Photonics Engineering, Technical University of Denmark, DK-2800 Kgs. Lyngby, Denmark*

[2]*DTU Mekanik, Department of Mechanical Engineering, Technical University of Denmark, DK-2800 Kgs. Lyngby, Denmark*

[3]*Institute of Photonics and Optical Science (IPOS), School of Physics, The University of Sydney, NSW 2006, Australia.*

[4]*CREOL, The College of Optics & Photonics, University of Central Florida, 4000 Central Florida Blvd., Orlando, FL 32816, USA*

[*]*gewoy@fotonik.dtu.dk*

Abstract: We have fabricated the first single-mode step-index and humidity insensitive polymer optical fiber operating in the 850 nm wavelength ranges. The step-index preform is fabricated using injection molding, which is an efficient method for cost effective, flexible and fast preparation of the fiber preform. The fabricated single-mode step-index (SI) polymer optical fiber (POF) has a 4.8μm core made from TOPAS grade 5013S-04 with a glass transition temperature of 134°C and a 150 μm cladding made from ZEONEX grade 480R with a glass transition temperature of 138°C. The key advantages of the proposed SIPOF are low water absorption, high operating temperature and chemical inertness to acids and bases and many polar solvents as compared to the conventional poly-methyl-methacrylate (PMMA) and polystyrene based POFs. In addition, the fiber Bragg grating writing time is short compared to microstructured POFs.

OCIS codes: (060.2280) Fiber design and fabrication, (130.5460) Polymer waveguides, (060.2270) Fiber characterization, (060.3735) Fiber Bragg gratings, (060.2370) Fiber optics sensors.

References and links

1. T. Kaino, M. Fujiki, and S. Nara, "Low-loss polystyrene core-optical fibers," J. Appl. Phys. **52**(12), 7061–7063 (1981).
2. T. Kaino, M. Fujiki, S. Oikawa, and S. Nara, "Low-loss plastic optical fibers," Appl. Opt. **20**(17), 2886–2888 (1981).
3. Y. Koike and M. Asai, "The future of plastic optical fiber," NPG Asia Mater. **1**(1), 22–28 (2009).
4. K. Peters, "Polymer optical fiber sensors – a review," Smart Mater. Struct. **20**(1), 013002 (2011).
5. D. J. Webb, "Fiber Bragg grating sensors in polymer optical fibers," Meas. Sci. Technol. **26**(9), 092004 (2015).
6. D. J. Webb and K. Kalli, "Polymer fiber bragg gratings," in *Fiber Bragg Grating Sensors: Thirty Years From Research to Market*, A. Cusano, A. Cutolo, and J. Albert eds. (Bentham Science, 2010).
7. J. Jensen, P. Hoiby, G. Emiliyanov, O. Bang, L. Pedersen, and A. Bjarklev, "Selective detection of antibodies in microstructured polymer optical fibers," Opt. Express **13**(15), 5883–5889 (2005).
8. G. Emiliyanov, J. B. Jensen, O. Bang, P. E. Hoiby, L. H. Pedersen, E. M. Kjaer, and L. Lindvold, "Localized biosensing with Topas microstructured polymer optical fiber," Opt. Lett. **32**(5), 460–462 (2007).
9. C. Markos, W. Yuan, K. Vlachos, G. E. Town, and O. Bang, "Label-free biosensing with high sensitivity in dual-core microstructured polymer optical fibers," Opt. Express **19**(8), 7790–7798 (2011).
10. H. Dobb, D. J. Webb, K. Kalli, A. Argyros, M. C. J. Large, and M. A. van Eijkelenborg, "Continuous wave ultraviolet light-induced fiber Bragg gratings in few- and single-mode microstructured polymer optical fibers," Opt. Lett. **30**(24), 3296–3298 (2005).

#254747 Received 27 Nov 2015; accepted 3 Jan 2016; published 14 Jan 2016

Corrected: 10 February 2016

11. Z. Xiong, G. D. Peng, B. Wu, and P. L. Chu, "Highly tunable Bragg gratings in single-mode polymer optical fibers," IEEE Photonics Technol. Lett. **11**(3), 352–354 (1999).
12. A. Stefani, S. Andresen, W. Yuan, N. Herholdt-Rasmussen, and O. Bang, "High sensitivity polymer optical fiber-Bragg-grating-based accelerometer," IEEE Photonics Technol. Lett. **24**(9), 763–765 (2012).
13. G. D. Peng, P. L. Chu, Z. Xiong, T. W. Whitbread, and R. P. Chaplin, "Dye-Doped Step-Index Polymer Optical Fiber for Broadband Optical Amplification," J. Lightwave Technol. **14**(10), 2215–2223 (1996).
14. G. Zhou, C.-F. J. Pun, H. Tam, A. C. L. Wong, C. Lu, and P. K. A. Wai, "Single-Mode Perfluorinated Polymer Optical Fibers With Refractive Index of 1.34 for Biomedical Applications," IEEE Photonics Technol. Lett. **22**(2), 106–108 (2010).
15. Y. Koike, Y. Takezawa, and Y. Ohtsuka, "New interfacial-gel copolymerization technique for steric GRIN polymer optical waveguides and lens arrays," Appl. Opt. **27**(3), 486–491 (1988).
16. M. Beckers, T. Schlüter, T. Vad, T. Gries, and C.-A. Bunge, "An overview on fabrication methods for polymer optical fibers," Polym. Int. **64**(1), 25–36 (2015).
17. M. van Eijkelenborg, M. Large, A. Argyros, J. Zagari, S. Manos, N. Issa, I. Bassett, S. Fleming, R. McPhedran, C. M. de Sterke, and N. A. Nicorovici, "Microstructured polymer optical fibre," Opt. Express **9**(7), 319–327 (2001).
18. A. Stefani, W. Yuan, C. Markos, and O. Bang, "Narrow bandwidth 850 nm fiber Bragg gratings in few-mode polymer optical fibers," IEEE Photonics Technol. Lett. **23**(10), 660–662 (2011).
19. A. Abang and D. J. Webb, "Demountable connection for polymer optical fiber grating sensors," Opt. Eng. **51**(8), 080503 (2012).
20. G. D. Marshall, D. J. Kan, A. A. Asatryan, L. C. Botten, and M. J. Withford, "Transverse coupling to the core of a photonic crystal fiber: the photo-inscription of gratings," Opt. Express **15**(12), 7876–7887 (2007).
21. I.-L. Bundalo, K. Nielsen, and O. Bang, "Angle dependent Fiber Bragg grating inscription in microstructured polymer optical fibers," Opt. Express **23**(3), 3699–3707 (2015).
22. H. G. Harbach, "Fiber Bragg gratings in polymer optical fibers," PhD Thesis, Lausanne, EPFL (2008).
23. C. Zhang, W. Zhang, D. J. Webb, and G. D. Peng, "Optical fiber temperature and humidity sensor," Electron. Lett. **46**(9), 643–644 (2010).
24. G. Khanarian and H. Celanese, "Optical properties of cyclic olefin copolymers," Opt. Eng. **40**(6), 1024–1029 (2001).
25. http://www.zeonex.com
26. http://www.topas.com
27. I. P. Johnson, W. Yuan, A. Stefani, K. Nielsen, H. K. Rasmussen, L. Khan, D. J. Webb, K. Kalli, and O. Bang, "Optical fiber Bragg grating recorded in TOPAS cyclic olefin copolymer," Electron. Lett. **47**(4), 271–272 (2011).
28. W. Yuan, L. Khan, D. J. Webb, K. Kalli, H. K. Rasmussen, A. Stefani, and O. Bang, "Humidity insensitive TOPAS polymer fiber Bragg grating sensor," Opt. Express **19**(20), 19731–19739 (2011).
29. C. Markos, A. Stefani, K. Nielsen, H. K. Rasmussen, W. Yuan, and O. Bang, "High-Tg TOPAS microstructured polymer optical fiber for fiber Bragg grating strain sensing at 110 degrees," Opt. Express **21**(4), 4758–4765 (2013).
30. K. Nielsen, H. K. Rasmussen, A. J. L. Adam, P. C. M. Planken, O. Bang, and P. U. Jepsen, "Bendable, low-loss Topas fibers for the terahertz frequency range," Opt. Express **17**(10), 8592–8601 (2009).
31. J. Anthony, R. Leonhardt, A. Argyros, and M. C. J. Large, "Characterization of a microstructured Zeonex terahertz fiber," J. Opt. Soc. Am. B **28**(5), 1013–1018 (2011).
32. Y. Zhang, K. Li, L. Wang, L. Ren, W. Zhao, R. Miao, M. C J Large, and M. A. van Eijkelenborg, "Casting preforms for microstructured polymer optical fibre fabrication," Opt. Express **14**(12), 5541–5547 (2006).
33. https://www.thorlabs.com/thorcat/6800/780HP-SpecSheet.pdf
34. https://www.thorlabs.com/thorcat/22100/SM800G80-SpecSheet.pdf
35. A. Stefani, K. Nielsen, H. K. Rasmussen, and O. Bang, "Cleaving of TOPAS and PMMA microstructured polymer optical fibers: Core-shift and statistical quality optimization," Opt. Commun. **285**(7), 1825–1833 (2012).
36. I.-L. Bundalo, K. Nielsen, C. Markos, and O. Bang, "Bragg grating writing in PMMA microstructured polymer optical fibers in less than 7 minutes," Opt. Express **22**(5), 5270–5276 (2014).
37. R. Oliveira, L. Bilro, and R. Nogueira, "Bragg gratings in a few mode microstructured polymer optical fiber in less than 30 seconds," Opt. Express **23**(8), 10181–10187 (2015).
38. I. P. Johnson, K. Kalli, and D. J. Webb, "827nm Bragg grating sensor in multimode microstructured polymer optical fiber," Electron. Lett. **46**(17), 1217–1218 (2010).

1. Introduction

A lot of research has gone into developing low loss polymer optical fibers (POFs) [1,2]. Mostly, it has been the area of short range communication that has been driving the research, development and commercialization of POFs, which now have a consolidated place in this field [3]. Loss in POFs has nevertheless been far from reaching that of silica fibers, in particular when it comes to single-mode fibers. However, POFs unique properties, such as

#254747 Received 27 Nov 2015; accepted 3 Jan 2016; published 14 Jan 2016

their very low processing temperature, high flexibility in bending, high fracture toughness, ease of handling, and non-brittle nature compared to glass fibers have now moved the interest about POFs towards the sensing field, where loss is not so crucial [4–6]. Biocompatibility further makes POFs ideal candidates for bio-sensing applications [7–9] and properties, such as a high elastic strain limit and low Young's modulus, makes it ideal for fiber Bragg grating based sensors [5,6], in particular in high strain and acceleration sensing applications [10–12]. Various types of POFs have been demonstrated so far, such as step-index [1,13,14], graded-index [2,15,16] and microstructured [17] POFs. In the quest for low loss POFs, highly multimode step-index and graded-index fibers have been developed and are now available commercially and widely used in short-range communication. However, single-mode fibers are necessary for FBG sensors. In order to obtain single-mode guidance, several fabrication techniques have been proposed: from reducing the diameter of commercially available graded-index fibers by re-drawing [14] to exploiting the endlessly single-mode behavior of microstructured optical fibers [17]. Single-mode step-index POFs have been available commercially, but they were very lossy (500 dB/m @ 850nm) and multi-mode at 850 nm because they were targeted to operate at 1550 nm (MORPOF02, Paradigm Optics, see [18]). However, POFs have lowest loss at visible wavelengths and only microstructured POFs have so far been demonstrated to be single-mode in this regime. The re-drawn commercial fiber presented in [14] was targeted to have single mode guidance at 1300nm and 1550nm.

Despite microstructured POFs being a good way of getting single-mode operation in the visible, solid fibers are preferable because this eliminates problems with (1) loss and degradation due to impurities getting into the holes, (2) the difficult to avoid loss due to scattering at the hole walls, and (3) cleaving, splicing, and connectorizing a fiber with holes in it [19]. Furthermore, in FBG sensor fabrication the holes of a microstructured POF strongly increased the writing time and quality of the grating due to scattering at the many- air-material interfaces [20,21].

Step-index and graded-index POFs that have been fabricated in the past are mostly PMMA or PS based [1,2,13,15,16] and therefore have low operating temperature and strong affinity for water, which makes them sensitive to humidity [22,23]. Thus, the strain and temperature response of FBG sensors based on these fibers will have a strong dependence on humidity.

As for the realization of the all-solid preform and/or fiber, techniques, such as batch extrusion, continuous extrusion, interfacial-gel polymerization, chemical vapor deposition, and centrifugation have been used [13–16]. Using these methods, fabrication of single mode POFs is difficult because it is not easy to control dopant diffusion from core to cladding during the polymerization of monomers in the preform making process. Thus, it is not easy to maintain the refractive index profile of POFs to ensure single-mode operation. In addition, these techniques are complex and time consuming. As a result, at the moment it is not possible to commercially buy a single-mode POF.

Here we demonstrate the first solid step-index POF, which is single-mode at 850 nm and which is humidity insensitive. The fiber is made of a TOPAS core and a ZEONEX cladding. Both materials are humidity insensitive and can operate at high temperature, because of their glass transition temperature exceeding 130°C. An injection molding technique has been used to fabricate the step index preform and heat drawing has been used for fiber fabrication. The fabricated fiber has a core size and a numerical aperture very close to that of a silica single mode fiber at the same wavelength, which is optimal for coupling. Moreover, since the main application for the fabricated fiber is FBG sensors, we also report the successful inscription and characterization of FBGs in the SIPOF.

#254747 Received 27 Nov 2015; accepted 3 Jan 2016; published 14 Jan 2016

2. TOPAS/ZEONEX step index POF fabrication

The SIPOF was fabricated in-house at DTU Fotonik. The preparation of the preform consisted of two steps: casting of the cladding material, ZEONEX, and injection molding of the core material, TOPAS. These two materials were chosen for the following reasons:

- They have very close chemical, mechanical and optical properties: as TOPAS is a cyclic olefin copolymer (COC) and ZEONEX is a cyclic-olefin polymer (COP).
- The selected grades of these polymers have almost the same glass transition temperature and very close refractive indices, with the refractive index of TOPAS 5013S-04 being slightly higher than that of ZEONEX 480R.
- These polymers are also a class of optical thermoplastics that are chemically inert to acids and bases and many polar solvents, have a very low moisture uptake, low birefringence, and superior moldability [24–26].
- FBG writing has been successfully demonstrated in different grades of TOPAS fibers and proved to be humidity insensitive, which makes them a potential candidate for humidity insensitive FBG sensors [27–29].
- TOPAS and ZEONEX have also good transparency at THz frequencies [30,31].

We started the preform fabrication by casting the cladding material, ZEONEX 480R produced by ZEON CORPORATION with a glass transition temperature of 138°C [25], from granulates into a solid rod. This method differs from chemical casting [32] as it does not involve any polymerization process. This polymer is suitable for engineering applications requiring mechanical stability at high temperature. After casting, the solid rod was machined to a uniform bulk preform of 60 mm diameter and 100 mm length. Then a single hole with a diameter of 4 mm was drilled at the center of the preform. In the second stage of the SI preform preparation TOPAS 5013S-04 was injected into the 4 mm hole. TOPAS 5013S-04 granulate was purchased from TOPAS Advanced Polymers and it has a glass transition temperature of 134°C [26]. An Engel ES 80/25 HL-Victory injection molding machine was used for injecting TOPAS into the host ZEONEX preform. Different injection temperatures were preliminarily tested. The aim was to optimize the transparency of the molten polymer before injection. This was done by visually inspecting the clarity of TOPAS while exiting the injection nozzle. Despite that a decrease in the injection temperature was seen to improve the transparency of the molten TOPAS, it was not possible to lower the temperature too much since TOPAS became too stiff to be processed. The optimal injection temperature was found to be around 200°C. Thereafter TOPAS was injection molded into the central hole of the ZEONEX solid rod with a melt pressure at the nozzle being slightly lower than the machine limit, which is approximately 2000 bar. The SI preform was then first drawn to a 5 mm cane. Then the 5 mm cane was sleeved and drawn to a fiber of 150 ± 3 μm diameter. The corresponding core diameter of the fiber is 4.8 μm. The end facet of the fabricated SIPOF is shown as inset in Fig. 1 (a).

3. TOPAS/ZEONEX single mode step index POF characterization

3.1 Refractive index profile and loss measurement

The refractive index contrast was measured at Azpect Photonics by interferometric optical phase measurement techniques with an accuracy of ± 0.0001. Figure 1(a) shows the measured refractive index contrast of this SIPOF. The core has a refractive index, which is 0.00591 larger than that of the cladding. With this refractive index difference and a core size of 4.8 μm, the numerical aperture of the fiber is 0.13 and the normalized frequency is 2.38 at 850 nm. The measured core/cladding eccentricity is less than 0.6 μm and the nominal mode field diameter of this fiber is 5.3 ± 0.3 μm. The geometrical and optical parameters of the fiber are

#254747 Received 27 Nov 2015; accepted 3 Jan 2016; published 14 Jan 2016

closely matching those of silica single mode fibers operating in 850 nm region [33,34], allowing for easy coupling and low coupling loss between these fibers.

The transmission loss of the fabricated SIPOF was measured using the cut-back method. One end of the SIPOF was connectorized with a single mode silica patch cable, which was connected to a supercontinuum source (SuperK Extreme, NKT Photonics). The other end of the fiber was butt-coupled to an optical spectrum analyzer (OSA, Ando AQ6315A) via a standard silica single mode fiber to record the SIPOF transmission spectrum. The end facet of the fiber was cleaved with a custom-made cleaver at a temperature of 76°C for both the blade and the fiber [35]. The fiber was cut-back from 5 m to 30 cm; recording the transmission spectrum of over 40 different fiber cuts in order to eliminate any uncertainties arising from power fluctuations, cleave quality and so on. The measured loss profile of the TOPAS SIPOF is shown in Fig. 1 (b). The minimum loss was found to be 4.197 dB/m at 862 nm. The fiber attenuation at 850 nm is 4.55 dB/m.

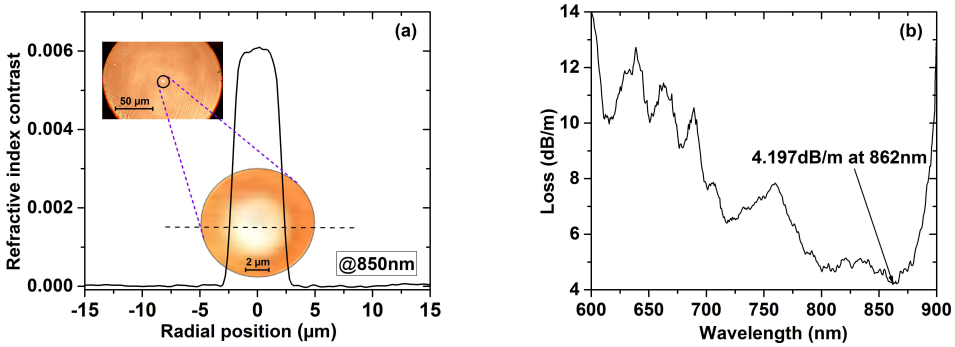

Fig. 1. (a) Measured refractive index contrast of SIPOF at 850 nm. Inset: microscope image of the end facet of the SIPOF. (b) Measured transmission loss of the SIPOF.

3.2 Fiber Bragg grating inscription and characterization

In order to explore the potential of this fiber for sensing, fiber Bragg gratings were inscribed in the fabricated SIPOF. The technique we used for inscribing the grating was the phase mask technique and the configuration setup used is the same as described in reference [36]. The phase mask used for inscribing the grating in the SIPOF has a 572.4 nm uniform period, making it suitable for writing FBGs in polymers fibers in the 850 nm region using a He-Cd 325 nm laser. The laser power used for inscription was only 6 mW and the writing time was 4 minutes as shown in Fig. 2(b). Despite the low power of 6 mW the writing time was shorter than the shortest writing time of 7 minutes reported for PMMA microstructured POF using 30 mW [36] and it is much shorter than the writing time of 338 minutes reported in TOPAS microstructured POF [28], all using a CW He-Cd laser. It is here worth mentioning that a writing time of 30 seconds was achieved using a pulsed excimer laser [37]. The typical reflection spectrum of a 2 mm long grating inscribed in the single mode SIPOF is shown in Fig. 2(a). The Bragg wavelength is located at 869.53 nm with a reflection strength of 30 dB and a full width half maximum (FWHM) of 0.29 nm. Before characterizing it for humidity, temperature and strain, the SIPOF was annealed for 24 hours at 110°C. Figure 2(a) shows the reflection spectrum of the FBG before and after annealing.

#254747 Received 27 Nov 2015; accepted 3 Jan 2016; published 14 Jan 2016

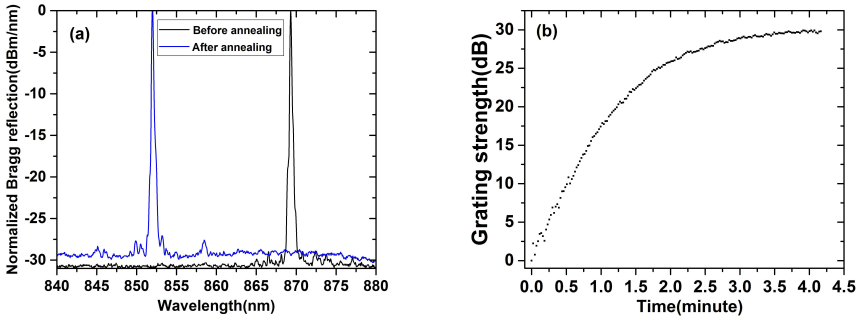

Fig. 2. (a) Bragg reflection of the SIPOFBG before and after annealing both normalized to the power of non-annealed grating. (b) Growth dynamic of the peak intensity of the 2 mm SIPOFBG during writing.

To study the humidity response, the fiber was first connectorized with a silica patch cable, which is single mode in the 850 nm region, and then placed in an environmental chamber (CLIMACELL, MMM group), which has a precision better than 0.3°C and 1% RH for relative humidity levels of 10-90%. Figure 3 illustrates the setup, in which a supercontinuum source (NKT Photonics A/S) has been used as a light source and a spectrometer (CCS175 - Compact Spectrometer, Thorlabs) has been used to continuously track the FBG peak during the humidity test. The humidity measurement has been done at 25°C. The relative humidity (RH) was first increased from 10% to 90% in steps of 10%. The chamber was programmed to increase the RH by 10% gradually within 30mins and then to keep the environmental conditions stable for another 30mins. Hence the total time allowed before increasing the relative humidity by 10% again was one hour. At the end of the ramp, the fiber was left inside the chamber for 24 hours at 90% RH to further investigate its humidity response. The total wavelength shift throughout the whole investigation was 40.85 pm, of which 35.13 pm was the change resulting from the increase from 10 to 90% and the 5.72 pm was the shift observed during the constant 90% RH period (occurred in the first 5 of the 24 hours). For the remaining 19hours no significant change in the Bragg wavelengths was measured. The humidity sensitivity when the RH was increased from 10 to 90% RH is 0.45 ± 0.22 pm/%RH, which is 78 times smaller than the sensitivity given by a step index PMMA POFBG [23].

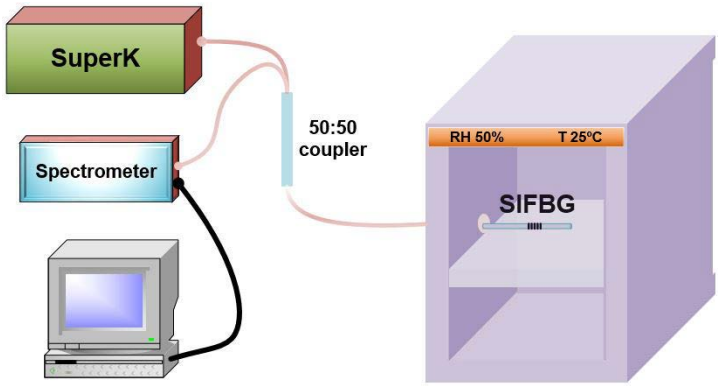

Fig. 3. Setup used for humidity and temperature measurement.

The temperature response of the SI POFBG was characterized with the same setup as the one used for humidity sensitivity measurements. The chamber was programmed to increase the temperature from 20°C to 105°C (the maximum operating temperature of the chamber)

#254747 Received 27 Nov 2015; accepted 3 Jan 2016; published 14 Jan 2016

and then to decrease down to 20°C, with a step of 5°C gradually within 5 minutes and stabilization time of 10 minutes at fixed 50% RH. Figure 4(b) shows the temperature response in the range 20°C to 105°C at 50% RH. The temperature sensitivity of this fiber is 17.57 ± 0.1 pm/°C for increasing temperature and 17.3 ± 0.02 pm/°C for decreasing temperature.

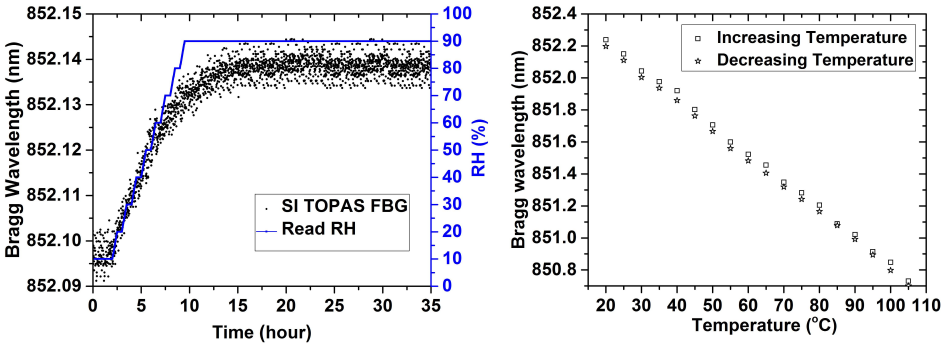

Fig. 4. (a) Humidity response of single-mode SIPOFBG at 25°C. (b) Temperature response single-mode SIPOFBG at 50% RH.

The strain response of the SI POFBG was studied by mechanically elongating the grating and monitoring its reflection spectrum. One end of the fiber was first connectorized with a single mode silica patch cable. Two centimeters away from the grating the fiber was clamped and glued to two micro-translation stages. One of the stages was used to apply axial strain manually to the grating. Every time strain was applied to the grating, 10 minutes were given for the grating to get stable before recording the reflection spectrum. The fiber was longitudinally strained up to 3% with steps of 0.25%. As shown in Fig. 5, the grating shows a linear response with an R-square value of 0.999 with no hysteresis. A linear fit of the results gives a strain sensitivity of 0.76 ± 0.02 pm/με, for both loading and unloading cases. This value matches the sensitivities of 0.71 pm/με reported for PMMA 3-ring mPOF FBGs at 850 nm [18] and 827 nm [38].

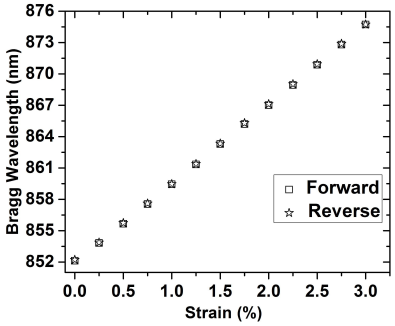

Fig. 5. Strain response of single-mode SIPOFBG.

4. Conclusion

In this work, we have fabricated for the first time a step-index single mode and humidity insensitive polymer optical fiber using injection molding technique. This technique provided a fast and flexible method of preparing step index preforms. The fabricated step index polymer optical fiber has a core made from TOPAS 5013S-04 with a glass transition temperature of 134°C and a cladding from ZEONEX 480R with a glass transition temperature of 138°C. The core and the cladding diameters of this fiber are 4.8 μm and 150μm,

#254747 Received 27 Nov 2015; accepted 3 Jan 2016; published 14 Jan 2016

respectively, which is compatible with a standard single mode silica fiber in the 850 nm region. The step index fiber has a minimum attenuation of 4.197 dB/m at 862 nm, which we anticipate can be further reduced by improving the preform production process. A fiber Bragg grating has also been inscribed in the proposed fiber in 4 minutes with as little as 6mW power from a CW He-Cd laser. We believe that FBGs inscribed in this step index fiber are particularly suitable for sensing applications that require high operating temperature and very low moisture absorption.

Acknowledgments

The research leading to these results has received funding from the People Programme (Marie Curie Actions) of the European Union's Seventh Framework Programme FP7/2007-2013/ under REA grant agreement n° 608382. The authors also acknowledge financial support from Innovation Fund Denmark for the project ShapeOCT (J. No. 4107-00011A), the Eugen Lommel Stipend for financial support and Danish Council for Independent Research (FTP Case No. 4184-00359B).

#254747 Received 27 Nov 2015; accepted 3 Jan 2016; published 14 Jan 2016

Paper 6

Zeonex microstructured polymer optical fiber: fabrication friendly fibers for high temperature and humidity insensitive Bragg grating sensing

G.Woyessa, A.Fasano, C. Markos, A. Stefani, H. K. Rasmussen, and O. Bang

Optical Material Express 7(1), 286-295 (2017).

Research Article | Vol. 7, No. 1 | 1 Jan 2017 | OPTICAL MATERIALS EXPRESS 286

Optical Materials EXPRESS

Zeonex microstructured polymer optical fiber: fabrication friendly fibers for high temperature and humidity insensitive Bragg grating sensing

GETINET WOYESSA,[1,*] ANDREA FASANO,[2] CHRISTOS MARKOS,[1] ALESSIO STEFANI,[1,3] HENRIK K. RASMUSSEN,[2] AND OLE BANG[1]

[1]*DTU Fotonik, Department of Photonics Engineering, Technical University of Denmark, DK-2800 Kgs. Lyngby, Denmark*
[2]*DTU Mekanik, Department of Mechanical Engineering, Technical University of Denmark, DK-2800 Kgs. Lyngby, Denmark*
[3]*Institute of Photonics and Optical Science (IPOS), School of Physics, The University of Sydney, NSW 2006, Australia*
**gewoy@fotonik.dtu.dk*

Abstract: In the quest of finding the ideal polymer optical fiber (POF) for Bragg grating sensing, we have fabricated and characterized an endlessly single mode microstructured POF (mPOF). This fiber is made from cyclo-olefin homopolymer Zeonex grade 480R which has a very high glass transition temperature of 138 °C and is humidity insensitive. It represents a significant improvement with respect to the also humidity insensitive Topas core fibers, in that Zeonex fibers are easier to manufacture, has better transmittance, higher sensitivity to temperature and better mechanical stability at high temperature. Furthermore, Zeonex has very good compatibility with PMMA in terms of dilatation coefficients for co-drawing applications. The Zeonex mPOF has a core and cladding diameter of 8.8 μm and 150 μm, respectively, with a hole to pitch ratio of 0.4 and a minimum propagation loss of 2.34 ± 0.39 dB/m at 690.78 nm. We have also inscribed and characterized fiber Bragg gratings (FBGs) in Zeonex mPOFs in the low loss 850 nm spectral band.

OCIS codes: (130.5460) Polymer waveguides, (060.2280) Fiber design and fabrication, (060.2270) Fiber characterization, (060.3735) Fiber Bragg gratings, (060.2370) Fiber optics sensors.

References and links

1. D. J. Webb and K. Kalli, "Polymer Fiber Bragg Gratings," in *Fiber Bragg Grating Sensors: Thirty Years From Research to Market*, A. Cusano, A. Cutolo, and J. Albert, eds. (Bentham Science, 2010).
2. D. J. Webb, "Fiber Bragg grating sensors in polymer optical fibers," Meas. Sci. Technol. **26**(9), 092004 (2015).
3. H. Dobb, D. J. Webb, K. Kalli, A. Argyros, M. C. J. Large, and M. A. van Eijkelenborg, "Continuous wave ultraviolet light-induced fiber Bragg gratings in few- and single-mode microstructured polymer optical fibers," Opt. Lett. **30**(24), 3296–3298 (2005).
4. A. Stefani, S. Andresen, W. Yuan, N. Herholdt-Rasmussen, and O. Bang, "High sensitivity polymer optical fiber Bragg grating based accelerometer," IEEE Photonics Technol. Lett. **24**(9), 763–765 (2012).
5. J. Jensen, P. Hoiby, G. Emiliyanov, O. Bang, L. Pedersen, and A. Bjarklev, "Selective detection of antibodies in microstructured polymer optical fibers," Opt. Express **13**(15), 5883–5889 (2005).
6. G. Emiliyanov, J. B. Jensen, O. Bang, P. E. Hoiby, L. H. Pedersen, E. M. Kjaer, and L. Lindvold, "Localized biosensing with Topas microstructured polymer optical fiber," Opt. Lett. **32**(5), 460–462 (2007).
7. C. Markos, W. Yuan, K. Vlachos, G. E. Town, and O. Bang, "Label-free biosensing with high sensitivity in dual-core microstructured polymer optical fibers," Opt. Express **19**(8), 7790–7798 (2011).
8. H. U. Hassan, K. Nielsen, S. Aasmul, and O. Bang, "Polymer optical fiber compound parabolic concentrator tip for enhanced coupling efficiency for fluorescence based glucose sensors," Biomed. Opt. Express **6**(12), 5008–5020 (2015).
9. C. Broadway, D. Gallego, G. Woyessa, A. Pospori, G. Carpintero, O. Bang, K. Sugden, and H. Lamela, "Fabry-Perot microstructured polymer optical fiber sensors for opto-acoustic endoscopy," Proc. SPIE **9531**, 953116 (2015).
10. S. Egusa, Z. Wang, N. Chocat, Z. M. Ruff, A. M. Stolyarov, D. Shemuly, F. Sorin, P. T. Rakich, J. D. Joannopoulos, and Y. Fink, "Multimaterial piezoelectric fibres," Nat. Mater. **9**(8), 643–648 (2010).

#278337 http://dx.doi.org/10.1364/OME.7.000286
Journal © 2016 Received 10 Oct 2016; revised 16 Dec 2016; accepted 18 Dec 2016; published 23 Dec 2016

Optical Materials EXPRESS

11. A. F. Abouraddy, M. Bayindir, G. Benoit, S. D. Hart, K. Kuriki, N. Orf, O. Shapira, F. Sorin, B. Temelkuran, and Y. Fink, "Towards multimaterial multifunctional fibres that see, hear, sense and communicate," Nat. Mater. **6**(5), 336–347 (2007).
12. H. G. Harbach, "Fiber Bragg gratings in polymer optical fibers," PhD Thesis, Lausanne, EPFL (2008).
13. C. Zhang, W. Zhang, D. J. Webb, and G. D. Peng, "Optical fiber temperature and humidity sensor," Electron. Lett. **46**(9), 643–644 (2010).
14. C. Zhang, X. Chen, D. J. Webb, and G. D. Peng, "Water detection in jet fuel using a polymer optical fiber Bragg grating," Proc. SPIE **7503**, 750380 (2009).
15. G. Woyessa, K. Nielsen, A. Stefani, C. Markos, and O. Bang, "Temperature insensitive hysteresis free highly sensitive polymer optical fiber Bragg grating humidity sensor," Opt. Express **24**(2), 1206–1213 (2016).
16. W. Yuan, L. Khan, D. J. Webb, K. Kalli, H. K. Rasmussen, A. Stefani, and O. Bang, "Humidity insensitive TOPAS polymer fiber Bragg grating sensor," Opt. Express **19**(20), 19731–19739 (2011).
17. I. P. Johnson, W. Yuan, A. Stefani, K. Nielsen, H. K. Rasmussen, L. Khan, D. J. Webb, K. Kalli, and O. Bang, "Optical fiber Bragg grating recorded in Topas cyclic olefin copolymer," Electron. Lett. **47**(4), 271–272 (2011).
18. C. Markos, A. Stefani, K. Nielsen, H. K. Rasmussen, W. Yuan, and O. Bang, "High-Tg TOPAS microstructured polymer optical fiber for fiber Bragg grating strain sensing at 110 degrees," Opt. Express **21**(4), 4758–4765 (2013).
19. G. Woyessa, A. Fasano, A. Stefani, C. Markos, K. Nielsen, H. K. Rasmussen, and O. Bang, "Single mode step-index polymer optical fiber for humidity insensitive high temperature fiber Bragg grating sensors," Opt. Express **24**(2), 1253–1260 (2016).
20. G. Khanarian and H. Celanese, "Optical properties of cyclic olefin copolymers," Opt. Eng. **40**(6), 1024–1029 (2001).
21. A. Fasano, G. Woyessa, P. Stajanca, C. Markos, A. Stefani, K. Nielsen, H. K. Rasmussen, K. Krebber, and O. Bang, "Fabrication and characterization of polycarbonate microstructured polymer optical fibers for high-temperature resistant fiber Bragg grating strain sensors," Opt. Mater. Express **6**(2), 649–659 (2016).
22. S. Roy, C. Y. Yue, Z. Y. Wang, and L. Anand, "Thermal bonding of microfluidic devices: Factors that affect interfacial strength of similar and dissimilar cyclic olefin copolymers," Sens. Actuators B Chem. **161**(1), 1067–1073 (2012).
23. J. Anthony, R. Leonhardt, A. Argyros, and M. C. J. Large, "Characterization of a microstructured Zeonex terahertz fiber," J. Opt. Soc. Am. B **28**(5), 1013–1018 (2011).
24. S. G. Leon-Saval, R. Lwin, and A. Argyros, "Multicore composite single-mode polymer fiber," Opt. Express **20**(1), 141–148 (2012).
25. A. Tuniz, R. Lwin, A. Argyros, S. C. Fleming, E. M. Pogson, E. Constable, R. A. Lewis, and B. T. Kuhlmey, "Stacked-and-drawn metamaterials with magnetic resonances in the terahertz range," Opt. Express **19**(17), 16480–16490 (2011).
26. N. Singh, A. Tuniz, R. Lwin, S. Atakaramians, A. Argyros, S. C. Fleming, and B. T. Kuhlmey, "Fiber draw double split ring resonators in the terahertz range," Opt. Mater. Express **2**(9), 1254–1259 (2012).
27. http://www.zeonex.com/optics.aspx.
28. Topas Advanced Polymers Inc, "Data Sheet - Topas 5013S-04," (Topas Advanced Polymers Inc., 2015), *http://www.topas.com/sites/default/files/TDS_5013S_04_e_1.pdf*.
29. É. Torres, M. N. Berberan-Santos, and M. J. Brites, "Synthesis, photophysical and electrochemical properties of perylene dyes," Dyes Pigments **112**, 298–304 (2015).
30. T. Bremner, A. Rudin, and D. G. Cook, "Melt Flow Index Values and Molecular Weight Distributions of Commercial Thermoplastics," J. Appl. Polym. Sci. **41**(78), 1617–1627 (1990).
31. A. Argyros, "Microstructured polymer optical fibers," J. Lightwave Technol. **27**(11), 1571–1579 (2009).
32. B. T. Kuhlmey, R. C. McPhedran, and C. Martijn de Sterke, "Modal cutoff in microstructured optical fibers," Opt. Lett. **27**(19), 1684–1686 (2002).
33. T. A. Birks, J. C. Knight, and P. St. J. Russell, "Endlessly single-mode photonic crystal fiber," Opt. Lett. **22**(13), 961–963 (1997).
34. A. Stefani, K. Nielsen, H. K. Rasmussen, and O. Bang, "Cleaving of Topas and PMMA microstructured polymer optical fibers: Core-shift and statistical quality optimization," Opt. Commun. **285**(7), 1825–1833 (2012).
35. A. Abang and D. J. Webb, "Demountable connection for polymer optical fiber grating sensors," Opt. Eng. **51**(8), 080503 (2012).
36. I.-L. Bundalo, K. Nielsen, C. Markos, and O. Bang, "Bragg grating writing in PMMA microstructured polymer optical fibers in less than 7 minutes," Opt. Express **22**(5), 5270–5276 (2014).
37. I.-L. Bundalo, K. Nielsen, and O. Bang, "Angle dependent Fiber Bragg grating inscription in microstructured polymer optical fibers," Opt. Express **23**(3), 3699–3707 (2015).
38. R. Oliveira, L. Bilro, and R. Nogueira, "Bragg gratings in a few mode microstructured polymer optical fiber in less than 30 seconds," Opt. Express **23**(8), 10181–10187 (2015).
39. K. E. Carroll, C. Zhang, D. J. Webb, K. Kalli, A. Argyros, and M. C. J. Large, "Thermal response of Bragg gratings in PMMA microstructured optical fibers," Opt. Express **15**(14), 8844–8850 (2007).
40. A. Stefani, W. Yuan, C. Markos, and O. Bang, "Narrow bandwidth 850 nm fiber Bragg gratings in few-mode polymer optical fibers," IEEE Photonics Technol. Lett. **23**(10), 660–662 (2011).
41. I. P. Johnson, K. Kalli, and D. J. Webb, "827nm Bragg grating sensor in multimode microstructured polymer optical fiber," Electron. Lett. **46**(17), 1217–1218 (2010).

Optical Materials EXPRESS

1. Introduction

Polymer optical fibers (POFs) share many of the merits that conventional silica optical fibers have for sensing applications such as immunity to electromagnetic interference, small size and multiplexing capabilities. POFs have unique features over those of silica fibers for many sensing applications. These include high flexibility in bending, non-brittle nature, low Young's modulus, high elastic strain limits and high fracture toughness, giving them great potential for fiber Bragg gratings (FBGs) based high strain and acceleration sensing applications [1–4]. POFs have also excellent compatibility with organic materials, making them ideal candidates for biomedical applications [5–9]. In addition, POFs have very low processing temperature and are easy to handle, hence low processing cost and safe disposability. Moreover, the integration of metals, insulators and semiconductors structures into extended length of polymer fibers have been demonstrated [10,11].

Some polymers, such as PMMA, strongly absorb water. As a result, PMMA based POFBGs are used for developing humidity sensors as the absorption or desorption of moisture leads to a change in refractive index and size of the fiber, both of which contribute to a change in Bragg wavelength [12–15]. However, PMMA based POFBGs suffer from strong cross sensitivity to humidity when they are used to develop strain and temperature sensors. To avoid such cross sensitivity to humidity, POFBGs made from a different class of polymers called cyclo-olefin copolymers, such as Topas grade 8007 [16,17], and 5013 [18,19], have been used as they have very low affinity to water. In addition to this, cyclo-olefin copolymers have good chemical inertness to bases and acids, and many polar solvents as compared to the conventional PMMA based POFs. They have also low birefringence and superior moldability [20]. Some grades of this class of polymers have high operating temperature, such as Topas grade 5013 [18,19]. Nevertheless, it is polycarbonate mPOFs, among currently exiting POFs, that have the highest operating temperature, having a glass transition temperature of 145 °C though it has affinity to water [21].

Here we demonstrate for the first time the fabrication of low loss, endlessly single mode and humidity insensitive microstructured polymer optical fiber made of Zeonex grade 480R with glass transition temperature (T_g) of 138 °C and also the first FBG inscribed in a Zeonex mPOF in the important low attenuation 850 nm region. The polymer Zeonex belongs to the class of cyclo-olefin polymers, in particular it is an amorphous homopolymer of norbornene. Although they are chemically different, Zeonex 480R shares most of Topas 5013 properties mentioned above. The difference in chemical structure lies in the presence of ethylene in Topas 5013, which is an amorphous ethylene-norbornene copolymer with a higher percentage of norbornene [22]. This makes the fabrication of Zeonex mPOF with micron sized holes and the writing of an FBG into it non-trivial, even knowing that a holey THz fiber and a step index POF could be fabricated in Zeonex [23, 24]. Our demonstration of low loss mPOF and FBG fabrication further underlines the excellent potential of Zeonex POF and mPOFs for sensing applications.

2. Advantages of Zeonex 480R over Topas 5013

Commercial Zeonex 480R rods have been used in the past not only for the fabrication of terahertz fibers [23], but also for multicore composite POFs, which consisted of Zeonex and PMMA, as Zeonex has a very good compatibility with PMMA in terms of dilatation coefficients for co-drawing applications and processing temperature [24]. Zeonex has also been used in the fabrication of drawn metamaterial fibers for the terahertz region [25, 26]. Recently, custom cast Zeonex 480R has been used as an optical cladding in the fabrication of single mode step index humidity insensitive high temperature Topas 5013 core POF [19]. At that point in time, Zeonex was worth using only as a cladding material due to its high material loss, despite combining Zeonex with different grades of various materials would have allowed obtaining the correct refractive index difference to use it as core material. In this work, the casting method has been optimized and the material loss has been significantly reduced as we

Optical Materials EXPRESS

will show later in the article. This polymer is also suitable for engineering applications requiring mechanical stability at high temperature, because of its high T_g [27].

When considering fabrication of step index or all solid POFs, the differences between Topas and Zeonex are not so evident. Contrary, when micron sized air holes are included in the material to create a regular microstructure, the superior drawability of Zeonex over Topas 5013 results in a clear advantage. It allows for more degrees of freedom in fiber design as the desired microstructures can be transferred to the final fiber more efficiently. For example, the cladding holes are symmetric with only minor distorted shape compared to Topas 5013 mPOFs. Due to the better stability of the drawing process, fluctuations in the fiber diameter are also reduced. The physical properties of Zeonex 480R are indeed well suited for high quality fiber drawing. Even if the T_g of Zeonex 480R is rather close to that of Topas 5013, 134 °C [28], a preform made of Zeonex ends up to be much easier to draw. This fact is a direct consequence of Zeonex greater molecular weight, which represents an average polymer chain length. The weight-average molecular weight (M_w) of Topas 5013 was measured to be 76400 g/mol [22] whereas the M_w of Zeonex 480R is approximately 480000 g/mol [29], which is six times larger than that of Topas 5013. The melt flow index that is the flowability, of a thermoplastic material in general decreases with increasing M_w [30]. Hence, Zeonex 480R preforms tend to flow slower than Topas 5013 under similar fiber drawing conditions, thereby ensuring highly controllable and stable fiber draw processes. The other important advantage of having a higher M_w or a lower melt flow rate is that, it can allow getting a wide range of drawing temperature and stress. Thus this wide range of drawing stress enables easier tuning of the final mechanical properties of the fiber. Nevertheless, it should be noted that either too high or too low values of M_w can make the fiber drawing very challenging or even unfeasible. The M_w of Zeonex 480R is sufficiently low to avoid this potential problem. Similar information can further be found by direct examination of the melt indices for the two polymers in the respective datasheets. At 260 °C the melt volume rate of Topas 5013 is 48 cm^3/10 min if a test load of 2.16 kg is used [28]. For Zeonex 480R the melt flow index is instead as low as 21 g/10 min with the same load at an even higher temperature, 280 °C [27], where the viscosity decreases when the temperature increases. Notice that, although the latter index is expressed in g/10 min, its value should not be numerically far from the corresponding melt volume rate datum, as the specific volume of Zeonex is in the range of 1.0-1.1 cm^3/g, between room temperature and its processing temperatures.

3. Zeonex preform casting and characterization

3.1 Preform casting

We cast commercial Zeonex 480R plastic pellets (Zeon Corporation) into an in-house made aluminum mold to produce an optical quality solid rod. The casting conditions were optimized in order to enhance the transparency of the Zeonex preform and minimize its tendency towards yellowing for long processing time at high temperature. Although moisture absorption of Zeonex is lower than 0.01% (ASTM D570, 23°C for 24 hours) [27], preheating of the polymer granulates is required. In particular, air trapped in the pellets may form bubbles and oxygen driven discoloration in the final preform, which consequently will result in higher material losses. The best results were obtained by applying a long and stepwise preheating phase. Prior to the melting phase, we preheated the preform under vacuum for 1 day: first at a temperature well below T_g for 16 hours and then around T_g for 8 hours. This led to a low-haze preform having significantly higher clarity than the one fabricated in reference [19], where Zeonex 480R could only be used as a cladding material due its elevated transmission loss.

Optical Materials EXPRESS

3.2 Refractive index measurement

The refractive index (RI) of the Zeonex 480R material used in our experiments was measured by using a commercially available ellipsometer VASE (J.A. Woollam). It covers a wavelength range of 210-1690 nm with a 5 nm and 10 nm resolutions for the range 210-1000 nm and 1000-1690 nm, respectively. The Zeonex sample used for the refractive index measurement had a disc shape with diameter of 25 mm and 10 mm thickness and with a surface roughness of 4.23 ± 0.022 nm. Cauchy model was used to fit the dispersion of the material. Figure 1(a) displays a direct comparison between the RIs of our own custom made Zeonex and the commercially available Zeonex (Zeon Corporation). The RI measurement was performed at 25 °C. As it can be seen from Fig. 1(a), our dispersion measurement is relatively close to the one obtained from the datasheet. The slight deviation between the two measured RIs could be attributed to the different molding and optimization approaches used.

3.3 Bulk material loss measurement

Bulk material propagation loss was measured within the interval 500-1600 nm based on a modified cut-back technique [21]. A 10 cm long initial cylindrical preform, which was prepared in the same way as done for the fiber drawing preform, was machined into an 8-step structure, with each step being 1 cm long as shown in the Fig. 1(b) inset. A broadband supercontinuum source (SuperK Versa, NKT Photonics) was used as an input light source. The beam divergence of the supercontinuum source is less than 5 mrad (half angle) and the beam diameter is 1 mm and 3 mm at 530 nm and 2000 nm, respectively.

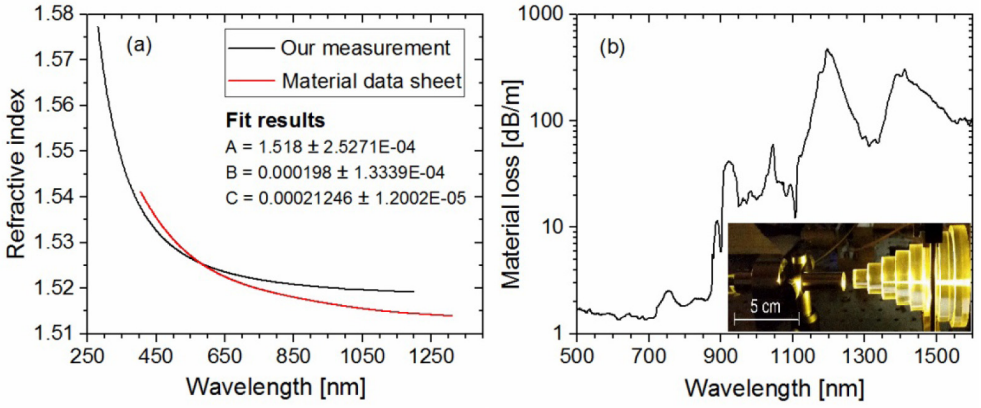

Fig. 1. (a) Material dispersion of Zeonex 480R. (b) Bulk material optical loss of Zeonex 480R. Inset: Zeonex step-like structure fabricated to measure the bulk loss.

The output light from the preform was collected and coupled to an optical spectrum analyzer (OSA, Ando AQ6315A) with a 1 mm core 2 m long multimode silica fiber patch cable (M35L02, Thorlabs) via an objective lens (10x, Zeiss). The numerical aperture of the MM fiber and the objective lens are 0.39 and 0.25, respectively. We made the measurement by recording the transmission spectrum for all step. For every step, we rotated the preform in order to record the spectrum at a different point and make sure the consistency of the measurement hence to minimize the error arising from possible surface defects on the preform or source power fluctuation. The rotation of the preform in every step was repeated five times and the final bulk loss is the average of the five measurements. Bulk material optical loss of Zeonex 480R is shown in Fig. 1(b).The material loss was relatively low in the visible range with a minimum recorded loss of 1.32 ± 0.18 dB/m at 689.98 nm while the minimum material loss for PMMA was reported to be 0.15 dB/m at 650 nm [31]. In the 500-880 nm region, the

Optical Materials EXPRESS

loss was found to be less than 2.54 ± 0.21 dB/m. However, the propagation loss significantly increased in the near infrared region as shown in Fig. 1(b).

4. Endlessly single mode Zeonex mPOF fabrication and characterization

4.1 Fiber fabrication

The prepared Zeonex solid rod was first machined into a polymer preform with 100 mm length and 60 mm diameter. By using a computer numerically controlled drilling machine, 3 mm holes with a pitch of 6 mm were drilled by 60° drill in a 3-ring hexagonal arrangement. The microstructured preform was then drawn down to a 6 mm cane. The cane was sleeved by a Zeonex tube, which was also made in house, and drawn to a fiber of 150 µm average outer diameter. Both the cane and the fiber were drawn at a temperature of 180 °C. For this temperature, the fiber drawing stress was 10 MPa. The core diameter of the fiber is 8.8 µm and the average size of holes diameter and the pitch are 2.2 µm and 5.5 µm, respectively. The hole to pitch ratio is 0.4 ensuring the fiber being endlessly single mode [32, 33]. A microscope image of the Zeonex mPOF end facet, which was cleaved with a custom made cleaver at a temperature of 78 °C of both blade and fiber [34], is shown as inset in Fig. 2(a).

4.2 Fiber characterization

4.2.1 Loss measurement

The transmission loss of the fabricated Zeonex mPOF was measured by cut-back method. One end of the Zeonex mPOF was connectorized [34] and connected to the visible wavelength output of a SuperK SPLIT (NKT photonics) which was connected to a supercontinuum source (SuperK Versa, NKT Photonics). The visible output of the SuperK SPLIT ranges from 450 nm to 900 nm. The light from the other end of the Zeonex mPOF was directed to a 1 mm core 2 m long multimode silica fiber patch cable via collimating (100x, Zeiss) and focusing (10x, Zeiss) objective lenses. The numerical apertures of the collimating and focusing lenses are 0.75 and 0.25, respectively, and that of the multimode fiber is 0.36. The other end of the fiber patch cable was connected to an OSA to record the Zeonex mPOF transmission spectrum. The fiber was cut back from 10 m to 50 cm, recording the transmission spectrum over 20 different fiber cuts in order to eliminate uncertainties arising from power fluctuations, coupling instabilities and cleaving quality. The measured loss profile of the Zeonex mPOF is shown in Fig. 2(a). The minimum loss was found to be 2.34 ± 0.39 dB/m at 690.78 nm. The fiber attenuation in the wavelength ranging from 550 nm to 875 nm is less than 3.2 ± 0.42 dB/m. As it can be seen in Fig. 2(a), the propagation loss of this mPOF is much lower than the previously reported microstructured [18], and step index TOPAS grade 5013 fibers [19], in particular in the visible region. The loss of our Zeonex mPOF is also much lower than the multicore step index POF having a core made of a composite of Zeonex 480R and PMMA and which has a lowest loss of 8 dB/m at 633 nm [24].

4.2.2 Fiber Bragg grating inscription and characterization

Fiber Bragg gratings were inscribed in the fabricated Zeonex mPOF in order to explore the potential of this fiber for sensing, as to our knowledge, no FBGs have been demonstrated in this material before. The grating inscription technique and the configuration setup used in this work were the same as the ones described in [36]. The phase mask used for the grating inscription in the Zeonex mPOF has a 572.4 nm uniform period, making it suitable for writing FBGs in polymers fibers in the low loss 850 nm region using a He-Cd 325 nm laser. The optimum inscription power for this fiber was found to be 5.5 mW and the corresponding writing time was less than 5 minutes. Inscription power higher than this resulted in weak gratings and also damaged the fiber, while inscription power lower than 5.5 mW resulted in longer inscription time without any improvement in the FBG strength. The writing time was shorter than the shortest writing time of 7 minutes reported for endlessly single mode PMMA

Optical Materials EXPRESS

microstructured POF [36] using 30 mW CW He-Cd laser power. However, it is comparable with the inscription time of 4 minutes at a power of 6 mW (CW He-Cd laser) reported for the Topas step-index fiber [19], despite the presence of the microstructure which generally affects the writing time [37]. However, it is pertinent to note that a writing time as low as 30 seconds has been already demonstrated using a pulsed excimer laser in a few mode PMMA mPOF [38].

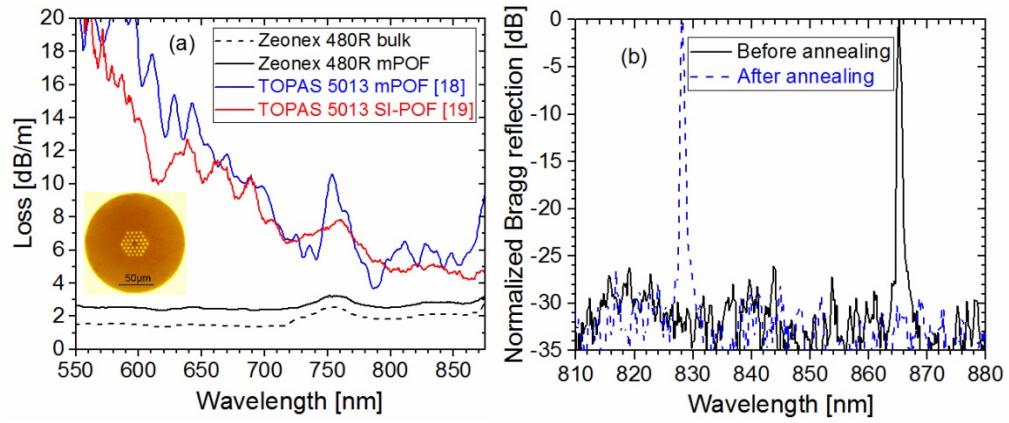

Fig. 2. (a) Measured transmission loss of bulk Zeonex 480R (dashed-black), single mode Zeonex 480R mPOF (black), single mode Topas 5013 mPOF (blue) [18], and single mode Topas 5013 SI-POF (red) [19]. Inset: microscope image of the fabricated Zeonex mPOF. (b) Bragg reflection of the Zeonex mPOF before and after annealing both normalized to the power of the non-annealed grating.

A typical reflection spectrum of a 2 mm long grating inscribed in the Zeonex mPOF is shown in Fig. 2(b). The Bragg wavelength is located at 865.24 nm with reflection strength of 30 dB and a full width half maximum of 0.522 nm. Before humidity, temperature and strain characterization, the Zeonex mPOFBG was annealed at 120 °C for 36 hours for stable operation of the sensor. After annealing, the grating blue shifted by 33.67 nm. Figure 2(b) shows the reflection spectrum of the FBG before and after annealing. Both grating reflection spectra, before and after annealing, were recorded with an optical spectrum analyzer and the spectra were then normalized to the power of the non-annealed grating. As it can be seen from Fig. 3(b) the grating was not degraded by thermal annealing.

The humidity and temperature responses of the Zeonex mPOFBG were measured using a characterization setup as described in [15]. The humidity measurement was done at 50 °C. The chamber was programmed to increase the relative humidity (RH) from 10% to 90% with a step of 10% RH. The time between each RH step was 1 hour, where 30 minutes was used to increase the RH, and 30 minutes was left for stabilization. Figure 3(a) shows the result of this process. The total wavelength change observed for the entire process was 60.2 pm and the relative humidity sensitivity measured was 0.75 ± 0.42 pm/%RH. The RH sensitivity of PMMA mPOFBG in the 850 nm region is 46 pm/%RH, which is 60 times higher than that of Zeonex mPOFBG. After reaching the value of 90% RH, the fiber was left inside the chamber for 24 hours to further investigate its humidity response. The Bragg wavelength red shifted by 8 pm in the first 4 hours of the 24 hour period and then blue shifted by 5.8 pm in the following 2 hours. These small fluctuations in the Bragg wavelength while the humidity was constant were due to the slight instability of the temperature in the chamber with time. The Bragg wavelength was almost stable in the remaining 18 hours of the constant 90% RH period as it can be seen from Fig. 3(a).

The temperature characterization was done at a fixed 50% RH by programming the chamber to increase the temperature from 20 °C to 100 °C (the maximum stable operating temperature of the chamber) and then to decrease it down to 20 °C, with steps of 10 °C

Optical Materials EXPRESS

gradually within 10 minutes and stabilization time of 60 minutes. Despite the fact that we demonstrated the temperature measurement only up to 100 °C, due to the limitation of the chamber, it is possible to operate a Zeonex mPOFBG up to 115 – 120 °C as its T_g is 138 °C. Figure 3(b) shows the temperature response in the stabilization period for the range 20 °C to 100 °C at 50% RH. The temperature sensitivity of this fiber is 24.01 ± 0.1 pm/°C for both increasing and decreasing temperature. No hysteresis was observed. This is because the grating was previously annealed 20 °C higher than the maximum reached temperature. This result shows that Zeonex mPOFBG has better temperature sensitivity than that of TOPAS 5013 mPOFBG [18]. The temperature sensitivity of PMMA mPOFBG in the 1550 nm wavelength region is –52 pm/ °C in the range 20 to 89 °C with a grating made in fiber pre-annealed for 7 hours at 80 °C [39].

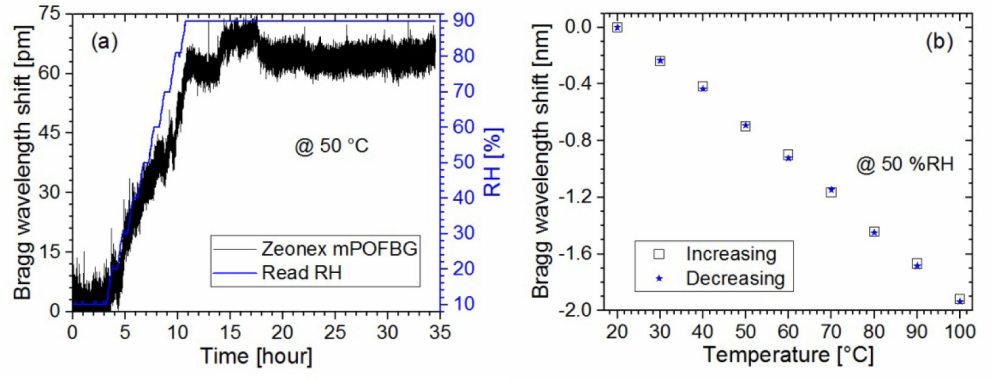

Fig. 3. (a) Humidity response at 50 °C and (b) temperature response at 50% RH of the Zeonex mPOFBG.

The strain response of the Zeonex mPOFBG was studied by mechanically elongating the grating and monitoring its reflection spectrum. A supercontinuum source (SuperK Extreme, NKT Photonics) was used as a light source and a spectrometer (CCS175-Compact Spectrometer, Thorlabs) was used to continuously track the FBG peak during strain test. The fiber was clamped and glued to two micro-translation stages, each being two centimeters away from the grating. One of the stages was used to apply axial strain to the grating manually. Every time a new strain was loaded or unloaded to the grating, 10 minutes was given to it to get stable. The fiber was longitudinally strained up to 3% with steps of 0.5%. As shown in Fig. 4, the grating shows a linear response with an R-square value of 0.999 with no hysteresis. This Zeonex mPOFBG has a strain sensitivity of 0.77 pm/με, for both loading and unloading cases. As expected, this value corresponds to the strain sensitivities reported for both step index and microstructured Topas 5013 POFBG [18,19] in the range 0-3% strain. In the same wavelength region, the strain sensitivities reported for a few [40] and multimode PMMA mPOFBG [41] in the range 0-2% and 0-1% strain, respectively, also match the value obtained for Zeonex mPOFBG.

Optical Materials EXPRESS

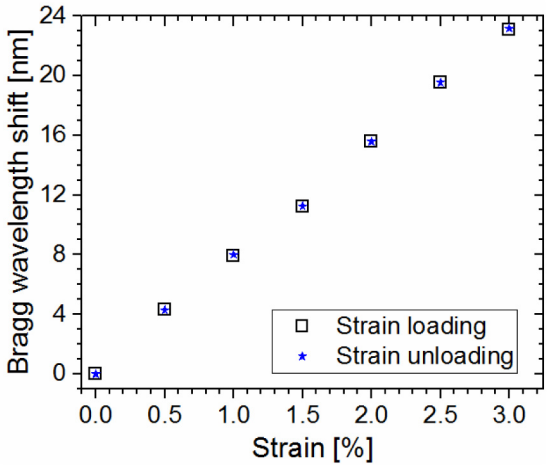

Fig. 4. Strain response of the Zeonex mPOFBG at ambient temperature and RH.

5. Conclusion

In this work, we have fabricated an endlessly single mode and humidity insensitive mPOF by the drill and drawing method. The mPOF was fabricated from norbornene homopolymer Zeonex 480R. Zeonex 480R is humidity insensitive and has a glass transition temperature of 138 °C, making it comparable with the other high operation temperature polymers for optical fibers. Two key points are related to the realization of this fiber. On one hand, the optimization of the casting method allowed reducing material loss to a level very close to other optical polymers, which eventually resulted in low fiber loss. Particularly, it provided an optical transmission one order of magnitude better in the short visible wavelengths compared to Topas core POFs. On the other hand, the higher molecular weight, compared to the ethylene-copolymerized counterpart, allowed for easier fabrication of microstructured fibers. Compared to Topas 5013, Zeonex 480R also provides a wider range of drawing temperature and stress, which gives more room for tailoring the mechanical properties of the resulting fiber to the specific application. The advantage in drawing further ensures a higher repeatability of the microstructured fiber in terms of microstructure and diameter. The realized mPOF has a core diameter and cladding diameter of 8.8 µm and 150 µm, respectively and the minimum measured material and fiber loss are 1.34 ± 0.18 dB/m and 2.34 ± 0.39 dB/m, respectively, around 690 nm. The measured average material and fiber loss in the visible wavelength range are less than 2.5 ± 0.21 dB/m and 3 ± 0.42 dB/m, respectively. A fiber Bragg grating was also inscribed in a Zeonex POF for the first time to our knowledge. The inscription process took less than 5 minutes with 5.5 mW power using a CW He-Cd laser, which we found to be the optimal power to write FBGs in this fiber. Zeonex 480R mPOFBG has shown a greater sensitivity to temperature than that of Topas 5013 mPOFBG.

The improvement in loss compared to Topas fibers allows to access working lengths over 10 m, required for most of polymer fiber sensors applications. Such achievement opens up the way to most of real life applications where the fibers cannot be embedded in water proof compounds or in applications where it is not possible to control moisture and the ambient conditions. We believe that Zeonex mPOFBGs will replace Topas-based FBGs for temperature and strain sensing with no cross sensitivity to humidity and mechanical stability at high temperature. Fiber Bragg gratings inscribed in Zeonex mPOFs are particularly suitable for engineering applications requiring mechanical stability at high temperature and very low moisture absorption. Examples of such applications would span within the automotive and composite materials. The low moisture absorption property also enables to realize high temperature and strain FBG sensor with no cross sensitivity to humidity.

Optical Materials EXPRESS

Funding

People Programme (Marie Curie Actions) of the European Union's Seventh Framework Programme (608382); Danish Research Council (FTP) (4184-00359B); Eugen Lommel stipend; Marie Sklodowska-Curie grant of the European Union's Horizon 2020 research and innovation programme (708860); Carslberg Foundation (CF14-0825) and Innovation Fund Denmark (ShapeOCT) (4107-00011A).

Paper 7

Zeonex-PMMA microstructured polymer optical FBGs for simultaneous humidity and temperature sensing

G. Woyessa, J.M.Pedersen, A. Fasano, K. Nielsen, C. Markos, H.K. Rasmussen, and O. Bang

Optics Letter 42(6), 1161-1164 (2017).

Optics Letters

Zeonex-PMMA microstructured polymer optical FBGs for simultaneous humidity and temperature sensing

Getinet Woyessa,[1,*] Jens K. M. Pedersen,[1] Andrea Fasano,[2] Kristian Nielsen,[1] Christos Markos,[1] Henrik K. Rasmussen,[2] and Ole Bang[1]

[1]DTU Fotonik, Department of Photonics Engineering, Technical University of Denmark, DK-2800 Kgs. Lyngby, Denmark
[2]DTU Mekanik, Department of Mechanical Engineering, Technical University of Denmark, DK-2800 Kgs. Lyngby, Denmark
*Corresponding author: gewoy@fotonik.dtu.dk

Received 26 December 2016; revised 10 February 2017; accepted 14 February 2017; posted 21 February 2017 (Doc. ID 282886); published 13 March 2017

In this Letter, we report for the first time, to the best of our knowledge, the fabrication and characterization of a Zeonex/PMMA microstructured polymer optical fiber (mPOF) Bragg grating sensor for simultaneous monitoring of relative humidity (RH) and temperature. The sensing element (probe) is based on two separate in-line fiber Bragg gratings (FBGs) inscribed in the fabricated mPOF. A root mean square deviation of 0.8% RH and 0.6°C in the range of 10%–90% RH and 20°C–80°C was found. The developed mPOFBG sensor constitutes an efficient route toward low-cost, easy-to-fabricate and compact multi-parameter sensing solutions.

OCIS codes: (060.2280) Fiber design and fabrication; (130.5460) Polymer waveguides; (060.3735) Fiber Bragg gratings; (060.2370) Fiber optics sensors.

https://doi.org/10.1364/OL.42.001161

The interest in polymer optical fibers (POFs) sensors is steadily increasing because of the high flexibility in bending, ease of handling, and non-brittle nature, which are properties that glass fibers do not have [1,2]. In addition, POFs have a high-yield strain with low Young's modulus and are biocompatible, which makes them advantageous for fiber Bragg grating (FBG)-based strain and bio-sensing applications [3–6]. Moreover, some polymers such as PMMA are humidity sensitive and strongly absorb water [7], while other polymers such as Topas and Zeonex were shown to have a very small affinity to water [8–10]. Due to the unique intrinsic properties of POFs, researchers have developed different single-parameter POFBG sensors to measure strain, temperature, humidity, pressure, and so on [11–14], but limited research has been carried out on the development of multi parameter sensing using POFBGs [15–17]. Particularly, simultaneous measurement of the relative humidity (RH) and temperature using POFBGs has not been achieved, although simultaneous monitoring of these two environmental parameters is critical in several areas such as industrial food processing and biomedical areas. The only work reported so far involving the simultaneous measurement of RH and temperature with the inclusion of a single-mode POFBG was by Zhang *et al.* [15]. The sensor head was fabricated by cascading silica FBG and PMMA POFBG. Despite the proposed fiber sensor exhibiting a well-conditioned response, cascading the silica with the polymer fiber with optical adhesive presents some challenging issues. Most of the commercially available optical adhesives cannot maintain their mechanical stability above a certain temperature and RH levels. Consequently, such sensing devices exhibit limited and narrow operational range. Oliveira *et al.* demonstrated a multi-parameter fiber optic sensor based on a multimode POFBG in an interferometer configuration [17]. The proposed sensor has a sensing element which requires gluing a multimode POF with a silica fiber, and this eventually reduces the sensor mechanical stability. In addition, it is difficult to accurately track the response of multimode FBGs and, therefore, these sensing devices suffer from low accuracy and resolution. The lack of consistently tracking of the multimode FBGs makes the ability to monitor humidity almost impossible. However, to date, several thermo-hygrometers were realized with dual in-line FBGs recorded in a standard silica fiber, where one of the FBGs was coated with a humidity sensitive material such as polymer and silica nanosphere films [18,19]. Here we demonstrate the first endlessly single-mode mPOFBGs for direct and simultaneous measurement of RH and temperature by combining the main material properties of two widely-known polymer materials (Zeonex and PMMA). One of the main advantages of the current fiber sensor is that it relies exclusively on polymer materials.

The presented mPOF was fabricated in-house at DTU Fotonik. The polymers used for the fiber fabrication are Zeonex 480R produced by Zeon Corporation and commercial PMMA from Nordisk Plast A/S. First, a Zeonex 480R cane was fabricated as described in [10]. The Zeonex cane was then sleeved with a Zeonex tube which was further sleeved with a PMMA tube, thereby forming an outer over-cladding. The

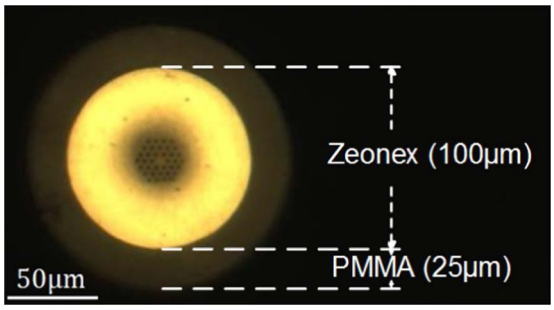

Fig. 1. Optical microscope image of the fabricated ESM Zeonex-PMMA mPOF.

Zeonex/PMMA secondary preform was then drawn to a fiber of ~150 μm diameter. The final fiber consisted of ~100 μm inner diameter of Zeonex material and ~25 μm outer layer of PMMA. The core diameter of the fiber was ~8 μm, and the hole-to-pitch ratio was 0.42, ensuring that the fiber was endlessly single mode (ESM) [20]. An optical microscope image of the Zeonex-PMMA mPOF end facet is shown in Fig. 1. From the fabricated fiber, a 50 cm long piece was connectorized with FC/APC fiber connector [21]. At the other end of the connectorized mPOF, 5 cm long PMMA over-cladding was etched out with acetone (laboratory reagent, ≥ 99.5%, Sigma-Aldrich), thus leaving only the inner Zeonex in this section, as shown in Fig. 2(a) [22]. It should be noted that Zeonex is acetone resistant polymer and, thus, remained unaffected during the etching process [23].

An FBG (FBG_1) with a Bragg wavelength at 865.62 nm was first inscribed in the PMMA etched section of the connectorized mPOF. In order to shift the Bragg wavelength of FBG_1, it was annealed in a conventional oven at 90°C for ~3 h which resulted in a permanent blueshift down to 847.79 nm. After annealing, a second FBG (FBG_2) was inscribed 2 cm away from FBG_1 in the section where the PMMA over-cladding was still intact. The Bragg wavelength of FBG_2 was measured to be 866.11 nm. The FBG inscription technique and the configuration setup used in this Letter have been previously described

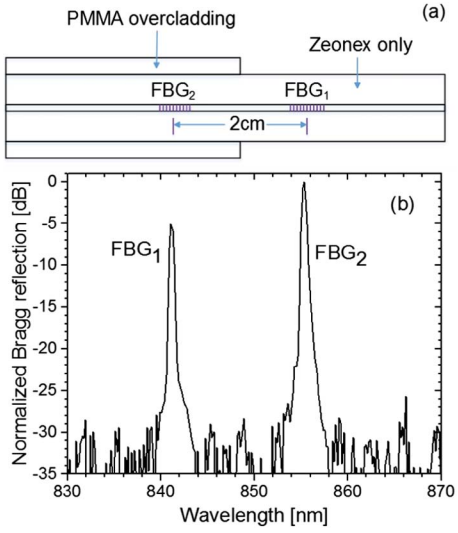

Fig. 2. (a) In-line dual FBGs configuration. (b) Normalized Bragg reflection spectrum of FBG_1 and FBG_2.

in [24]. The two FBGs were finally annealed together in an environmental controlled climate chamber (CLIMACELL, MMM group) at 85°C and 90% RH for 24 h to ensure stable operation of the final sensor [13]. The final locations of the Bragg wavelengths of FBG_1 and FBG_2 after annealing were found to be 841.21 and 855.32 nm, respectively. Figure 2(a) shows a schematic representation of the physical locations of the two gratings, and Fig. 2(b) shows their corresponding reflection spectra at ambient conditions. The two main reasons for using these two particular materials (Zeonex and PMMA) are (1) it has already been demonstrated that Zeonex is humidity insensitive, while PMMA is highly sensitive to humidity [10,13]; and (2) these two materials are compatible in terms of dilatation coefficients for co-drawing [25]. The basic principle behind humidity measurement with the Zeonex/PMMA mPOF relies on the swelling effect caused by PMMA over-cladding while it absorbs moisture, thus inducing an indirect strain on the FBG_2, effectively leading to a shift in the Bragg wavelength.

When we started the design and development of the sensor for simultaneous measurement of temperature and humidity, the first attempt involved the use of a dual grating inscribed in a pure PMMA mPOF. The gratings were superimposed at a single point by using two phase masks, one after the other. The two gratings were inscribed at 780 and at 850 nm [26]. The RH response of the developed sensor was determined, and sensitivities of 40 and 46 pm/%RH were obtained for the shorter and longer Bragg wavelength, respectively. We also attempted to measure the temperature sensitivity of the dual FBGs several times at different RH levels, but it was challenging to accurately determine using our climate chamber. This was because the humidity sensitivity of the PMMA mPOF was significantly high and, therefore, it was causing a considerable influence on the temperature response for 1% RH precision of our climate chamber. In order to overcome this problem, we pre-strained the grating which led to an increase in temperature sensitivity and a decrease in humidity sensitivity [27,28]. Based on this approach, we successfully measured both parameters. However, the adhesive used to fix the strained fiber, was softening; thus, the fiber tended to slip when the temperature and the RH were increased beyond 60°C and 70% RH levels, respectively. Therefore, this experimental limitation did not allow us to fully investigate the potential of the sensor over its maximum operational limits. In addition, the aforementioned approach required additional mechanical components to maintain the fiber strained, thus making the idea of a compact sensing system, for instance, suitable for structural health monitoring, even more challenging. Moreover, the two gratings required being distinctively apart from each other in wavelength in order to obtain a well-conditioned response. Even though dual gratings that are distinctively apart provide a well-conditioned response, the use of a very broad light source such as supercontinuum sources is required to interrogate the gratings which increases the cost of the sensor system. Last but not least, the requirement of two different phase masks for writing the two gratings further increases the cost of the sensor development.

We also considered Topas 5013S-04 as the fiber core material because of its low water affinity compared to PMMA. However, due to the high flowability of Topas, it was impossible to draw it with a PMMA sleeve while still maintaining the microstructure during the drawing process.

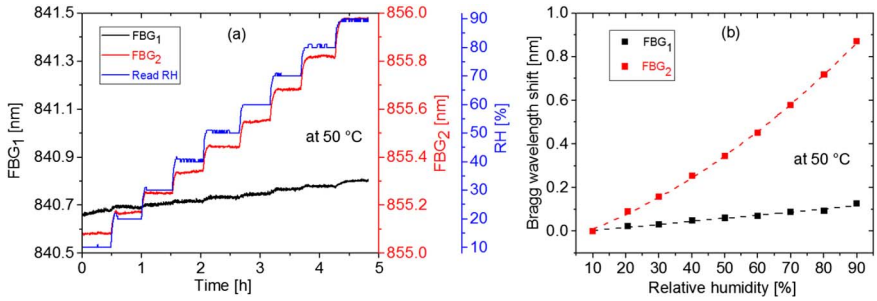

Fig. 3. (a) Measured humidity response and (b) corresponding stabilized humidity response of FBG_1 and FBG_2 at 50°C. The dashed lines correspond to a linear fit of FBG_1 data and a second-order polynomial fit of FBG_2 data.

Topas was flowing very fast inside the PMMA sleeving tube and collapsing to produce a step index structure, which was not desirable, as the resulting fiber was highly multimoded. At the same drawing conditions, Zeonex 480R shows flowability properties more suited for fiber drawing than that of Topas 5013S-04. In particular, at the same draw temperature, the flowability of Zeonex is lower than that of Topas 5013S-04. In addition, a multicore step index fiber has already been fabricated based on Zeonex 480R and PMMA which confirms that the compatibility of these two materials is well suited for co-drawing [24].

The calibration of the fabricated sensor was made in a climate chamber (CLIMACELL, MMM group) with a RH and temperature precision of 1% and 0.3°C, respectively, in the range 20°C–100°C and 10%–90% RH. A supercontinuum source (SuperK Compact, NKT Photonics) was used as a broadband light source, and a spectrometer (CCS175 - Compact Spectrometer, Thorlabs) was used to continuously track and record the reflection spectrum from the sensors during the experiments. First, the RH calibration was performed at 50°C by increasing the RH from 10% to 90% in steps of 10% RH. The chamber was programmed to change the RH in a minute and then to maintain the environmental conditions stable for 30 min for each step. Figure 3 shows the humidity responses of both FBG_1 and FBG_2 at 50°C. The temperature calibration was done in the range 20°C–80°C at 50% RH, following the RH measurement. The chamber was programmed to ramp the temperature by 10°C in 30 min and then to maintain the environmental conditions constant for 30 min. Figure 4 shows the temperature responses of both FBG_1 and FBG_2 at 50% RH.

A suitable model for the responses of the two FBGs, including the nonlinear humidity response of FBG_2, is

$$\Delta\lambda_1 = \alpha_1\Delta T + \beta_1\Delta H, \tag{1}$$

$$\Delta\lambda_2 = \alpha_2\Delta T + \beta_2\Delta H + \gamma_2\Delta H^2, \tag{2}$$

where $\Delta\lambda_1$ and $\Delta\lambda_2$ are the Bragg wavelength shifts of FBG_1 and FBG_2, respectively, as a result of changes in RH ΔH and temperature ΔT. By combining (1) and (2) we derive the following expression for the change in RH:

$$\Delta H = \frac{1}{2\gamma_2}\left(\frac{\alpha_2}{\alpha_1}\beta_1 - \beta_2 + \sqrt{D}\right), \tag{3}$$

where

$$D = \left(\beta_2 - \frac{\alpha_2}{\alpha_1}\beta_1\right)^2 - 4\gamma_2\left(\frac{\alpha_2}{\alpha_1}\Delta\lambda_1 - \Delta\lambda_2\right).$$

Once the coefficients $\alpha_{1,2}$, $\beta_{1,2}$ and γ_2 have been determined by fitting the polynomial equations to the calibration data, we are then able to determine the RH using Eq. (3) and, subsequently, the temperature from Eq. (1) by simultaneously measuring the Bragg wavelength shifts of the two FBGs. By fitting the data in Figs. 3(b) and 4(b), we found the following parameters, with $\Delta T = 0$ at $T = 50$°C and $\Delta H = 0$ at $H = 50\%$ RH corresponding to $\Delta\lambda_1 = \Delta\lambda_2 = 0$, and the stated uncertainties are the standard errors of the fitting parameters shown in Table 1.

Using these coefficients, we reconstructed the values measured during the calibration from the corresponding measured values of λ_1 and λ_2; see Fig. 5. The root mean square deviations of the reconstructed values were 0.8% RH and 0.6°C for the RH and temperature, respectively, which should be compared with the precision of the climate chamber of 1% RH and 0.3°C. These results show that the proposed sensor system is a viable way of effectively separating the responses to temperature and humidity. In order to estimate the resolution of the sensor, which is limited by the resolution related to the detection of λ_1 and λ_2, we calculated the combined variance:

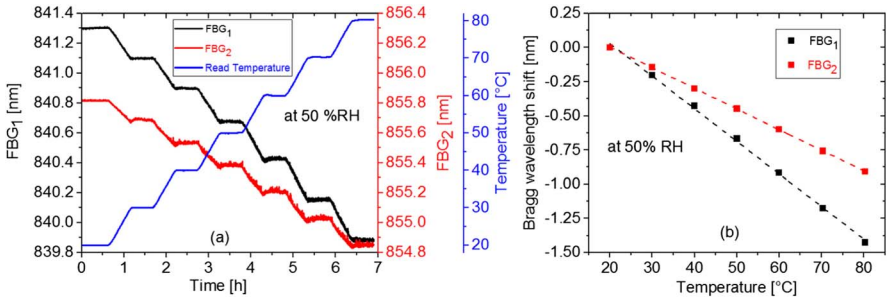

Fig. 4. (a) Measured temperature response and (b) corresponding stabilized temperature response of FBG_1 and FBG_2 at 50% RH. The dashed lines correspond to the linear fitting of the data.

Table 1. Standard Errors of the Fitting Parameters

i	α_i (pm/°C)	β_i (pm/% RH)	γ_i (pm/(% RH)^2)
1	−23.9 ± 0.4	1.4 ± 0.1	—
2	−15.1 ± 0.1	6.4 ± 0.5	0.057 ± 0.004

$$\sigma_H^2 = \left(\frac{\partial \Delta H}{\partial \Delta\lambda_1}\sigma_\lambda\right)^2 + \left(\frac{\partial \Delta H}{\partial \Delta\lambda_{21}}\sigma_\lambda\right)^2, \tag{4}$$

$$\sigma_T^2 = \left(\frac{\partial \Delta T}{\partial \Delta\lambda_1}\sigma_\lambda\right)^2 + \left(\frac{\partial \Delta T}{\partial \Delta\lambda_{21}}\sigma_\lambda\right)^2, \tag{5}$$

where σ_λ is the standard deviation related to the detection of $\Delta\lambda_1$ and $\Delta\lambda_2$, which was measured to be 5 pm during the experiments. Using Eqs. (3)–(5), the RH and temperature resolution of the sensor at a 68% confidence level can be expressed as

$$\sigma_H = \sigma_\lambda \sqrt{\frac{1}{D}\left(1 + \frac{\alpha_2^2}{\alpha_1^2}\right)} \quad \text{and}$$

$$\sigma_T = \frac{\sigma_\lambda}{|\alpha_1|}\sqrt{\left(1 + \frac{\alpha_2}{\alpha_1}\frac{\beta_1}{\sqrt{D}}\right)^2 + \frac{\beta_1^2}{D}}. \tag{6}$$

Figure 6 shows the RH and temperature resolution of the sensor calculated using Eq. (6).

As can be seen from Fig. 6(a), due to the nonlinear humidity response of FBG_2, the RH resolution is not constant over the sensing range. It improves at higher levels of RH due to the increased sensitivity, whereas it remains invariant to temperature changes, as can be seen from Fig. 6(b).

In conclusion, we reported an all-fiber sensor suitable for the simultaneous measurement of the temperature and humidity using mPOFBGs. The fiber was fabricated from two types of polymers: Zeonex, which has a low affinity to water, and PMMA, which is highly humidity sensitive. Root mean square deviations of 0.8% RH and 0.6°C were observed in our experimental results in the measured range of 10%–90% RH and 20°C–80°C. The developed sensor system offers a number of advantages such as ease of fabrication, cost-effectiveness, and compactness. In addition, as the Bragg wavelengths of the two gratings are close to each other, it would be possible to use not only a low-cost light source to interrogate the grating but also the multiplex multiple dual gratings in a single fiber. Moreover, only one phase mask is required for the FBG inscription, thus making the development of the sensor cost-effective.

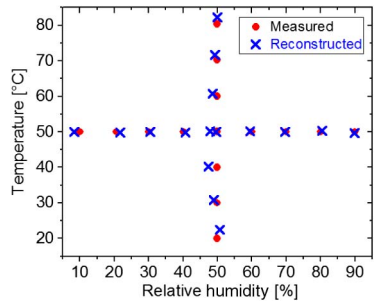

Fig. 5. Reconstruction of the temperature and RH from the measured values of λ_1 and λ_2.

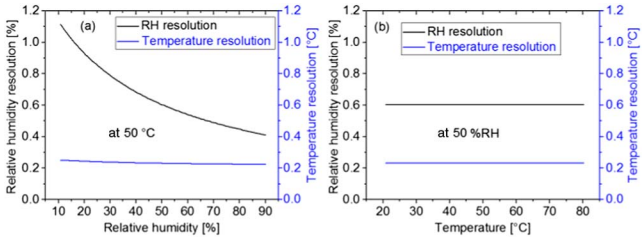

Fig. 6. RH and temperature resolution of the sensor as a function of (a) RH and (b) temperature.

Funding. People Programme (Marie Curie Actions) of the European Union's Seventh Framework Programme (FP7) (608382); Innovation Fund Denmark (1382-00058B); ShapeOCT (4107-00011A); Danish Council for Independent Research (4184-00359B).

REFERENCES

1. K. Peters, Smart Mater. Struct. **20**, 013002 (2011).
2. D. J. Webb, Meas. Sci. Technol. **26**, 092004 (2015).
3. H. Dobb, D. J. Webb, K. Kalli, A. Argyros, M. C. J. Large, and M. A. van Eijkelenborg, Opt. Lett. **30**, 3296 (2005).
4. Z. Xiong, G. D. Peng, B. Wu, and P. L. Chu, IEEE Photon. Technol. Lett. **11**, 352 (1999).
5. A. Stefani, S. Andresen, W. Yuan, N. Herholdt-Rasmussen, and O. Bang, IEEE Photon. Technol. Lett. **24**, 763 (2012).
6. J. Jensen, P. Hoiby, G. Emiliyanov, O. Bang, L. Pedersen, and A. Bjarklev, Opt. Express **13**, 5883 (2005).
7. N. G. Harbach, "Fiber Bragg gratings in polymer optical fibers," Ph.D. thesis (EPFL, 2008).
8. C. Markos, A. Stefani, K. Nielsen, H. K. Rasmussen, W. Yuan, and O. Bang, Opt. Express **21**, 4758 (2013).
9. G. Woyessa, A. Fasano, A. Stefani, C. Markos, K. Nielsen, H. K. Rasmussen, and O. Bang, Opt. Express **24**, 1253 (2016).
10. G. Woyessa, A. Fasano, C. Markos, A. Stefani, H. K. Rasmussen, and O. Bang, Opt. Mater. Express **7**, 286 (2017).
11. W. Yuan, A. Stefani, M. Bache, T. Jacobsen, B. Rose, N. Herholdt-Rasmussen, F. K. Nielsen, S. Andresen, O. B. Sørensen, K. S. Hansen, and O. Bang, Opt. Commun. **284**, 176 (2011).
12. I. P. Johnson, D. J. Webb, and K. Kalli, Proc. SPIE **8351**, 835106 (2012).
13. G. Woyessa, K. Nielsen, A. Stefani, C. Markos, and O. Bang, Opt. Express **24**, 1206 (2016).
14. K. E. Carroll, C. Zhang, D. J. Webb, K. Kalli, A. Argyros, and M. C. J. Large, Opt. Express **15**, 8844 (2007).
15. C. Zhang, W. Zhang, D. J. Webb, and G. D. Peng, Electron. Lett. **46**, 643 (2010).
16. K. Bhowmik, G. D. Peng, E. Ambikairajah, V. Lovric, W. Walsh, B. Prusty, and G. Rajan, IEEE Photon. Technol. Lett. **27**, 604 (2015).
17. R. Oliveira, T. H. R. Marques, L. Bilro, R. Nogueira, and C. M. B. Cordeiro, J. Lightwave Technol. **35**, 3 (2017).
18. N. A. David, P. M. Wild, J. Jensen, T. Navessin, and N. Djilali, J. Electrochem. Soc. **157**, B1173 (2010).
19. D. Viegas, M. Hernaéz, J. Goicoechea, J. L. Santos, F. M. Araújo, F. Arregui, and I. R. Matias, IEEE Sens. **11**, 162 (2011).
20. T. A. Birks, J. C. Knight, and P. St.J. Russell, Opt. Lett. **22**, 961 (1997).
21. A. Abang and D. J. Webb, Opt. Eng. **51**, 080503 (2012).
22. X. Hu, C. F. J. Pun, H.-Y. Tam, P. Mégret, and C. Caucheteur, Opt. Express **22**, 18807 (2014).
23. S. Bäumer, *Handbook of Plastic Optics* (Wiley-VCH, 2011).
24. I.-L. Bundalo, K. Nielsen, C. Markos, and O. Bang, Opt. Express **22**, 5270 (2014).
25. S. G. Leon-Saval, R. Lwin, and A. Argyros, Opt. Express **20**, 141 (2012).
26. G. Statkiewicz-Barabach, K. Tarnowski, D. Kowal, P. Mergo, and W. Urbanczyk, Opt. Express **21**, 8521 (2013).
27. W. Zhang, D. J. Webb, and G. D. Peng, Opt. Lett. **40**, 4046 (2015).
28. W. Zhang and D. J. Webb, Opt. Lett. **39**, 3026 (2014).

Bibliography

[1] E. Udd, 'An overview of fiber-optic sensors', *Review of Scientific Instruments*, vol. 66, no. 8. pp. 4015–4030, 1995.

[2] B. Culshaw and J. Dakin, *Optical fiber sensors: Systems and applications. Volume 2*. Boston, MA: Artech House, 1989.

[3] K. Bohnert, P. Gabus, and H. Brändle, 'Fiber-Optic Current and Voltage Sensors for High-Voltage Substations', *Invit. Pap. 16th Int. Conf. Opt. Fiber Sensors, Nara Japan,Technical Dig.*, pp. 752–754, 2003.

[4] L. Sun, S. Jiang, and J. R. Marciante, 'All-fiber optical magnetic-field sensor based on Faraday rotation in highly terbium-doped fiber', *Opt. Express*, vol. 18, no. 6, pp. 5407–5412, 2010.

[5] G. Zhou and L. M. Sim, 'Damage detection and assessment in fibre-reinforced composite structures with embedded fibre optic sensors-review', *Smart Mater. Struct.*, vol. 11, no. 6, pp. 925–939, 2002.

[6] N. D. W. Glossop *et al.*, 'Optical fibre damage detection for an aircraft composite leading edge', *Composites*, vol. 21, no. 1, pp. 71–80, 1990.

[7] R. Chen *et al.*, 'Acoustic Emission detection using a novel fibre optic sensor', *Acoust. Emiss. Test.*, vol. 13–14, pp. 99–104, 2006.

[8] A. Inoue, M. Shigehara, M. Ito, M. Inai, Y. Hattori, and T. Mizunami, 'Fabrication and Application of Fiber Bragg Grating - a Review', *Optoelectron. Technol.*, vol. 10, no. 1, pp. 119–130, 1995.

[9] Y. J. Rao, 'In-fibre Bragg grating sensors', *Meas. Sci. Technol.*, vol. 8, no. 4, pp. 355–375, 1997.

[10] K. O. Hill, Y. Fujii, D. C. Johnson, and B. S. Kawasaki, 'Photosensitivity in optical fiber waveguides: Application to reflection filter fabrication', *Appl. Phys. Lett.*, vol. 32, no. 10, pp. 647–649, 1978.

[11] A. Cusano, D. Paladino, A. Cutolo, A. Iadicicco, and S. Campopiano, *Fiber Bragg Grating Sensors: Recent Advancements, Industrial Applications and Market Exploitation*. Bentham Science Publishers Ltd., 2012.

[12] D. J. Webb, 'Fibre Bragg grating sensors in polymer optical fibres', *Meas. Sci. Technol.*, vol. 26, no. 9, p. 92004, 2015.

[13] H. Dobb, D. J. Webb, K. Kalli, A. Argyros, M. C. J. Large, and M. A. van Eijkelenborg, 'Continuous wave ultraviolet light-induced fiber Bragg gratings in few- and single-mode microstructured polymer optical fibers', *Opt. Lett.*, vol. 30, no. 24, pp. 3296–3298, 2005.

[14] A. Stefani, S. Andresen, W. Yuan, N. Herholdt-Rasmussen, and O. Bang, 'High sensitivity polymer optical fiber-bragg-grating-based accelerometer', *IEEE Photonics Technol. Lett.*, vol. 24, no. 9, pp. 763–765, 2012.

[15] J. B. Jensen, P. E. Hoiby, G. Emiliyanov, O. Bang, L. H. Pedersen, and A. Bjarklev, 'Selective detection of antibodies in microstructured polymer optical fibers', *Opt. Express*, vol. 13, no. 15, p. 5883, 2005.

[16] G. Emiliyanov *et al.*, 'Localized biosensing with Topas microstructured polymer optical fiber', *Opt. Lett.*, vol. 32, no. 5, pp. 460–2, 2007.

[17] C. Markos, W. Yuan, K. Vlachos, G. E. Town, and O. Bang, 'Label-free biosensing with high sensitivity in dual-core microstructured polymer optical fibers', *Opt. Express*, vol. 19, no. 8, pp. 7790–8, 2011.

[18] H. Ul Hassan, K. Nielsen, S. Aasmul, and O. Bang, 'Compound parabolic concentrator optical fiber tip for FRET based fluorescent sensors', *Biomed. Opt. Express*, vol. 9634, no. 12, pp. 1–4, 2015.

[19] C. Broadway *et al.*, 'Fabry-Perot micro-structured polymer optical fibre sensors for opto-acoustic endoscopy', in *Progress in Biomedical Optics and Imaging - Proceedings of SPIE*, 2015, vol. 9531.

[20] S. Egusa *et al.*, 'Multimaterial piezoelectric fibres', *Nat. Mater.*, vol. 9, no. 8, pp. 643–648, 2010.

[21] F. Abouraddy *et al.*, 'Towards multimaterial multifunctional fibres that see, hear, sense and communicate', *Nat. Mater.*, vol. 6, no. 5, pp. 336–347, 2007.

[22] J. Zubia and J. Arrue, 'Plastic optical fibers: An introduction to their technological processes and applications', *Opt. Fiber Technol.*, vol. 7, no. 2, pp. 101–140, 2001.

[23] M. C. J. Large, L. Poladian, G. W. Barton, and M. A. Van Eijkelenborg, *Microstructured polymer optical fibres*. Springer US, 2008.

[24] A. Yeniay, R. Gao, K. Takayama, R. Gao, and A. F. Garito, 'Ultra-Low-Loss Polymer Waveguides', in *Journal of Lightwave Technology*, 2004, vol. 22, no. 1, pp. 154–158.

[25] Y. Koike and T. Ishigure, 'High-bandwidth plastic optical fiber for fiber to the display', *J. Light. Technol.*, vol. 24, no. 12, pp. 4541–4553, 2006.

[26] T. Kaino, K. Jinguji, and S. Nara, 'Low loss poly(methylmethacrylate-d8) core optical fibers', *Appl. Phys. Lett.*, vol. 42, no. 7, pp. 567–569, 1983.

[27] N. Tanio and Y. Koike, 'What Is the Most Transparent Polymer?', *Polym. J.*, vol. 32, no. 1, pp. 43–50, 2000.

[28] M. A. van Eijkelenborg *et al.*, 'Microstructured polymer optical fibre', *Opt. Express*, vol. 9, no. 7, pp. 319–327, 2001.

[29] A. Othonos, K. Kalli, and G. E. Kohnke, 'Fiber Bragg Gratings: Fundamentals and Applications in Telecommunications and Sensing', *Phys. Today*, vol. 53, no. 5, p. 61, 2000.

[30] 'Graded-Index Polymer Optical Fiber (GI-POF)'. [Online]. Available: https://www.thorlabs.com/catalogPages/1100.pdf.

[31] A. Argyros, 'Microstructured Polymer Optical Fibers', *J. Light. Technol.*, vol. 27, no. 11, pp. 1571–1579, 2009.

[32] J. Wilson, 'Optoelectronics: An Introduction', *American Journal of Physics*, vol. 52, no. 5. p. 479, 1984.

[33] T. A. Birks, J. C. Knight, P. S. Russell, and D. M. Atkin, 'All-silica single-mode optical fiber with photonic crystal cladding', *Opt. Lett.*, vol. 21, no. 19, pp. 1547–1549, 1996.

[34] J. C. Knight, J. Broeng, T. A. Birks, and P. S. J. Russell, 'Photonic Band Gap Guidance in Optical Fibers', *Science (80-.).*, vol. 282, no. 5393, pp. 1476–1478, 1998.

[35] T. A. Birks, J. C. Knight, and P. S. J. Russell, 'Endlessly single-mode photonic crystal fiber', *Opt. Lett.*, vol. 22, no. 13, p. 961, 1997.

[36] N. A. Mortensen, 'Semianalytical approach to short-wavelength dispersion and modal properties of photonic crystal fibers', *Opt. Lett.*, vol. 30, no. 12, pp. 1455–1457, 2005.

[37] N. A. Mortensen, J. R. Folkenberg, M. D. Nielsen, and K. P. Hansen, 'Modal cutoff and the V parameter in photonic crystal fibers', *Opt. Lett.*, vol. 28, no. 20, pp. 1879–1881, 2003.

[38] R. Lwin *et al.*, 'Suspended Core Microstructured Polymer Optical Fibre: Connecting to Reality', in *Proceedings of the Australian Conference on Optical Fibre Technology*, pp. 2–4, 2005.

[39] A. Argyros, M. A. van Eijkelenborg, M. C. J. Large, and I. M. Bassett, 'Hollow-core microstructured polymer optical fiber', *Opt. Lett.*, vol. 31, no. 2, pp. 172–174, 2006.

[40] M. A. van Eijkelenborg, N. Issa, M. Hiscocks, C. Lwin, C. von Korff Schmising, and R. Lwin, 'Rectangular-core microstructured polymer optical fibre for interconnect applications', *Electron. Lett.*, vol. 42, no. 4, pp. 201–202, 2006.

[41] M. A. van Eijkelenborg *et al.*, 'Bandwidth and loss measurements of graded-index microstructured polymer optical fibre', *Electron. Lett.*, vol. 40, no. 10, pp. 592–593, 2004.

[42] M. K. Szczurowski, O. Frazão, J. M. Baptista, K. Nielsen, O. Bang, and W. Urbańczyk, 'Sensing characteristics of birefringent microstructured polymer optical fiber', in *21st International Conference on Optical Fiber Sensors*, 2011, vol. 7753, p. 77533Z.

[43] W. E. P. Padden, M. A. van Eijkelenborg, A. Argyros, and N. A. Issa, 'Coupling in a twin-core microstructured polymer optical fiber', *Appl. Phys. Lett.*, vol. 84, no. 10, p. 1689, 2004.

[44] M. A. van Eijkelenborg, A. Argyros, and A. Bachmann, 'Imaging with microstructured polymer fibre', *Opt. Express*, vol. 12, no. 2, pp. 342–6, 2004.

[45] O. Ziemann, J. Krauser, P. E. Zamzow, and W. Daum, *POF handbook: Optical short range transmission systems*. Springer-Verlag Berlin Heidelberg, 2008.

[46] H. Y. Liu, G. D. Peng, and P. L. Chu, 'Thermal tuning of polymer optical fiber Bragg gratings', *IEEE Photonics Technol. Lett.*, vol. 13, no. 8, pp. 824–826, 2001.

[47] W. Yuan *et al.*, 'Improved thermal and strain performance of annealed polymer optical fiber Bragg gratings', *Opt. Commun.*, vol. 284, no. 1, pp. 176–182, 2011.

[48] H. B. Liu, H. Y. Liu, G. D. Peng, and P. L. Chu, 'Strain and temperature sensor using a combination of polymer and silica fibre Bragg gratings', *Opt. Commun.*, vol. 219, no. 1, pp. 139–142, 2003.

[49] 'Cyclic Olefin Copolymer (COC)'. [Online]. Available: http://www.topas.com/sites/default/files/files/TOPAS_Brochure_E_2014_06(1).pdf.

[50] I. P. Johnson *et al.*, 'Optical fibre Bragg grating recorded in TOPAS cyclic olefin copolymer', *Electron. Lett.*, vol. 47, no. 4, pp. 271–272, 2011.

[51] C. Markos, A. Stefani, K. Nielsen, H. K. Rasmussen, W. Yuan, and O. Bang, 'High-Tg TOPAS microstructured polymer optical fiber for fiber Bragg grating strain sensing at 110 degrees', *Opt. Express*, vol. 21, no. 4, pp. 4758–65, 2013.

[52] C. Emslie, 'Review: Polymer optical fibres', *J. Mater. Sci.*, vol. 23, no. 7, pp. 2281–2293, 1988.

[53] M. Beckers, T. Schlüter, T. Vad, T. Gries, and C. A. Bunge, 'An overview on fabrication methods for polymer optical fibers', *Polym. Int.*, vol. 64, no. 1, pp. 25–36, 2015.

[54] D. Bosc and C. Toinen, 'Fully polymer single-mode optical fibre', *IEEE Photonics Technol. Lett.*, vol. 4, no. 7, pp. 794–751, 1992.

[55] M. G. Kuzyk, U. C. Paek, and C. W. Dirk, 'Guest-host polymer fibre for nonlinear optics', *Appl. Phys. Lett.*, vol. 59, no. 8, pp. 902–904, 1991.

[56] G. Peng, P. Chu, Z. Xiong, T. Whitbread, and R. Chaplin, 'Dye-doped step-index polymer optical fibre for broadband optical amplification', *J. Light. Technoolgy*, vol. 14, no. 10, pp. 2215–2223, 1996.

[57] H. H. Park, B. G. Shin, and J. J. Kim, 'Fabrication of plastic holey polymer fibers', in *in Proceedings of the 11 th international Plastic Optical Fibers Conference*, pp. 9–11, 2002.

[58] H. Ebendorff-Heidepriem *et al.*, 'Extrusion of complex preforms for microstructured optical fibers', *Cryst*, vol. 446, pp. 219–231, 2006.

[59] Y. Zhang *et al.*, 'Casting preforms for microstructured polymer optical fibre fabrication', *Opt. Express*, vol. 14, no. 12, pp. 5541–5547, 2006.

[60] G. Barton, M. A. Van Eijkelenborg, G. Henry, M. C. J. Large, and J. Zagari, 'Fabrication of microstructured polymer optical fibres', *Opt. Fiber Technol.*, vol. 10, pp. 325–335, 2004.

[61] Z. Xiong, G. D. Peng, B. Wu, and P. L. Chu, 'Highly Tunable Bragg Gratings in Single-Mode Polymer Optical Fibers', *IEEE Photonics Technol. Lett.*, vol. 11, no. 3, pp. 352–354, 1999.

[62] W. J. Tomlinson, I. P. Kaminow, E. A. Chandross, R. L. Fork, and W. T. Silfvast, 'Photoinduced refractive index increase in poly(methylmethacrylate) and its applications', *Appl. Phys. Lett.*, vol. 16, no. 12, pp. 486–489, 1970.

[63] G. Rajan and K. Iniewski, *Optical fiber sensors: advanced techniques and applications*. CRC Press, 2015.

[64] J. Yu, X. Tao, and H. Tam, 'Trans-4-stilbenemethanol-doped photosensitive polymer fibers and gratings', *Opt. Lett.*, vol. 29, no. 2, pp. 156–8, 2004.

[65] W. Yuan, A. Stefani, and O. Bang, 'Tunable Polymer Fiber Bragg Grating (FBG) Inscription: Fabrication of Dual-FBG Temperature Compensated Polymer Optical Fiber Strain Sensors', *IEEE Photonics Technol. Lett.*, vol. 24, no. 5, pp. 401–403, 2012.

[66] I. P. Johnson, D. J. Webb, K. Kalli, M. C. J. Large, and A. Argyros, 'Multiplexed FBG sensor recorded in multimode microstructured polymer optical fibre', *Proc. SPIE-The Int. Soc. Opt. Eng.*, vol. 7714, p. 77140D–77140D, 2010.

[67] B. Malo, K. O. Hill, F. Bilodeau, D. C. Johnson, and J. Albert, 'Point-by-point fabrication of micro-Bragg gratings in photosensitive fibre using single excimer pulse refractive index modification techniques', *Electron. Lett.*, vol. 29, no. 18, p. 1668, 1993.

[68] A. Martinez, M. Dubov, I. Khrushchev, and I. Bennion, 'Direct writing of fibre Bragg gratings by femtosecond laser', *Electron. Lett.*, vol. 40, no. 19, pp. 1170–1172, 2006.

[69] A. Stefani, M. Stecher, G. E. Town, and O. Bang, 'Direct writing of fiber bragg grating in microstructured polymer optical fiber', *IEEE Photonics Technol. Lett.*, vol. 24, no. 13, pp. 1148–1150, 2012.

[70] A. Lacraz, M. Polis, A. Theodosiou, C. Koutsides, and K. Kalli, 'Femtosecond Laser Inscribed Bragg Gratings in Low Loss CYTOP Polymer Optical Fiber', *IEEE Photonics Technol. Lett.*, vol. 27, no. 7, pp. 693–696, 2015.

[71] K. Kalli, A. Theodosiou, and A. Lacraz, 'Femtosecond laser inscribed Bragg grating arrays in long lengths of polymer optical fibres; a route to practical sensing with POF', *Electron. Lett.*, vol. 52, no. 19, pp. 1626–1627, 2016.

[72] M. Stecher, R. J. Williams, O. Bang, G. D. Marshall, M. J. Withford, and G. E. Town, 'Periodic refractive index modifications inscribed in polymer optical fibre by focussed femtosecond pulses', *Int. Conf. Plast. Opt. Fibers*, pp. 3–5, 2009.

[73] G. D. Marshall, D. J. Kan, A. A. Asatryan, L. C. Botten, and M. J. Withford, 'Transverse coupling to the core of a photonic crystal fiber: the photo-inscription of gratings', *Opt. Express*, vol. 15, no. 12, pp. 7876–7887, 2007.

[74] T. Baghdasaryan, T. Geernaert, F. Berghmans, and H. Thienpont, 'Geometrical study of a hexagonal lattice photonic crystal fiber for efficient femtosecond laser grating inscription', *Opt. Express*, vol. 19, no. 8, pp. 7705–7716, 2011.

[75] I. L. Bundalo, K. Nielsen, and O. Bang, 'Angle dependent Fiber Bragg grating inscription in microstructured polymer optical fibers', *Opt. Express*, vol. 23, no. 3, p. 3699, 2015.

[76] A. Stefani, W. Yuan, C. Markos, and O. Bang, 'Narrow bandwidth 850-nm fiber Bragg gratings in few-mode polymer optical fibers', *IEEE Photonics Technol. Lett.*, vol. 23, no. 10, pp. 660–662, 2011.

[77] H. Y. Liu, H. B. Liu, G. D. Peng, and P. L. Chu, 'Observation of type I and type II gratings behavior in polymer optical fiber', *Opt. Commun.*, vol. 220, no. 4–6, pp. 337–343, 2003.

[78] W. Yuan *et al.*, 'Humidity insensitive TOPAS polymer fiber Bragg grating sensor', *Opt. Express*, vol. 19, no. 20, pp. 19731–9, 2011.

[79] I. L. Bundalo, K. Nielsen, C. Markos, and O. Bang, 'Bragg grating writing in PMMA microstructured polymer optical fibers in less than 7 minutes', *Opt. Express*, vol. 22, no. 5, pp. 5270–6, 2014.

[80] R. Oliveira, L. Bilro, and R. Nogueira, 'Bragg gratings in a few mode microstructured polymer optical fiber in less than 30 seconds', *Opt. Express*, vol. 23, no. 8, pp. 10181–10187, 2015.

[81] I. Johnson, K. Kalli, and D. J. Webb, '827nm Bragg grating sensor in multimode microstructured polymer optical fibre', *Electron. Lett.*, vol. 46, no. 17, pp. 3–4, 2010.

[82] J. Terblanche, D. Schmieder, and J. Meyer, 'Fibre Bragg gratings in polymer optical fibre at 980 nm', in *Proc. SPIE 7503, 20th International Conference on Optical Fibre Sensors, 75037F*, 2009.

[83] G. Statkiewicz-Barabach, K. Tarnowski, D. Kowal, P. Mergo, and W. Urbanczyk, 'Fabrication of multiple Bragg gratings in microstructured polymer fibers using a phase mask with several diffraction orders', *Opt. Express*, vol. 21, no. 7, pp. 8521–8534, 2013.

[84] D. Sáez-Rodríguez, K. Nielsen, H. K. Rasmussen, O. Bang, and D. J. Webb, 'Highly photosensitive polymethyl methacrylate microstructured polymer optical fiber with doped core', *Opt. Lett.*, vol. 38, no. 19, pp. 3769–3772, 2013.

[85] X. Hu *et al.*, 'Bragg grating photo-inscription in doped microstructured polymer optical fiber by 400 nm femtosecond laser pulses', in *Proceedings of the 25th International Conference on Plastic Optical Fibers*, 2016.

[86] L. Bjerkan, 'Application of fiber-optic bragg grating sensors in monitoring environmental loads of overhead power transmission lines', *Appl. Opt.*, vol. 39, no. 4, pp. 554–560, 2000.

[87] É. Pinet, 'Medical applications: Saving lives', *Nat. Photonics*, vol. 2, no. 3, pp. 150–152, 2008.

[88] M. Aufleger, M. Conrad, M. Goltz, S. Perzlmaier, and P. Porras, 'Innovative Dam Monitoring Tools Based on Distributed Temperature Measurement', *Jordan J. Civ. Eng.*, vol. 1, no. 1, 2007.

[89] P. M. Tracey, 'Intrinsic Fiber-Optic Sensors', *IEEE Trans. Ind. Appl.*, vol. 27, no. 1, pp. 96–98, 1991.

[90] A. D. Kersey *et al.*, 'Fiber grating sensors', *J. Light. Technol.*, vol. 15, no. 8, pp. 1442–1463, 1997.

[91] D. X. Yang, J. Yu, X. Tao, and H. Tam, 'Structural and mechanical properties of polymeric optical fiber', *Mater. Sci. Eng. A*, vol. 364, no. 1–2, pp. 256–259, 2004.

[92] M. C. J. Large, J. Moran, and L. Ye, 'The role of viscoelastic properties in strain testing using microstructured polymer optical fibres (mPOF)', *Meas. Sci. Technol.*, vol. 20, no. 3, p. 34014, 2009.

[93] J. Brandrup, E. Immergut, and E. A. Grulke, 'Polymer handbook', *John Wiley Sons, Inc*, vol. 12, no. 3, p. 265, 1990.

[94] K. Peters, 'Polymer optical fiber sensors - A review', *Smart Mater. Struct.*, vol. 20, no. 1, 2011.

[95] 'Materials Data Book', *Cambridge University Engineering Department*, 2003. [Online]. Available: http://www-mdp.eng.cam.ac.uk/web/library/enginfo/cueddatabooks/materials.pdf.

[96] S. F. H. Correia *et al.*, 'Optical fiber relative humidity sensor based on a FBG with a di-ureasil coating', *Sensors (Switzerland)*, vol. 12, no. 7, pp. 8847–8860, 2012.

[97] T. L. Yeo, K. T. V. Grattan, D. Parry, R. Lade, and B. D. Powell, 'Polymer-coated fiber Bragg grating for relative humidity sensing', *IEEE Sens. J.*, vol. 5, no. 5, pp. 1082–1089, 2005.

[98] B. N. Shivananju *et al.*, 'Highly sensitive carbon nanotubes coated etched fiber bragg grating sensor for humidity sensing', *IEEE Sens. J.*, vol. 14, no. 8, pp. 2615–2619, 2014.

[99] N. G. Harbach, 'Fiber bragg gratings in Polymer Optical Fibers', Ph.D. dissertation, Faculty Eng. Sci. Technol., École Polytechnique Fédérale de Lausanne, Lausanne, Switzerland, 2008.

[100] W. Zhang and D. J. Webb, 'Humidity responsivity of poly(methyl methacrylate)-based optical fiber Bragg grating sensors', *Opt. Lett.*, vol. 39, no. 10, pp. 3026–3029, 2014.

[101] C. Zhang, X. Chen, D. J. Webb, and G. D. Peng, 'Water detection in jet fuel using a polymer optical fibre Bragg grating', in *Proc. SPIE 7503, 20th International Conference on Optical Fibre Sensors*, 7503, vol. 2009.

[102] C. Zhang, W. Zhang, D. J. Webb, and G.-D. Peng, 'Optical fibre temperature and humidity sensor', *Electron. Lett.*, vol. 46, no. 9, pp. 643–644, 2010.

[103] K. E. Carroll, C. Zhang, D. J. Webb, K. Kalli, A. Argyros, and M. C. Large, 'Thermal response of Bragg gratings in PMMA microstructured optical fibers', *Opt. Express*, vol. 15, no. 14, pp. 8844–50, 2007.

[104] 'Nordisk Plast'. [Online]. Available: http://www.nordiskplast.dk/.

[105] 'GEHR Plastics Inc. - PMMA (Acrylic)'. [Online]. Available: https://www.gehrplastics.com/pmma-acrylic.html.

[106] 'Makrolon LED2245 Polycarbonate'. [Online]. Available: http://www.plastics.covestro.com/en/Products/Makrolon/ProductList/201305212210/Makrolon-LED2245.

[107] 'Topas Advanced Polymers Topas 5013S-04'. [Online]. Available: http://www.topas.com/sites/default/files/TDS_5013S_04_e_1.pdf.

[108] 'Zeon Corporation Zeonex'. [Online]. Available: http://www.zeonex.com/optics.aspx.

[109] A. Stefani, K. Nielsen, H. K. Rasmussen, and O. Bang, 'Cleaving of TOPAS and PMMA microstructured polymer optical fibers: Core-shift and statistical quality optimization', *Opt. Commun.*, vol. 285, no. 7, pp. 1825–1833, Apr. 2012.

[110] A. Abang and D. J. Webb, 'Demountable connection for polymer optical fiber grating sensors', *Opt. Eng.*, vol. 51, pp. 80501–80503, 2012.

[111] M. K. Szczurowski, T. Martynkien, G. Statkiewicz-Barabach, W. Urbanczyk, L. Khan, and D. J. Webb, 'Measurements of stress-optic coefficient in polymer optical fibers', *Opt. Lett.*, vol. 35, no. 12, p. 2013, 2010.

[112] T. Ishigure, M. Hirai, M. Sato, and Y. Koike, 'Graded-index plastic optical fiber with high mechanical properties enabling easy network installations I', *J. Appl. Polym. Sci.*, vol. 91, no. 1, pp. 404–409, 2004.

[113] E. E. Shafee, 'Effect of photodegradation on the β-relaxation in poly(methylmethacrylate)', *Polym. Degrad. Stab.*, vol. 53, no. 1, pp. 57–61, 1996.

[114] L. Smith and V. Schmitz, 'The effect of water on the glass transition temperature of poly(methyl methacrylate)', *Polymer (Guildf).*, vol. 29, no. 10, pp. 1871–1878, 1988.

[115] D. R. G. Williams, P. E. M. Allen, and T. Van Tan, 'Glass transition temperature and stress relaxation of methanol equilibrated poly(methyl methacrylate)', *Eur. Polym. J.*, vol. 22, no. 11, pp. 911–919, 1986.

[116] Z. F. Zhang and X. M. Tao, 'Synergetic effects of humidity and temperature on PMMA based fiber Bragg gratings', *J. Light. Technol.*, vol. 30, no. 6, pp. 841–845, 2012.

[117] G. Khanarian and H. Celanese, 'Optical properties of cyclic olefin copolymers', *Opt. Eng.*, vol. 40, no. 6, pp. 1024–1029, 2001.

[118] S. Roy, C. Y. Yue, Z. Y. Wang, and L. Anand, 'Thermal bonding of microfluidic devices: Factors that affect interfacial strength of similar and dissimilar cyclic olefin copolymers', *Sensors Actuators, B Chem.*, vol. 161, no. 1, pp. 1067–1073, 2012.

[119] E. Torres, M. N. Berberan-Santos, and M. J. Brites, 'Synthesis, photophysical and electrochemical properties of perylene dyes', *Dye. Pigment.*, vol. 112, pp. 298–304, 2015.

[120] T. Bremner, A. Rudin, and D. G. Cook, 'Melt flow index values and molecular weight distributions of commercial thermoplastics', *J. Appl. Polym. Sci.*, vol. 41, no. 7–8, pp. 1617–1627, 1990.

[121] S. G. Leon-Saval, R. Lwin, and A. Argyros, 'Multicore composite single-mode polymer fiber', *Opt. Express*, vol. 20, no. 1, pp. 141–148, 2012.

[122] K. Bhowmik *et al.*, 'Intrinsic high-sensitivity sensors based on etched single-mode polymer optical fibers', *IEEE Photonics Technol. Lett.*, vol. 27, no. 6, pp. 604–607, 2015.

[123] R. Oliveira, T. H. R. Marques, L. Bilro, R. Nogueira, and C. M. B. Cordeiro, 'Multiparameter POF Sensing based on Multimode Interference and Fiber Bragg Grating', *J. Light. Technol.*, vol. 35, no. 1, pp. 3–9, 2016.

[124] W. Zhang, D. J. Webb, and G. D. Peng, 'Investigation Into Time Response of Polymer Fiber Bragg Grating Based Humidity Sensors', *J. Light. Technol.*, vol. 30, no. 8, pp. 1090–1096, 2012.

[125] X. Chen, W. Zhang, C. Liu, Y. Hong, and D. J. Webb, 'Enhancing the humidity response time of polymer optical fiber Bragg grating by using laser micromachining', *Opt. Express*, vol. 23, no. 20, pp. 25942–25949, 2015.